

**DEVELOPMENT OF CURVED-PLATE ELEMENTS FOR THE EXACT
BUCKLING ANALYSIS OF COMPOSITE PLATE ASSEMBLIES INCLUDING
TRANSVERSE-SHEAR EFFECTS**

by

David Michael McGowan
B.S.M.E., May 1989, Old Dominion University

A Thesis Submitted to the Faculty of
Old Dominion University in Partial Fulfillment of the
Requirements for the Degree of

MASTER OF SCIENCE


ENGINEERING MECHANICS

OLD DOMINION UNIVERSITY
May 1997


Approved by:



Chuh Mei (Co-adviser)



Melvin S. Anderson (Co-adviser)



Norman F. Knight, Jr. (Member)

DEVELOPMENT OF CURVED-PLATE ELEMENTS FOR THE EXACT BUCKLING ANALYSIS OF COMPOSITE PLATE ASSEMBLIES INCLUDING TRANSVERSE-SHEAR EFFECTS

ABSTRACT

The analytical formulation of curved-plate non-linear equilibrium equations including transverse-shear-deformation effects is presented. The formulation uses the principle of virtual work. A unified set of non-linear strains that contains terms from both physical and tensorial strain measures is used. Linearized, perturbed equilibrium equations (stability equations) that describe the response of the plate just after buckling occurs are then derived after the application of several simplifying assumptions. These equations are then modified to allow the reference surface of the plate to be located at a distance z_c from the centroidal surface. The implementation of the new theory into the VICONOPT exact buckling and vibration analysis and optimum design computer program is described as well. The terms of the plate stiffness matrix using both classical plate theory (CPT) and first-order shear-deformation plate theory (SDPT) are presented. The necessary steps to include the effects of in-plane transverse and in-plane shear loads in the in-plane stability equations are also outlined. Numerical results are presented using the newly implemented capability. Comparisons of results for several example problems with different loading states are made. Comparisons of analyses using both physical and tensorial strain measures as well as CPT and SDPT are also made. Results comparing the computational effort required by the new analysis to that of the analysis currently in the VICONOPT program are presented. The effects of including terms related to in-plane transverse and in-plane shear loadings in the in-plane stability equations are also examined. Finally, results of a design-optimization study of two different cylindrical shells subject to uniform axial compression are presented.

ACKNOWLEDGMENTS

The author expresses sincere gratitude to Dr. Melvin S. Anderson for his patience, guidance and encouragement during the course of this research. Sincere appreciation is also extended to Dr. James H. Starnes, Jr., Head of the Structural Mechanics Branch, Structures Division, NASA Langley Research Center, for his technical, editorial, and moral support during the completion of this thesis. Many thanks are offered to my co-adviser, Dr. Chuh Mei, and Dr. Norman F. Knight, Jr., committee member and Graduate Program Director of the Aerospace Engineering Department at Old Dominion University, for all of their efforts in helping me complete this work. Thanks are also due to Dr. Michael P. Nemeth for his helpful discussions on plate and shell theory. I also thank Dr. F. W. Williams and Dr. D. Kennedy of the Cardiff School of Engineering, University of Wales, for their helpful discussions and suggestions during the implementation of this work into the VICONOPT computer program. Finally, to the family and friends that have supported me for so long, I express my sincere thanks and deep appreciation for everything you have done for me.

DEDICATION

The author dedicates this thesis to his loving wife, Christie White McGowan, for her love, support, encouragement, and endless patience during this entire effort. Thank you for believing in me.

TABLE OF CONTENTS

ABSTRACT	ii
ACKNOWLEDGMENTS.....	iii
DEDICATION.....	iv
TABLE OF CONTENTS.....	v
LIST OF TABLES.....	vii
LIST OF FIGURES.....	viii
LIST OF SYMBOLS.....	x
CHAPTER I.....	1
INTRODUCTION.....	1
1.1 Purpose of Study	1
1.2 Literature Review	4
1.3 Scope of Study.....	10
CHAPTER II	12
ANALYTICAL FORMULATION	12
2.1 Plate Geometry, Loadings, and Sign Conventions.....	12
2.2 Strain-Displacement Relations.....	13
2.3 Equilibrium Equations.....	16
2.4 Stability Equations	19
2.5 Stability Equations Transformed to the Plate Reference Surface	23
2.6 Constitutive Relations	27

CHAPTER III.....	31
IMPLEMENTATION INTO VICONOPT	31
3.1 Simplifications to the Theory	31
3.2 Continuity of Rotations at a Plate Junction.....	32
3.3 Derivation of the Curved-Plate Stiffness Matrix.....	36
3.4 The Wittrick-Williams Eigenvalue Algorithm.....	42
CHAPTER IV	44
NUMERICAL RESULTS.....	44
4.1 Convergence of the Segmented-Plate Approach.....	44
4.2 Buckling of Curved Plates With Widely Varying Curvatures	46
4.3 Buckling of an Unsymmetrically Laminated Curved Plate.....	48
4.4 Effect of N_{22} Terms in the In-Plane Stability Equations	49
4.5 Design Optimization of a Cylindrical Shell Subject to Uniaxial Compression	53
CHAPTER V.....	56
CONCLUDING REMARKS	56
REFERENCES	59
APPENDIX A	63
MATRICES FOR DETERMINING CHARACTERISTIC ROOTS.....	63

LIST OF TABLES

Table 1.	Material properties for boron/epoxy plies and 2024 aluminum (SI units).	72
Table 2.	Geometric parameters used to vary the curvature parameter, $\frac{b^2}{R_2 t}$	72
Table 3.	Critical value of stress resultant N_{11} for buckling of a symmetrically laminated long curved plate with clamped longitudinal edges.	73
Table 4.	Critical value of stress resultant N_{22} for buckling of a symmetrically laminated long curved plate with clamped longitudinal edges.	74
Table 5.	Critical value of stress resultant N_{12} for buckling of a symmetrically laminated long curved plate with clamped longitudinal edges.	75
Table 6.	Critical value of stress resultant $N_{11} = N_{22} = N_{12}$ for buckling of a symmetrically laminated long curved plate with clamped longitudinal edges.	76
Table 7.	Critical value of stress resultant N_{11} for buckling of an unsymmetrically laminated long curved plate with simply supported longitudinal edges.	77
Table 8.	Critical value of stress resultant N_{12} for buckling of an unsymmetrically laminated long curved plate with simply supported longitudinal edges.	77
Table 9.	Material properties for aluminum and Korex™ honeycomb core (English Engineering units).	78
Table 10.	Critical value of hoop stress resultant N_{22} for buckling of a long, isotropic cylinder subject to uniform external compression (results are in lbs/in.).	78
Table 11.	Design-optimization results for a honeycomb-sandwich cylinder subjected to N_{11} loading.	78
Table 12.	Design-optimization results for a solid-wall cylinder subjected to N_{11} loading.	79

LIST OF FIGURES

Figure 1.1	Typical longitudinally stiffened plate structures.	80
Figure 1.2	Segmented representation of curved-plate geometry currently used by VICONOPT.....	80
Figure 2.1	Curved-plate geometry and sign convention for buckling displacements, rotations, moments, and forces.....	81
Figure 2.2	Sign convention for applied in-plane loads and relation of reference surface to centroidal surface.	82
Figure 2.3	Curved-laminate geometry.	83
Figure 3.1	Displacements and rotations at a typical plate junction.....	84
Figure 4.1	Long isotropic (aluminum) cylinder subjected to uniaxial compression....	85
Figure 4.2	Convergence of VICONOPT segmented-plate results as a function of the number of segments used in the approximation.	86
Figure 4.3	Normalized CPU time requirements for the segmented-plate approach as a function of the number of segments used in the approximation.....	87
Figure 4.4	Positive applied in-plane loads on a long curved plate.....	88
Figure 4.5	Symmetrically laminated long curved plate with clamped longitudinal edges subjected to applied in-plane loads.	88
Figure 4.6	Critical value of stress resultant N_{11} for buckling of a symmetrically laminated curved plate with clamped longitudinal edges.	89
Figure 4.7	Critical value of stress resultant N_{22} for buckling of a symmetrically laminated curved plate with clamped longitudinal edges.	90
Figure 4.8	Critical value of stress resultant N_{12} for buckling of a symmetrically laminated curved plate with clamped longitudinal edges.	91
Figure 4.9	Critical value of stress resultants $N_{11} = N_{22} = N_{12}$ for buckling of a symmetrically laminated curved plate with clamped longitudinal edges.	92
Figure 4.10	Unsymmetrically laminated aluminum and boron/epoxy (B/E) curved plate with simply supported edges subjected to applied in-plane loads.....	93
Figure 4.11	Critical value of stress resultant N_{11} for buckling of an unsymmetrically laminated aluminum and boron/epoxy (B/E) curved plate with simply supported longitudinal edges.	94
Figure 4.12	Critical value of stress resultant N_{12} for buckling of an unsymmetrically laminated aluminum and boron/epoxy (B/E) curved plate with simply supported longitudinal edges.	95

Figure 4.13	Isotropic (aluminum) long cylindrical tube subjected to uniform external pressure loading.....	96
Figure 4.14	Cylindrical shell subjected to uniform axial compression (N_{11} loading).....	97
Figure 4.15	Optimized cylinder mass as a function of the applied loading for a cylindrical shell.....	98

LIST OF SYMBOLS

A	extensional stiffness matrix
a	upper half of the eigenvectors of matrix R , associated with displacements
B	coupling stiffness matrix
B , C , E ,	
E , G , H	coefficients used to select physical or tensor strains
b	lower half of the eigenvectors of matrix R , associated with forces
b	plate width (arc length)
C	matrix whose columns contain the eigenvectors of matrix R
c	single eigenvector of matrix R
D	bending stiffness matrix
d	vector of displacement amplitudes at the two edges of a plate
ds	arc length of a line element in a body before deformation
ds *	arc length of a line element in a body after deformation
E_{ii}	Young's modulus in the i-i direction
E	matrix used to define vector d , see Eq. (3.19)
F	matrix used to define vector f , see Eq. (3.20)
f	vector of force amplitudes at the two edges of a plate
f_i	body forces
G₁₂	in-plane shear stiffness
G₁₃ , G₂₃	transverse shear stiffnesses
h_{ij}	coefficient of the partially inverted constitutive relations, see Eqs. (3.11) and (3.12)
I	identity matrix
I	moment of inertia
i	imaginary number, square root of -1

K	plate stiffness matrix
k	transverse-shear compliance matrix
M_{11}, M_{22}, M_{12}	applied (prebuckling) moment resultants
m_{11}, m_{22}, m_{12}	perturbation values of moment resultants just after buckling has occurred
$\tilde{m}_{11}, \tilde{m}_{22}, \tilde{m}_{12}$	moment resultants
N_{11}, N_{22}, N_{12}	applied (prebuckling) stress resultants
n_{11}, n_{22}, n_{12}	perturbation values of stress resultants just after buckling has occurred
$\tilde{n}_{11}, \tilde{n}_{22}, \tilde{n}_{12}$	stress resultants
$\hat{n}_{22}, \hat{n}_{12}$	effective forces per unit length at an edge $\xi_2 = \text{constant}$
n_l	number of layers in a general curved laminate
P	coefficient matrix of the set of first-order plate differential equations, see Eq. (3.14)
p	applied external pressure
p_2, p_3	perturbation values of the applied pressure load in the buckled state in the ξ_2 - and ξ_3 -directions
Q	lamina reduced stiffness matrix
\bar{Q}	lamina reduced transformed stiffness matrix
Q_1, Q_2	applied (prebuckling) shear stress resultants
$q_1, q_2,$	perturbation values of shear stress resultants just after buckling has occurred
\tilde{q}_1, \tilde{q}_2	shear stress resultants
\hat{q}_2	effective transverse shear force per unit length at an edge $\xi_2 = \text{constant}$
R	matrix whose eigenvalues are the characteristic roots of the plate differential equations, see Eq. (3.16b)

R_1, R_2	radii of lines of principal curvature
\mathbf{T}	coefficient matrix of the set of first-order plate differential equations, see Eq. (3.14)
T_i	surface tractions
t	plate thickness
U_1, U_2	prebuckling displacements
u_1, u_2	perturbation values of displacements just after buckling has occurred
v	volume
w	normal displacement in the ξ_3 -direction
\mathbf{Z}	vector of the forces and displacements in the plate
\mathbf{z}	vector containing the amplitudes of the forces and displacements in the plate assuming a sinusoidal variation in the ξ_1 -direction
z_c	distance from the plate centroidal surface to the plate reference surface
z_k	distance from laminate reference surface to the k th layer in the laminate

Greek

α_1, α_2	Lamé parameters
β	angle included by a curved plate
ϵ	vector containing strains ϵ_{11} , ϵ_{22} , and γ_{12}
$\epsilon_{11}, \epsilon_{22}$	in-plane direct strains
$\epsilon_{12}, \gamma_{12}$	in-plane shear strains
$\epsilon_{13}, \gamma_{13}$	transverse shear strains
$\epsilon_{23}, \gamma_{23}$	transverse shear strains

ϕ_1, ϕ_2	rotations
ϕ_n	rotation about the normal to the plate middle surface
κ_{11}, κ_{22}	middle surface changes in curvatures
κ_{12}	middle surface twisting curvature
λ	half wavelength of buckling mode
ν	Poisson's ratio
θ_k	angular orientation of ply k in a laminate with respect to the laminate coordinate system
ρ	density
σ	vector containing stresses σ_{11} , σ_{22} , and τ_{12}
σ_{11}, σ_{22}	in-plane direct stresses
τ_{12}	in-plane shear stress
ξ_1, ξ_2, ξ_3	coordinate measures in the 1-, 2-, and 3-directions, respectively

Subscripts and Superscripts

cr	critical value for buckling
k	k th layer in a laminated composite plate
n	normal to middle surface
1, 2, 3	1-, 2-, and 3-directions, respectively
o	value at centroidal surface

CHAPTER I

INTRODUCTION

1.1 Purpose of Study

Longitudinally stiffened plate structures occur frequently in aerospace vehicle structures. These structures can typically be represented by long, thin, flat or curved plates that are rigidly connected along their longitudinal edges, see Figure 1.1. The designs for these structures often exploit the increased structural efficiency that can be obtained by the use of advanced composite materials. Therefore, the plates used to represent the structure may consist of anisotropic laminates. The buckling and vibration behavior of this type of structure must be understood to design the structure. Additionally, to satisfy the current demands for more cost-effective and structurally efficient aerospace vehicles, these structures are frequently optimized to obtain an optimal design that satisfies either buckling or vibration constraints or a combination of these two constraints. There is a need for analytical tools that can provide the analysis capability required to optimize panel designs.

The VICONOPT computer code [1] is an exact analysis and optimum design program that includes the buckling and vibration analyses of prismatic assemblies of flat, in-plane-loaded anisotropic plates. The code also includes approximations for curved and tapered plates, discrete supports, and transverse stiffeners. Anisotropic composite laminates having fully populated **A**, **B** and **D** stiffness matrices may be analyzed. Either classical plate theory (CPT) or first-order transverse-shear-deformation plate theory (SDPT) may be used [2]. The analyses of the plate assemblies assume a sinusoidal response along the plate length. The analysis used in the code is referred to as “exact” because it uses

stiffness matrices that result from the exact solution to the differential equations that describe the behavior of the plates.

Currently, VICONOPT approximates a curved plate by subdividing it into a series of flat-plate segments that are joined along their longitudinal edges to form the complete curved-plate structure, see Figure 1.2. This procedure is analogous to the discretization approach used in finite element analysis. The code uses exact stiffnesses for the flat-plate segments and enforces continuity of displacements and rotations at the segment connections. Thus, the analyst must ensure that an adequate number of flat-plate segments is used in the analysis. The next logical step in the development of the VICONOPT code is to eliminate the need to approximate curved-plate geometries by flat-plate segments by adding the capability to analyze curved-plate segments exactly. By adding this capability, the accuracy of the solutions can be improved. Furthermore, since the curvature of a plate is modeled directly, there will be no need to determine if a sufficient amount of flat-plate segments have been used to model the curved plate. Another benefit of adding this capability is that the computational efficiency of the code will be improved since only one stiffness calculation for the entire curved plate is required, rather than the several that are currently required for the individual flat plates that are used to approximate the curved plate. This improvement in computational efficiency is important for structural optimization. In this thesis, the capability to analyze curved-plate segments exactly has been added to the VICONOPT code. The present thesis will describe the methodology used to accomplish this enhancement of the code and will present results obtained utilizing this new capability.

The procedure used in the present thesis is an extension of the procedure described in [2]. This procedure involves deriving the appropriate differential equations of equilibrium for the analysis of fully anisotropic curved plates, including transverse-shear-deformation effects. These coupled equations are of eighth-order if transverse-shear effects are neglected, and of tenth-order if transverse-shear effects are included. For the

analysis of flat plates, the coupling of these equations occurs through the laminate extension-bending **B** matrix; however, coupling can also be produced by including curvature terms in the equilibrium equations. The numerical solution technique that was developed in [2] to solve such systems of equations will apply for either type of coupling, and the stiffnesses of the plates are derived from the numerical solution to these equations.

Several features have been added to the VICONOPT code as part of the present thesis. The current version of VICONOPT only analyzes flat-plate elements based on a tensorial strain-displacement relation. However, the choice of strain-displacement relations can affect the contribution of prebuckling forces in curved plates. Therefore, a unified set of nonlinear strain-displacement relations that contains terms from both physical and tensorial strain measures is used to derive the plate equilibrium equations. The unified set of strains is used throughout the derivation of the equilibrium equations, and the selection of either physical or tensorial strains is achieved by appropriately setting coefficients in the equilibrium equations equal to one or zero. The option to use physical strain-displacement relations for the analysis of flat plates is included as well. Another addition is the treatment of the effects of in-plane transverse and in-plane shear loadings in the in-plane equilibrium equations. These effects are currently ignored in the VICONOPT code (see [1]). In the present thesis, an in-plane transverse loading, denoted N_{22} , is a loading that acts perpendicular to the longitudinal edges of the plate. The present study has added the option to include the effects of these loadings in the in-plane equilibrium equations. Finally, either CPT or SDPT may be used. The SDPT used in VICONOPT and in the present thesis uses the usual first-order assumption that straight lines originally normal to the centroidal surface are assumed to remain straight and inextensional but not necessarily normal to the centroidal surface during deformation of the plate. All of these features have been implemented such that they are available for use in the analysis of both flat and curved plates.

1.2 Literature Review

The buckling and vibration analysis of assemblies of prismatic plates has received a great deal of attention over the last thirty years. One method of analysis for this class of structure that has been studied extensively is the finite-strip method, FSM [3]. A popular application of this method involves determining a stiffness matrix for each individual plate in the assembly and then assembling those individual matrices into a global stiffness matrix for use in determining the response of the entire structure. This method is therefore analogous in form to the finite element method [4]. The main difference between the two methods is that the finite element method discretizes the individual plates into elements in both the longitudinal and transverse directions. The stiffness matrix for each individual element is then calculated and assembled into a global stiffness matrix. In the FSM, the response of the plate in the longitudinal direction is represented as a continuously differentiable smooth series that satisfies the boundary conditions at the two ends of the plate. Therefore, discretization of the structure is only required to be performed in the transverse direction, and depending on the method being used, discretization of the individual plates may or may not be required [3].

The work in the area of finite strip analysis of assemblies of prismatic plates may be broadly classified based upon different characteristics of the analysis method used. One classification distinguishes whether the properties of the individual plates are derived by direct solution to the equations of equilibrium or by application of potential energy or virtual work principles, i.e., exact versus approximate methods. Another classification distinguishes whether classical plate theory (CPT) or first-order shear-deformation plate theory (SDPT) is used in the analysis. Finally, a distinction may be made as to whether or not complex quantities are used in the development of the individual stiffness matrices. A review of the literature in the area of finite strip analysis methods is presented below. Approximate methods are discussed separately from exact methods.

The approximate FSM was first proposed for the static analysis of plate bending by Cheung in 1968 [5]. The approximate FSM involves subdividing each plate into a series of finite-width strips that are linked together at their longitudinal edges in a manner similar to that depicted in Figure 1.2. Separate expressions for in-plane and out-of-plane displacements as well as rotations about the in-plane x and y axes over the middle surface of each strip are assumed. Each of these fundamental quantities are expressed as a summation of the products of longitudinal series and transverse polynomials [3]. The longitudinal series are typically sinusoidal and are selected to satisfy displacement conditions at the transverse edges of each strip that match the desired plate boundary conditions along those edges. The potential energy of an individual finite strip is then evaluated, and the total potential energy of the plate is obtained by summing the potential energies of the individual strips. Following the application of any appropriate zero-displacement boundary conditions at the longitudinal edges, the potential energy is minimized with respect to each plate degree of freedom to generate the equilibrium equations for the plate. Displacements are then calculated for a given loading condition using this system of equations.

The analysis of [5] utilized CPT for the static bending analysis of isotropic plates. In 1971, Cheung and Cheung [6] applied the approximate FSM to the analysis of natural vibrations of thin, flat-walled structures with different combinations of the standard edge boundary conditions (i.e., clamped, simply supported, or free). Their analysis was based upon CPT and the displacements in the longitudinal direction were approximated using the normal modes of Timoshenko beam theory to allow for various boundary conditions on the transverse edges.

Przemieniecki [7] used an approximate FSM based upon CPT to calculate the initial buckling of assemblies of flat plates subjected to a biaxial stress state. This method only considered local buckling modes since it assumed that the line junctions between plates remained straight during buckling. Plank and Wittrick [8] extended the work of

Przemieniecki by considering global as well as local modes and by admitting a more general loading state that included uniform transverse and longitudinal shear stress and longitudinal direct stress that varies linearly across the width of the plate. When in-plane shear loading is present, a spatial phase difference occurs between the perturbation forces and displacements which occur at the edges of the plates during buckling. This phase difference causes skewing of the nodal lines and is accounted for in [8] by defining the magnitude of these quantities using complex quantities. This method is referred to as a complex finite strip method.

In 1977, Dawe [9 and 10] used an approximate FSM based upon CPT for the static and linear buckling analysis of curved-plate assemblies. The plates studied were isotropic, and in-plane shear loads were not allowed. Morris and Dawe extended this analysis to study the free vibration of curved-plate assemblies in 1980 [11].

All of the analyses discussed thus far have been based upon CPT. In 1978, Dawe [12] presented an approximate FSM based upon SDPT [13] for the vibration of isotropic plates with a pair of opposite edges simply supported. Roufaeil and Dawe [14] and Dawe and Roufaeil [15] extended this analysis to the vibration and buckling, respectively, of isotropic and transversely isotropic plates with general boundary conditions. The latter two analyses admitted the general boundary conditions through the use of the normal modes of Timoshenko beam theory, as was done in [6].

In 1986, Craig and Dawe [16] considered the vibration of single symmetrically laminated plates using an approximate FSM based upon SDPT. Dawe and Craig [17] then extended this analysis to study the buckling of single symmetrically laminated plates subject to uniform shear stress and direct in-plane stress. This analysis allowed for anisotropic material properties. General boundary conditions were once again admitted through the use of the normal modes of Timoshenko beam theory. The analysis of [17] was extended in 1987 to the vibration of complete plate assemblies [18]. However, it was shown in this work that the problem size increased dramatically as attempts to

increase the accuracy of the solution were made by further subdivision of the component plates.

In 1988, Dawe and Craig [19] presented a complex FSM based upon SDPT for the buckling and vibration of prismatic plate structures in which the component plates could consist of anisotropic laminates and could be subject to in-plane shear loads. This work also made use of substructuring to create “superstrips” that eliminated the internal degrees-of-freedom from each component plate. This analysis was later extended to consider finite-length structures [20 and 21] and to add multi-level substructuring to couple several “superstrips” to further decrease the problem size. Dawe and Peshkam [22] also developed a complementary analysis to that presented in [20 and 21] for long plate structures. Analyses using both SDPT and CPT were presented. This work also added the capability to define eccentric connections of component plates.

Wittrick laid the groundwork for the exact FSM in 1968 [23]. The basic assumption in this work is that the deformation of any component plate varies sinusoidally in the longitudinal direction. Using this assumption, a stiffness matrix may be derived that relates the amplitudes of the edge forces and moments to the corresponding edge displacements and rotations for a single component plate. For the exact FSM, this stiffness matrix is derived directly from the equations of equilibrium that describe the behavior of the plate. In [23], Wittrick developed an exact stiffness matrix for a single isotropic, long flat plate subject to uniform axial compression. His analysis used CPT. Wittrick and Curzon [24] extended this analysis to account for the spatial phase difference between the perturbation forces and displacements which occur at the edges of the plate during buckling due to the presence of in-plane shear loading. This phase difference is accounted for by defining the magnitude of these quantities using complex quantities. Wittrick [25] then extended his analysis to consider flat isotropic plates under any general state of stress that remains uniform in the longitudinal direction (i.e., combinations of bi-axial direct stress and in-plane shear). A method very similar to that

described in [23] was presented by Smith in 1968 [26] for the bending, buckling, and vibration of plate-beam structures.

In 1972, Williams [27] presented two computer programs, GASVIP and VIPAL to compute the natural frequencies and initial buckling stress of prismatic plate assemblies subjected to uniform longitudinal stress or uniform longitudinal compression, respectively. GASVIP was used to set up the overall stiffness matrix for the structure, and VIPAL demonstrated the use of substructuring. In 1974, Wittrick and Williams [28] first reported on the VIPASA computer code for the buckling and vibration analyses of prismatic plate assemblies. This code allowed for isotropic or anisotropic plates as well as a general state of stress (including in-plane shear). The complex stiffnesses described in [8] were incorporated, as well as allowances for eccentric connections between component plates. This code also incorporated an algorithm, referred to as the Wittrick-Williams algorithm, for determining any natural frequency or buckling load for any given wavelength [29]. The development of this algorithm was necessary because the complex stiffnesses described above are transcendental functions of the load factor and half wavelength of the buckling modes of the structure. The eigenvalue problem for determining natural frequencies and buckling load factors is therefore transcendental. Further discussion of the Wittrick-Williams algorithm will be presented in Chapter III.

In 1973, Viswanathan and Tamekuni [30 and 31] presented an exact FSM based upon CPT for the elastic stability analysis of composite stiffened structures subjected to biaxial inplane loads. The structure is idealized as an assemblage of laminated plate elements (flat or curved) and beam elements. The analysis assumes that the component plates are orthotropic. The transverse edges are assumed to be simply supported, and any combination of boundary conditions may be applied to the longitudinal edges. The analysis was included in an associated computer code, BUCLAP2. Viswanathan, Tamekuni, and Baker extended this analysis in [32] to consider long curved plates subject to any general state of stress, including in-plane shear loads. Anisotropic material

properties were also allowed. This analysis utilized complex stiffnesses as described in [8]. The analyses described in [26, 28, and 32] are very similar. The differences between the three are discussed in [28].

When applied in-plane shear loads or anisotropy is present, the assumption of a sinusoidal variation of deformation in the longitudinal direction is only exact for structures that are infinitely long. Significant errors for structures of finite length can occur due to the skewing of nodal lines. In 1983, Williams and Anderson [33] presented modifications to the eigenvalue algorithm described in [29]. The modifications presented in [33] allowed the buckling mode corresponding to a general loading to be represented as a series of sinusoidal modes in combination with Lagrangian multipliers to apply point constraints at any location on those edges. Each sinusoidal mode is represented by an exact stiffness matrix. This technique allows infinitely long structures supported at repeating intervals with anisotropy or applied in-plane shear loads to be analyzed. Thus, a panel supported at its transverse edges is approximated by one with a series of point supports along those edges. These modifications formed the basis for the computer code VICON (VIpasa with CONstraints) described in [34]. However, the analysis capability of VICON was limited to plates analyzed with CPT having a zero **B** matrix. The VICON code was later modified to include structures supported by Winkler foundations [35]. An optimum design feature was also added in 1990 [36 and 37], and the VICONOPT (VICON with OPTimization) code was introduced.

Anderson and Kennedy [2] incorporated SDPT into VICONOPT in 1993. A numerical approach to obtain exact plate stiffnesses that include the effects of transverse-shear deformation was presented. The generality of VICONOPT was also expanded in [2] to allow for the analysis of laminates with fully populated **A**, **B**, and **D** stiffness matrices.

1.3 Scope of Study

The analytical formulation of the curved-plate non-linear equilibrium equations including transverse-shear-deformation effects are presented in Chapter II. A unified set of non-linear strains that contains terms from both physical and tensorial strain measures is used. The equilibrium equations are derived using the principle of virtual work following the method presented by Sanders [38 and 39]. Linearized, perturbed equilibrium equations that describe the response of the plate just after buckling occurs are then derived after the application of several simplifying assumptions. Modifications to these equations that allow the reference surface of the plate to be located at a distance z_c from the centroidal surface are then made.

In Chapter III, the implementation of the new theory into the VICONOPT code is described. A derivation of the terms of the plate stiffness matrix using MATHEMATICA [40] is presented. The form of these terms for both CPT and SDPT is discussed. The necessary steps to include the effects of in-plane transverse and in-plane shear loads in the in-plane equilibrium equations are also outlined.

In Chapter IV, numerical results are presented using the newly implemented capability. A convergence study using the current segmented-plate approach in VICONOPT is performed for a simple example problem to obtain baseline results for use in future comparisons. Results comparing the computational effort required by the new analysis to that of the analysis currently in the VICONOPT program are also presented. Comparisons of results for several example problems with different loading states are then made. Comparisons of analyses using both physical and tensorial strain measures as well as CPT and SDPT are made. The effects of including terms related to in-plane transverse and in-plane shear loads in the in-plane stability equations are also examined.

In Chapter V, the characteristics of the newly implemented curved-plate elements in VICONOPT is presented. A brief summary of the effects of several analytical features that have been implemented into VICONOPT is given. Finally, potential future work in this area is discussed.

CHAPTER II

ANALYTICAL FORMULATION

In this chapter, the non-linear equilibrium equations are derived for a curved plate including transverse-shear effects. A unified set of non-linear strains that contain terms from both physical and tensorial strain measures is used. The equilibrium equations are derived using the principle of virtual work following the method presented by Sanders [38 and 39]. Linearized stability equations that describe the response of the plate just after buckling occurs are then derived following the application of several simplifying assumptions. Modifications to these equations that allow the reference surface of the plate to be located at a distance z_c from the centroidal surface are then made.

2.1 Plate Geometry, Loadings, and Sign Conventions

The geometry of the basic plate element being studied is given in Figure 2.1. This figure depicts the orthogonal curvilinear coordinate system (ξ_1, ξ_2, ξ_3) used in the present analysis. The ξ_1 - and ξ_2 -axes shown in the figure are along lines of principal curvature and they have radii of curvature R_1 and R_2 , respectively. The ξ_3 -axis is normal to the middle surface of the plate. The first fundamental form of the plate middle surface is given by

$$ds^2 = \alpha_1^2 d\xi_1^2 + \alpha_2^2 d\xi_2^2 \quad (2.1)$$

where α_1 and α_2 are the Lamé parameters. The coordinates ξ_1 and ξ_2 are measured as arc lengths along the ξ_1 - and ξ_2 -axes, respectively. The result of measuring the coordinates in

this manner is that $\alpha_1 = \alpha_2 = 1$. The sign conventions for buckling displacements, moments, rotations, and forces are also shown in Figure 2.1. The sign convention for the applied in-plane loadings being considered and the relation of the reference surface of the plate to the centroidal surface of the plate are shown in Figure 2.2. Note that that centroidal surface can be offset from the reference surface by a distance z_c . The centroidal surface is defined to be located at the centroid of the face of the panel that is normal to the ξ_1 -axis. The loading N_{22} shown in this figure is referred to in the present thesis as an in-plane transverse loading.

2.2 Strain-Displacement Relations

The nonlinear strain-displacement relations used for the present study are given by

$$\varepsilon_{11} = u_{1,1} + \frac{w}{R_1} + \frac{1}{2} \left[w_{,1} - \frac{u_1}{R_1} \right]^2 + \frac{B}{2} u_{2,1}^2 + \frac{C}{2} \left[u_{1,1} + \frac{w}{R_1} \right]^2 \quad (2.2a)$$

$$\varepsilon_{22} = u_{2,2} + \frac{w}{R_2} + \frac{1}{2} \left[w_{,2} - \frac{u_2}{R_2} \right]^2 + \frac{E}{2} u_{1,2}^2 + \frac{F}{2} \left[u_{2,2} + \frac{w}{R_2} \right]^2 \quad (2.2b)$$

$$\begin{aligned} 2\varepsilon_{12} = \gamma_{12} = & u_{1,2} + u_{2,1} + w_{,1} w_{,2} - w_{,1} \frac{u_2}{R_2} - w_{,2} \frac{u_1}{R_1} + \frac{u_1 u_2}{R_1 R_2} \\ & - \frac{G}{2} \left[u_{1,2} u_{2,2} + u_{2,1} u_{1,1} + u_{1,2} \frac{w}{R_2} + u_{2,1} \frac{w}{R_1} \right] \\ & + \frac{H}{2} \left[u_{1,2} u_{1,1} + u_{2,1} u_{2,2} + u_{1,2} \frac{w}{R_1} + u_{2,1} \frac{w}{R_2} \right] \end{aligned} \quad (2.2c)$$

$$2\varepsilon_{13} = \gamma_{13} = w_{,1} - \frac{u_1}{R_1} - \phi_1 \quad (2.2d)$$

$$2\varepsilon_{23} = \gamma_{23} = w_{,2} - \frac{u_2}{R_2} - \phi_2 \quad (2.2e)$$

where the following notation for partial derivatives is used: $\frac{\partial u_i}{\partial \xi_j} = u_{i,j}$. The displacement quantities in Eqs. (2.2a) through (2.2e) are displacements of the centroidal surface of the plate. The constants B, C, E, F, and H are set equal to one and G is set equal to zero in Eqs. (2.2a) through (2.2e) to use tensorial strain measures. The constants B, E, and G are set equal to one and C, F, and H are set equal to zero to use physical strain measures. Note that the linear portions of the tensorial and physical strain measures are identical. To obtain Donnell theory from the strain-displacement relations in Eqs. (2.2a) through (2.2e) the constants B, C, E, F, G, and H must be set equal to zero, and all terms involving the quantities $\frac{u_1}{R_1}$ and $\frac{u_2}{R_2}$ must be neglected. Sander's theory [39] may be obtained by setting the constants B, C, E, F, G, and H equal to zero and adding the term $\frac{1}{2}\phi_n^2$ to Eqs. (2.2a) and (2.2b), where ϕ_n is the rotation about the normal to the plate middle surface.

The tensorial strain measures used in the present study are those of Novozhilov [41]. These strains are obtained by taking the difference between the square of the arc length of a line element in a body after deformation, $(ds^*)^2$, and before deformation $(ds)^2$. The tensorial strain measures, ε_{jk} , are defined by the relationship

$$\frac{1}{2} \left[(ds^*)^2 - (ds)^2 \right] = \varepsilon_{jk} d\xi_j d\xi_k \quad i, j = 1, 3 \quad (2.3)$$

The repeated indices in Eq. (2.3) indicate summation over i and j . The physical strain measures are strains that can be measured in the laboratory. The physical strains used in the present thesis are derived in a manner similar to that presented by Stein in [42] and they were communicated to the author in lines of curvature coordinates by Dr. Michael P. Nemeth¹. Physical extensional strains are defined as the ratio of the change in arc length of a line element in a body, ds^* , to the original length of that line element, ds ,

$$\varepsilon_{jj} = \frac{(ds^*)_j - (ds)_j}{(ds)_j} \quad j = 1, 2 \text{ (no summation)} \quad (2.4a)$$

Physical shearing strains are defined as the change in the angles between three line elements that are orthogonal before deformation and are oriented in the direction of three unit vectors, \hat{e}_j^* , after deformation. The physical shearing strains are defined by the following expressions

$$\sin(\gamma_{12}) \approx \gamma_{12} = \hat{e}_1^* \bullet \hat{e}_2^* \quad (2.4b)$$

$$\sin(\gamma_{j3}) \approx \gamma_{j3} = \hat{e}_j^* \bullet \hat{e}_3^* \quad j = 1, 2 \quad (2.4c)$$

The definitions for the changes in curvatures of the centroidal surface used for both theories are

$$\kappa_{11} = -\phi_{1,1} \quad (2.5a)$$

$$\kappa_{22} = -\phi_{2,2} \quad (2.5b)$$

$$\kappa_{12} = -(\phi_{1,2} + \phi_{2,1}) \quad (2.5c)$$

¹ Structural Mechanics Branch, Structures Division, NASA Langley Research Center, Hampton, Virginia, 23681-0001

These changes in curvatures are equivalent to those given by Sanders in [39] with the terms involving rotations about the normal neglected.

2.3 Equilibrium Equations

The nonlinear equilibrium equations for the curved plate illustrated in Figures 2.1 and 2.2 are derived using the principle of virtual work [43]. This principle states that, if a structure in equilibrium is subject to a virtual distortion while remaining in equilibrium, then the external virtual work done by the external forces on the structure is equal to the internal virtual work done by the internal stresses. The principle of virtual work can therefore be written in the form

$$\int_{\text{surface}} T_i \delta u_i ds + \int_{\text{volume}} f_i \delta u_i dv = \int_{\text{volume}} \sigma_{ij} \delta \epsilon_{ij} dv \quad (2.6)$$

The present derivation uses the principle of virtual work in the manner of Sanders [38] written in the following form

$$\begin{aligned} & \iint_{\text{area}} \left[\bar{n}_{11} \delta \epsilon_{11} + \bar{n}_{22} \delta \epsilon_{22} + 2\bar{n}_{12} \delta \epsilon_{12} + \bar{m}_{11} \delta \kappa_{11} \right. \\ & \quad \left. + \bar{m}_{22} \delta \kappa_{22} + 2\bar{m}_{12} \delta \kappa_{12} + \bar{q}_1 \delta \gamma_{13} + \bar{q}_2 \delta \gamma_{23} \right] d\xi_1 d\xi_2 \\ & + \oint_c [N_{11} \delta u_1 + N_{12} \delta u_2 + Q_1 \delta w - M_{11} \delta \phi_1 - M_{12} \delta \phi_2] d\xi_2 \\ & - \oint_c [N_{12} \delta u_1 + N_{22} \delta u_2 + Q_2 \delta w - M_{12} \delta \phi_1 - M_{22} \delta \phi_2] d\xi_1 = 0 \end{aligned} \quad (2.7)$$

The terms \bar{n}_{12} and \bar{m}_{12} are effective stress measures as defined by Sanders in [38]. The terms \bar{q}_1 and \bar{q}_2 are also effective stress measures as defined by Cohen in [44]. The uppercase terms in Eq. (2.7) are applied loadings on the boundary of the plate.

Substituting Eqs. (2.2a) through (2.2e) and Eqs. (2.5a) through (2.5c) into Eq. (2.7) and integrating by parts results in

$$\begin{aligned}
& \iint_{\text{area}} - \left(\left[\tilde{n}_{11,1} + \tilde{n}_{12,2} + \frac{\tilde{n}_{11}}{R_1} \left(w_{,1} - \frac{u_1}{R_1} \right) + \frac{\tilde{n}_{12}}{R_1} \left(w_{,2} - \frac{u_2}{R_2} \right) + \frac{\tilde{q}_1}{R_1} \right. \right. \\
& + \underline{C} \left(\tilde{n}_{11} \left[u_{1,1} + \frac{w}{R_1} \right] \right)_{,1} + \underline{E} (\tilde{n}_{22} u_{1,2})_{,2} \\
& - \underline{G} \left(\left[\tilde{n}_{12} \left\{ u_{2,2} + \frac{w}{R_2} \right\} \right]_{,2} + [\tilde{n}_{12} u_{2,1}]_{,1} \right) \\
& \left. + \underline{H} \left(\left[\tilde{n}_{12} \left\{ u_{1,1} + \frac{w}{R_1} \right\} \right]_{,2} + [\tilde{n}_{12} u_{1,2}]_{,1} \right) \right] \delta u_1 \\
& + \left[\tilde{n}_{12,1} + \tilde{n}_{22,2} + \frac{\tilde{n}_{22}}{R_2} \left(w_{,2} - \frac{u_2}{R_2} \right) + \frac{\tilde{n}_{12}}{R_2} \left(w_{,1} - \frac{u_1}{R_1} \right) + \frac{\tilde{q}_2}{R_2} \right. \\
& + \underline{B} (\tilde{n}_{11} u_{2,1})_{,1} + \underline{F} \left(\tilde{n}_{22} \left[u_{2,2} + \frac{w}{R_2} \right] \right)_{,2} \\
& - \underline{G} \left(\left[\tilde{n}_{12} \left\{ u_{1,1} + \frac{w}{R_1} \right\} \right]_{,1} + [\tilde{n}_{12} u_{1,2}]_{,2} \right) \\
& \left. + \underline{H} \left(\left[\tilde{n}_{12} \left\{ u_{2,2} + \frac{w}{R_2} \right\} \right]_{,1} + [\tilde{n}_{12} u_{2,1}]_{,2} \right) \right] \delta u_2 \\
& + \left[\tilde{q}_{1,1} + \tilde{q}_{2,2} - \left(\frac{\tilde{n}_{11}}{R_1} + \frac{\tilde{n}_{22}}{R_2} \right) + \left[\tilde{n}_{11} \left(w_{,1} - \frac{u_1}{R_1} \right) \right]_{,1} \right. \\
& + \left[\tilde{n}_{22} \left(w_{,2} - \frac{u_2}{R_2} \right) \right]_{,2} + \left[\tilde{n}_{12} \left(w_{,2} - \frac{u_2}{R_2} \right) \right]_{,1} \\
& + \left[\tilde{n}_{12} \left(w_{,1} - \frac{u_1}{R_1} \right) \right]_{,2} + \frac{\underline{C} \tilde{n}_{11}}{R_1} \left(\frac{w}{R_1} + u_{1,1} \right) \\
& - \frac{\underline{F} \tilde{n}_{22}}{R_2} \left(\frac{w}{R_2} + u_{2,2} \right) + \underline{G} \tilde{n}_{12} \left(\frac{u_{1,2}}{R_2} + \frac{u_{2,1}}{R_1} \right) \\
& \left. - \underline{H} \tilde{n}_{12} \left(\frac{u_{1,2}}{R_1} + \frac{u_{2,1}}{R_2} \right) \right] \delta w
\end{aligned}$$

$$\begin{aligned}
& + \left[\tilde{m}_{11,1} + \tilde{m}_{12,2} - \tilde{q}_1 \right] \delta \phi_1 + \left[\tilde{m}_{12,1} + \tilde{m}_{22,2} - \tilde{q}_2 \right] \delta \phi_2 \Bigg) d\xi_1 d\xi_2 \\
& + \oint_c \left(\left[N_{11} + \tilde{n}_{11} + \underline{C}\tilde{n}_{11} \left(u_{1,1} + \frac{w}{R_1} \right) - \underline{G}\tilde{n}_{12} u_{2,1} + \underline{H}\tilde{n}_{12} u_{1,2} \right] \delta u_1 \right. \\
& + \left[N_{12} + \tilde{n}_{12} + \underline{B}\tilde{n}_{11} u_{2,1} - \underline{G}\tilde{n}_{12} \left(u_{1,1} + \frac{w}{R_1} \right) + \underline{H}\tilde{n}_{12} \left(u_{2,2} + \frac{w}{R_2} \right) \right] \delta u_2 \\
& + \left[Q_1 + \tilde{q}_1 + \tilde{n}_{11} \left(w_{,1} + \frac{u_1}{R_1} \right) + \tilde{n}_{12} \left(w_{,2} + \frac{u_2}{R_2} \right) \right] \delta w \\
& \left. - [M_{11} + \tilde{m}_{11}] \delta \phi_1 - [M_{12} + \tilde{m}_{12}] \delta \phi_2 \right) d\xi_2 \\
& + \oint_c \left(\left[N_{12} + \tilde{n}_{12} + \underline{E}\tilde{n}_{22} u_{1,2} - \underline{G}\tilde{n}_{12} \left(u_{2,2} + \frac{w}{R_2} \right) + \underline{H}\tilde{n}_{12} \left(u_{1,1} + \frac{w}{R_1} \right) \right] \delta u_1 \right. \\
& + \left[N_{22} + \tilde{n}_{22} + \underline{F}\tilde{n}_{22} \left(u_{2,2} + \frac{w}{R_2} \right) - \underline{G}\tilde{n}_{12} u_{1,2} + \underline{H}\tilde{n}_{12} u_{2,1} \right] \delta u_2 \\
& + \left[Q_2 + \tilde{q}_2 + \tilde{n}_{12} \left(w_{,1} + \frac{u_1}{R_1} \right) + \tilde{n}_{22} \left(w_{,2} + \frac{u_2}{R_2} \right) \right] \delta w \\
& \left. - [M_{12} + \tilde{m}_{12}] \delta \phi_1 - [M_{22} + \tilde{m}_{22}] \delta \phi_2 \right) d\xi_1 = 0 \tag{2.8}
\end{aligned}$$

For arbitrary displacements u_1 , u_2 , w , ϕ_1 , and ϕ_2 , the coefficients of the displacements in the area integral in Eq. (2.8) are the five equilibrium equations. The coefficients of the displacement variables in the first line integral in Eq. (2.8) are the natural boundary

conditions for an edge $\xi_1 = \text{constant}$, and the coefficients of the displacement variables in the second line integral are the natural boundary conditions for an edge $\xi_2 = \text{constant}$.

2.4 Stability Equations

A set of perturbation equilibrium equations that govern the stability of the plate, referred to herein as the stability equations, may now be written by taking the difference between the equilibrium equations evaluated for an equilibrium state just prior to buckling and an adjacent (perturbed) equilibrium state just after buckling has occurred. Let the prebuckling state be represented by:

$$\begin{aligned} \tilde{n}_{11} &= -N_{11}, \quad \tilde{n}_{22} = -N_{22}, \quad \tilde{n}_{12} = -N_{12}, \quad \tilde{m}_{11} = -M_{11}, \\ \tilde{m}_{22} &= -M_{22}, \quad \tilde{m}_{12} = -M_{12}, \quad \tilde{q}_1 = -Q_1, \quad \tilde{q}_2 = -Q_2, \\ U_1, U_2, W \end{aligned} \quad (2.9)$$

The minus signs in the loading terms reflect the sign convention used in which the applied loads are opposite in direction to the loads that develop after buckling. Let the perturbed state just after buckling has occurred be represented by:

$$\begin{aligned} \tilde{n}_{11} &= n_{11} - N_{11}, \quad \tilde{n}_{22} = n_{22} - N_{22}, \quad \tilde{n}_{12} = n_{12} - N_{12}, \\ \tilde{m}_{11} &= m_{11} - M_{11}, \quad \tilde{m}_{22} = m_{22} - M_{22}, \quad \tilde{m}_{12} = m_{12} - M_{12}, \\ \tilde{q}_1 &= q_1 - Q_1, \quad \tilde{q}_2 = q_2 - Q_2, \quad u_1 + U_1, \quad u_2 + U_2, \quad w + W \end{aligned} \quad (2.10)$$

where the lower case variables are perturbation variables. Taking the difference between the two equilibrium states represented by Eqs. (2.9) and (2.10), linearizing the resulting equations for the perturbation variables, and applying the following simplifying assumptions:

- 1) Prebuckling deformations, moments, and transverse-shear stresses are negligible
- 2) The in-plane prebuckling stress state is uniform

yields the following stability equations:

$$\begin{aligned}
 & n_{11,1} + n_{12,2} + \frac{q_1}{R_1} - \frac{N_{11}}{R_1} \left(w_{,1} - \frac{u_1}{R_1} \right) - \frac{N_{12}}{R_1} \left(w_{,2} - \frac{u_2}{R_2} \right) \\
 & - \underline{C}N_{11} \left(\frac{w_{,1}}{R_1} + u_{1,11} \right) - \underline{E}N_{22} u_{1,22} + \underline{G}N_{12} \left(\frac{w_{,2}}{R_2} + u_{2,11} + u_{2,22} \right) \\
 & - \underline{H}N_{12} \left(\frac{w_{,2}}{R_1} + 2u_{1,12} \right) = 0
 \end{aligned} \tag{2.11a}$$

$$\begin{aligned}
 & n_{12,1} + n_{22,2} + \frac{q_2}{R_2} - \frac{N_{22}}{R_2} \left(w_{,2} - \frac{u_2}{R_2} \right) - \frac{N_{12}}{R_2} \left(w_{,1} - \frac{u_1}{R_1} \right) \\
 & - \underline{B}N_{11} u_{2,11} - \underline{F}N_{22} \left(\frac{w_{,2}}{R_2} + u_{2,22} \right) + \underline{G}N_{12} \left(\frac{w_{,1}}{R_1} + u_{1,11} + u_{1,22} \right) \\
 & - \underline{H}N_{12} \left(\frac{w_{,1}}{R_2} + 2u_{2,12} \right) = 0
 \end{aligned} \tag{2.11b}$$

$$\begin{aligned}
 & q_{1,1} + q_{2,2} - \frac{n_{11}}{R_1} - \frac{n_{22}}{R_2} - N_{11} \left(w_{,11} - \frac{u_{1,1}}{R_1} \right) - N_{12} \left(w_{,21} - \frac{u_{2,1}}{R_2} \right) \\
 & - N_{12} \left(w_{,12} - \frac{u_{1,2}}{R_1} \right) - N_{22} \left(w_{,22} - \frac{u_{2,2}}{R_2} \right) + \frac{\underline{C}N_{11}}{R_1} \left(\frac{w}{R_1} + u_{1,1} \right) \\
 & + \frac{\underline{F}N_{22}}{R_2} \left(\frac{w}{R_2} + u_{2,2} \right) - \underline{G}N_{12} \left(\frac{u_{2,1}}{R_1} + \frac{u_{1,2}}{R_2} \right) \\
 & + \underline{H}N_{12} \left(\frac{u_{1,2}}{R_1} + \frac{u_{2,1}}{R_2} \right) = 0
 \end{aligned} \tag{2.11c}$$

$$m_{11,1} + m_{12,2} - q_1 = 0 \tag{2.11d}$$

$$m_{12,1} + m_{22,2} - q_2 = 0 \tag{2.11e}$$

The boundary conditions for an edge $\xi_1 = \text{constant}$ are

$$\delta u_1 = 0$$

$$\text{or} \quad (2.12a)$$

$$n_{11} - \underline{C}N_{11}\left(u_{1,1} + \frac{w}{R_1}\right) + \underline{G}N_{12}u_{2,1} - \underline{H}N_{12}u_{1,2} = 0$$

$$\delta u_2 = 0$$

$$\text{or} \quad (2.12b)$$

$$n_{12} - \underline{B}N_{11}u_{2,1} + \underline{G}N_{12}\left(u_{1,1} + \frac{w}{R_1}\right) - \underline{H}N_{12}\left(u_{2,2} + \frac{w}{R_2}\right) = 0$$

$$\delta w = 0$$

$$\text{or} \quad (2.12c)$$

$$q_1 - N_{11}\left(w_{,1} + \frac{u_1}{R_1}\right) - N_{12}\left(w_{,2} + \frac{u_2}{R_2}\right) = 0$$

$$\delta \phi_1 = 0 \quad \text{or} \quad m_{11} = 0 \quad (2.12d)$$

$$\delta \phi_2 = 0 \quad \text{or} \quad m_{12} = 0 \quad (2.12e)$$

As will be discussed in Chapter III, a sinusoidal variation of displacements and forces is assumed in the ξ_1 direction. Therefore, these boundary conditions are ignored herein.

The boundary conditions for an edge $\xi_2 = \text{constant}$ are

$$\delta u_1 = 0$$

$$\text{or} \quad (2.13a)$$

$$\hat{n}_{12} = n_{12} - \underline{E}N_{22}u_{1,2} + \underline{G}N_{12}\left(u_{2,2} + \frac{w}{R_2}\right) - \underline{H}N_{12}\left(u_{1,1} + \frac{w}{R_1}\right) = 0$$

$$\delta u_2 = 0$$

$$\text{or} \quad (2.13b)$$

$$\hat{n}_{22} = n_{22} - \underline{F}N_{22}\left(u_{2,2} + \frac{w}{R_2}\right) + \underline{G}N_{12}u_{1,2} - \underline{H}N_{12}u_{2,1} = 0$$

$$\delta w = 0$$

or

$$\hat{q}_2 = q_2 - N_{12} \left(w_{,1} + \frac{u_1}{R_1} \right) - N_{22} \left(w_{,2} + \frac{u_2}{R_2} \right) = 0 \quad (2.13c)$$

$$\delta \phi_1 = 0 \quad \text{or} \quad m_{12} = 0 \quad (2.13d)$$

$$\delta \phi_2 = 0 \quad \text{or} \quad m_{22} = 0 \quad (2.13e)$$

where the terms with a caret (^) are effective force quantities per unit length at an edge $\xi_2 = \text{constant}$. The effective forces, \hat{n}_{12} , \hat{n}_{22} , and \hat{q}_2 are equal to forces in the original (undeformed) ξ_1 -, ξ_2 -, and ξ_3 -directions along the longitudinal edges of the plate ($\xi_2 = \text{constant}$). Introduction of these force quantities facilitates the derivation of the stiffness matrix in Chapter III which relates the forces along the longitudinal edges of the plate in the original coordinate directions to the corresponding displacements along those edges.

The first three stability equations given in Eqs. (2.11a) through (2.11c) are now written in a simplified form using the definitions of the effective forces per unit length given in Eqs. (2.13a) through (2.13c)

$$\begin{aligned} n_{11,1} + \hat{n}_{12,2} + \frac{q_1}{R_1} - \frac{N_{11}}{R_1} \left(w_{,1} - \frac{u_1}{R_1} \right) - \frac{N_{12}}{R_1} \left(w_{,2} - \frac{u_2}{R_2} \right) \\ - \underline{C}N_{11} \left(\frac{w_{,1}}{R_1} + u_{1,11} \right) + \underline{G}N_{12}u_{2,11} - \underline{H}N_{12}u_{1,12} = 0 \end{aligned} \quad (2.14a)$$

$$\begin{aligned} n_{12,1} + \hat{n}_{22,2} + \frac{q_2}{R_2} - \frac{N_{22}}{R_2} \left(w_{,2} - \frac{u_2}{R_2} \right) - \frac{N_{12}}{R_2} \left(w_{,1} - \frac{u_1}{R_1} \right) \\ - \underline{B}N_{11}u_{2,11} + \underline{G}N_{12} \left(\frac{w_{,1}}{R_1} + u_{1,11} \right) - \underline{H}N_{12} \left(\frac{w_{,1}}{R_2} + u_{2,12} \right) = 0 \end{aligned} \quad (2.14b)$$

$$\begin{aligned}
& q_{1,1} + \hat{q}_{2,2} - \frac{n_{11}}{R_1} - \frac{\hat{n}_{22}}{R_2} - N_{11} \left(w_{,11} - \frac{u_{1,1}}{R_1} \right) - N_{12} \left(w_{,21} - \frac{u_{2,1}}{R_2} \right) \\
& + \frac{CN_{11}}{R_1} \left(\frac{w}{R_1} + u_{1,1} \right) - \frac{GN_{12}u_{2,1}}{R_1} + \frac{HN_{12}u_{1,2}}{R_1} = 0
\end{aligned} \tag{2.14c}$$

This form of these stability equations will be used herein. Note that Eq. (2.14b) contains the perturbation variables n_{12} and q_2 . These variables are related to the effective forces, \hat{n}_{12} and \hat{q}_2 , through Eqs. (2.13a) and (2.13c).

2.5 Stability Equations Transformed to the Plate Reference Surface

The stability equations given in Eqs. (2.11a) through (2.11e) describe the response at the centroidal surface of the plate. A superscript o may be added to the displacement quantities in these equations to indicate that they are centroidal quantities. These equations are now written such that they describe the response at the reference surface of the plate, which can be located a distance z_c from the centroidal surface, Figure 2.2. To write the stability equations at the reference surface, the following information is used:

- 1) The relations of the displacements at the centroidal surface, u_1^o and u_2^o , to the displacements at the reference surface, u_1 and u_2 are:

$$u_1^o = u_1 - z_c \phi_1 \tag{2.15a}$$

$$u_2^o = u_2 - z_c \phi_2 \tag{2.15b}$$

- 2) The relations of the moments at the centroidal surface, m_{11}^o , m_{22}^o , and m_{12}^o , to the displacements at the reference surface, m_{11} , m_{22} , and m_{12} are:

$$m_{11}^o = m_{11} - z_c n_{11} \quad (2.15c)$$

$$m_{22}^o = m_{22} - z_c n_{22} \quad (2.15d)$$

$$m_{12}^o = m_{12} - z_c n_{12} \quad (2.15e)$$

3) The following quantities do not vary with z :

$$N_{11}, N_{22}, N_{12}, n_{11}, n_{22}, n_{12}, q_1, q_2, \text{ and } w$$

4) The applied in-plane stresses, N_{11} , N_{22} , and N_{12} act at the centroidal surface.

Substitution of Eqs. (2.15a) through (2.15e) into Eqs. (2.14a) through (2.14c) and Eqs. (2.11d) and (2.11e) yields the following equations

$$\begin{aligned} n_{11,1} + \hat{n}_{12,2} + \frac{q_1}{R_1} - \frac{N_{11}}{R_1} \left(w_{,1} - \frac{u_1 - z_c \phi_1}{R_1} \right) - \frac{N_{12}}{R_1} \left(w_{,2} - \frac{u_2 - z_c \phi_2}{R_2} \right) \\ - \underline{C}N_{11} \left(\frac{w}{R_1} + u_{1,1} - z_c \phi_1 \right)_{,1} + \underline{G}N_{12} [u_2 - z_c \phi_2]_{,11} \\ - \underline{H}N_{12} [u_1 - z_c \phi_1]_{,12} = 0 \end{aligned} \quad (2.16a)$$

$$\begin{aligned} n_{12,1} + \hat{n}_{22,2} + \frac{q_2}{R_2} - \frac{N_{22}}{R_2} \left(w_{,2} - \frac{u_2 - z_c \phi_2}{R_2} \right) - \frac{N_{12}}{R_2} \left(w_{,1} - \frac{u_1 - z_c \phi_1}{R_1} \right) \\ - \underline{B}N_{11} (u_2 - z_c \phi_2)_{,11} + \underline{G}N_{12} \left(\frac{w_{,1}}{R_1} + [u_1 - z_c \phi_1]_{,11} \right) \\ - \underline{H}N_{12} \left(\frac{w_{,1}}{R_2} + [u_2 - z_c \phi_2]_{,12} \right) = 0 \end{aligned} \quad (2.16b)$$

$$\begin{aligned}
& q_{1,1} + \hat{q}_{2,2} - \frac{n_{11}}{R_1} - \frac{\hat{n}_{22}}{R_2} - N_{11} \left(w_{,1} - \frac{u_1 - z_c \phi_1}{R_1} \right)_{,1} \\
& - N_{12} \left(w_{,2} - \frac{u_2 - z_c \phi_2}{R_2} \right)_{,1} + \frac{CN_{11}}{R_1} \left(\frac{w}{R_{,1}} + [u_1 - z_c \phi_1]_{,1} \right) \\
& + \frac{GN_{12}[u_2 - z_c \phi_2]_{,1}}{R_1} + \frac{HN_{12}[u_1 - z_c \phi_1]_{,2}}{R_1} = 0
\end{aligned} \tag{2.16c}$$

$$m_{11,1} + m_{12,2} - z_c (n_{11,1} + n_{12,2}) - q_1 = 0 \tag{2.16d}$$

$$m_{12,1} + m_{22,2} - z_c (n_{12,1} + n_{22,2}) - q_2 = 0 \tag{2.16e}$$

The natural boundary conditions are also rewritten after substitution of Eqs. (2.15a) through (2.15e) into Eqs. (2.13a) through (2.13e). For an edge $\xi_2 = \text{constant}$, the natural boundary conditions become

$$\begin{aligned}
\hat{n}_{12} = n_{12} - \underline{E}N_{22}[u_1 - z_c \phi_1]_{,2} + \underline{G}N_{12} \left([u_2 - z_c \phi_2]_{,2} + \frac{w}{R_2} \right) \\
- \underline{H}N_{12} \left([u_1 - z_c \phi_1]_{,1} + \frac{w}{R_1} \right) = 0
\end{aligned} \tag{2.17a}$$

$$\begin{aligned}
\hat{n}_{22} = n_{22} - \underline{F}N_{22} \left([u_2 - z_c \phi_2]_{,2} + \frac{w}{R_2} \right) + \underline{G}N_{12}[u_1 - z_c \phi_1]_{,2} \\
- \underline{H}N_{12}[u_2 - z_c \phi_2]_{,1} = 0
\end{aligned} \tag{2.17b}$$

$$\hat{q}_2 = q_2 - N_{12} \left(w_{,1} + \frac{[u_1 - z_c \phi_1]}{R_1} \right) - N_{22} \left(w_{,2} + \frac{[u_2 - z_c \phi_2]}{R_2} \right) = 0 \tag{2.17c}$$

$$m_{12} - z_c n_{12} = 0 \quad (2.17d)$$

$$m_{22} - z_c n_{22} = 0 \quad (2.17e)$$

The last two stability equations, Eqs. (2.16d) and (2.16e), are now rewritten by substituting expressions for the quantities $(n_{11,1} + n_{12,2})$ and $(n_{12,1} + n_{22,2})$ that can be obtained using Eqs. (2.16a) and (2.16b), respectively, and the definitions for the effective forces per unit length, Eqs. (2.17a) through (2.17c). The definitions for the effective forces are needed since the terms n_{12} and n_{22} that appear in the two above are the perturbation values, not the effective forces. Substitution of the expressions for the two quantities above into Eqs. (2.16d) and (2.16e), respectively, yields the final form of the last two stability equations

$$\begin{aligned} & m_{11,1} + m_{12,2} - q_1 + z_c \left[\frac{q_1}{R_1} - \frac{N_{11}}{R_1} \left(w_{,1} - \frac{u_1 - z_c \phi_1}{R_1} \right) \right. \\ & - \frac{N_{12}}{R_1} \left(w_{,2} - \frac{u_2 - z_c \phi_2}{R_2} \right) - \underline{C}N_{11} \left(\frac{w}{R_1} + u_{1,1} - z_c \phi_1 \right)_{,1} \\ & - \underline{E}N_{22} (u_1 - z_c \phi_1)_{,22} + \underline{G}N_{12} \left(\frac{w_{,2}}{R_2} + [u_2 - z_c \phi_2]_{,11} \right. \\ & \left. \left. + [u_2 - z_c \phi_2]_{,22} \right) - \underline{H}N_{12} \left(\frac{w_{,2}}{R_1} + 2[u_1 - z_c \phi_1]_{,12} \right) \right] = 0 \end{aligned} \quad (2.18a)$$

$$\begin{aligned} & m_{12,1} + m_{22,2} - q_2 + z_c \left[\frac{q_2}{R_2} - \frac{N_{22}}{R_2} \left(w_{,2} - \frac{u_2 - z_c \phi_2}{R_2} \right) \right. \\ & - \frac{N_{12}}{R_2} \left(w_{,1} - \frac{u_1 - z_c \phi_1}{R_1} \right) - \underline{B}N_{11} (u_2 - z_c \phi_2)_{,11} \\ & - \underline{F}N_{22} \left(\frac{w_{,2}}{R_2} + [u_2 - z_c \phi_2]_{,22} \right) + \underline{G}N_{12} \left(\frac{w_{,1}}{R_1} + [u_1 - z_c \phi_1]_{,11} \right. \\ & \left. \left. + [u_1 - z_c \phi_1]_{,22} \right) - \underline{H}N_{12} \left(\frac{w_{,1}}{R_2} + 2[u_2 - z_c \phi_2]_{,12} \right) \right] = 0 \end{aligned} \quad (2.18b)$$

The stability equations in the form given in Eqs. (2.16a) through (2.16c) and Eqs. (2.18a) and (2.18b) are those implemented into the VICONOPT code.

2.6 Constitutive Relations

The present analysis allows for generally laminated composite materials. The geometry of a general, curved laminate is given in Figure 2.3. As shown in the figure, the number of layers in the laminate is n , and the width of the laminate is b . The radius of curvature of the ξ_2 -axis, R_2 is shown in the figure as well. . The radius of curvature of the ξ_1 -axis, R_1 is not shown; however, its direction may be inferred from that of R_2 . The lamina coordinate system is the (ξ_1, ξ_2, ξ_3) system and the laminate coordinate system is the (ξ_1, ξ_2, ξ_3) system. The lamina coordinate system is aligned with the principal material direction of the lamina, and the laminate coordinate system is aligned with the principal geometric directions of the laminate. The coordinate system for the k th lamina is oriented at an angle θ_k with respect to the laminate coordinate system. The stress-strain relations in the lamina coordinate system for a lamina of orthotropic material in a state of plane stress are

$$\begin{Bmatrix} \sigma_{11}' \\ \sigma_{22}' \\ \tau_{12}' \end{Bmatrix} = \begin{bmatrix} Q_{11} & Q_{12} & 0 \\ Q_{12} & Q_{22} & 0 \\ 0 & 0 & Q_{66} \end{bmatrix} \begin{Bmatrix} \varepsilon_{11}' \\ \varepsilon_{22}' \\ \gamma_{12}' \end{Bmatrix} \quad (2.19)$$

where the $[Q]$ matrix is referred to as the reduced stiffness matrix for the lamina and is defined in [45] in terms of the elastic engineering constants of the lamina. These relations may be written in the laminate coordinate system by use of transformation matrices as defined in [45]. The transformed relations are

$$\begin{Bmatrix} \sigma_{11} \\ \sigma_{22} \\ \tau_{12} \end{Bmatrix} = \begin{bmatrix} \bar{Q}_{11} & \bar{Q}_{12} & \bar{Q}_{16} \\ \bar{Q}_{12} & \bar{Q}_{22} & \bar{Q}_{26} \\ \bar{Q}_{16} & \bar{Q}_{26} & \bar{Q}_{66} \end{bmatrix} \begin{Bmatrix} \varepsilon_{11} \\ \varepsilon_{22} \\ \gamma_{12} \end{Bmatrix} \quad (2.20)$$

where the $[\bar{Q}]$ matrix is the reduced transformed stiffness matrix for the lamina. Both of Eqs. (2.19) and (2.20) may be thought of as stress-strain relations for the k th lamina in a multi-layer laminate. Therefore, Eq. (2.20) may be written as

$$\{\sigma\}_k = [\bar{Q}]_k \{\varepsilon\}_k \quad (2.21)$$

The constitutive relations for a thin, elastic laminated composite shell may now be defined as

$$\begin{Bmatrix} N_{11} \\ N_{22} \\ N_{12} \\ M_{11} \\ M_{22} \\ M_{12} \end{Bmatrix} = \begin{bmatrix} A_{11} & A_{12} & A_{16} & B_{11} & B_{12} & B_{16} \\ A_{12} & A_{22} & A_{26} & B_{12} & B_{22} & B_{26} \\ A_{16} & A_{26} & A_{66} & B_{16} & B_{26} & B_{66} \\ B_{11} & B_{12} & B_{16} & D_{11} & D_{12} & D_{16} \\ B_{12} & B_{22} & B_{26} & D_{12} & D_{22} & D_{26} \\ B_{16} & B_{26} & B_{66} & D_{16} & D_{26} & D_{66} \end{bmatrix} \begin{Bmatrix} \varepsilon_{11} \\ \varepsilon_{22} \\ \gamma_{12} \\ \kappa_{11} \\ \kappa_{22} \\ \kappa_{12} \end{Bmatrix} \quad (2.22)$$

where the resultant forces and moments acting on the laminate, $\{N\}$ and $\{M\}$, respectively, are defined as

$$\begin{Bmatrix} N_{11} \\ N_{22} \\ N_{12} \end{Bmatrix} = \sum_{k=1}^{n_l} \int_{z_{k-1}}^{z_k} \begin{Bmatrix} \sigma_{11} \\ \sigma_{22} \\ \tau_{12} \end{Bmatrix} d\xi_3 \quad (2.23)$$

$$\begin{Bmatrix} M_{11} \\ M_{22} \\ M_{12} \end{Bmatrix} = \sum_{k=1}^{n_l} \int_{z_{k-1}}^{z_k} \begin{Bmatrix} \sigma_{11} \\ \sigma_{22} \\ \tau_{12} \end{Bmatrix} \xi_3 d\xi_3 \quad (2.24)$$

where n_l is the total number of layers in the laminate. The extensional, coupling, and bending stiffness matrices, \mathbf{A} , \mathbf{B} , and \mathbf{D} , respectively, are defined as

$$(\mathbf{A}, \mathbf{B}, \mathbf{D}) = \sum_{k=1}^{n_l} \int_{z_{k-1}}^{z_k} [\bar{\mathbf{Q}}]_k (1, \xi_3, \xi_3^2) d\xi_3 \quad (2.25)$$

The analysis in VICONOPT allows for laminates with fully populated \mathbf{A} , \mathbf{B} , and \mathbf{D} matrices.

The constitutive relations for transverse shear used in VICONOPT are those presented by Cohen in [44]. The constitutive relations for transverse shear are written in inverted form as

$$\begin{Bmatrix} \gamma_{13} \\ \gamma_{23} \end{Bmatrix} = \begin{bmatrix} k_{11} & k_{12} \\ k_{12} & k_{22} \end{bmatrix} \begin{Bmatrix} q_1 \\ q_2 \end{Bmatrix} \quad (2.26)$$

where $[\mathbf{k}]$ is a symmetric 2-by-2 transverse shear compliance matrix whose terms are defined in [44]. The terms of the $[\mathbf{k}]$ matrix were derived for general, anisotropic, multi-layered composite shells and they are a generalization of results for a shell with a homogeneous wall for which the transverse shear correction factor for the shear stiffness is 5/6. The procedure used in [44] for obtaining the terms of the $[\mathbf{k}]$ matrix follows. Statically correct expressions of in-plane stresses and transverse-shear stresses were derived in terms of the transverse-shear stress resultants and arbitrary constants that were interpreted by Cohen as redundant “forces”. The expressions for in-plane stresses were obtained using the constitutive relations given in Eq. (2.22) and linear distribution of in-plane strains through the wall thickness. The expressions of transverse-shear stresses were obtained by integrating in the ξ_3 -direction the three-dimensional equilibrium equations. The transverse-shear stress resultants were then used to derive an expression

of the volumetric density of the transverse-shear strain energy. A statically correct expression of the area density of the transverse-shear strain energy was then obtained by integrating in the ξ_3 -direction this volumetric density. The transverse-shear constitutive relations given in Eq. (2.26) were then derived by applying Castigliano's theorem of least work [46] by minimizing the area density of the transverse-shear strain energy with respect to the redundant forces mentioned previously.

CHAPTER III

IMPLEMENTATION INTO VICONOPT

In this chapter, the implementation of the present theory into the VICONOPT code is described. Additional simplifications made to the theory are described first. A discussion of the use of the transverse-shear strain, γ_{13} , as a fundamental displacement variable in the problem to maintain continuity of rotations at plate junctions is then presented. The derivation of an expression for the curved-plate stiffness matrix is described. The terms of matrices that are needed to calculate this stiffness matrix were obtained using MATHEMATICA [40], and they are presented in Appendix A. The terms for both CPT and SDPT are presented, and the terms that result from the inclusion of direct in-plane transverse and in-plane shear loads in the in-plane stability equations are specified. As stated previously, the implementation of the curved-plate theory into VICONOPT follows very closely the method presented in Reference [2]. Therefore, the following discussion is necessarily similar to that presented in that reference.

3.1 Simplifications to the Theory

Before proceeding with the derivation of the curved-plate stiffness matrix, a discussion of several simplifications to be implemented is presented. First, the theory implemented into the VICONOPT code considers structures that are prismatic in the longitudinal direction. Therefore, for the curved plates being considered in the present thesis, the radius of curvature in the longitudinal direction, R_1 , is infinite; and any terms involving the quantity $\frac{1}{R_1}$ are zero. Although these terms are set equal to zero for the calculation of the terms of the stiffness matrix, they are retained for completeness in the

theory presented in this chapter. Another simplification to the theory involves limiting the capability to locate the reference surface a distance z_c from the centroidal surface. This capability has only been implemented for the case where the effects of N_{22} and N_{12} loads in the in-plane stability equations are neglected. The expressions for the stiffness terms that result when N_{22} and N_{12} are included in the in-plane stability equations **and** z_c is non-zero are prohibitively long. Therefore, in the derivation to follow, only the following two cases are presented:

- 1) N_{22} and N_{12} are included in the in-plane stability equations and z_c is zero (i.e., reference surface is coincident with the centroidal surface); and ,
- 2) N_{22} and N_{12} are neglected in the in-plane stability equations and z_c is non-zero (i.e., reference surface may be translated from the centroidal surface).

3.2 Continuity of Rotations at a Plate Junction

One important issue to be addressed in the analysis of plate assemblies is the continuity of rotations at a plate junction. The original VIPASA code is based upon CPT, and the theory only treats four degrees of freedom (DOF) at a longitudinal plate edge. These DOF are the three displacement quantities, u_1 , u_2 , and w , and a rotation about the ξ_1 -axis, ϕ_2 . Maintaining continuity of these DOF at a typical plate junction is very straightforward. However, when SDPT is considered, there are five DOF at a longitudinal plate edge. These DOF are the four from CPT as well as an additional rotation, ϕ_1 , that results from the inclusion of transverse-shear deformation. Another problem that must be addressed is that when two plates are joined together such that one is rotated at an arbitrary angle, θ , to the other, rotations about the normals to the centroidal surfaces of the two plates must be included to satisfy continuity of rotations. This rotation, ϕ_n , is not accounted for in the present plate theory. The procedure used in

VICONOPT to maintain continuity of rotations follows that used by Cohen in [47]. This procedure introduces the shear strain, γ_{13} , as a fundamental displacement variable instead of the rotation, ϕ_1 . The justification for using this approach is described subsequently.

The displacements and rotations at a typical plate junction are shown in Figure 3.1. The two plates, numbered 1 and 2, are shown viewed along the 1-axis, and it is obvious that the u_1 displacements are easily matched regardless of the orientation of plate 2. The displacements and rotations for which continuity must be maintained are u_2 , w , ϕ_1 , and ϕ_n . Upon inspection of Figure 3.1(a), the following expressions for coplanar plates ($\theta = 0$) may be written as

$$u_2^1 = u_2^2 \quad (3.1a)$$

$$w^1 = w^2 \quad (3.1b)$$

$$\phi_1^1 = \phi_1^2 \quad (3.1c)$$

$$\phi_n^1 = \phi_n^2 \quad (3.1d)$$

where the superscripts 1 and 2 refer to the plate numbers. Similarly, upon inspection of Figure 3.1(b), the following expressions for $\theta = +90^\circ$ may be written as

$$u_2^1 = w^2 \quad (3.2a)$$

$$w^1 = -u_2^2 \quad (3.2b)$$

$$\phi_1^1 = -\phi_n^2 \quad (3.2c)$$

$$\phi_n^1 = \phi_1^2 \quad (3.2d)$$

Finally, upon inspection of Figure 3.1(c), the following expressions for arbitrary θ may be written as

$$u_2^1 = u_2^2 \cos \theta + w^2 \sin \theta \quad (3.3a)$$

$$w^1 = w^2 \cos \theta - u_2^2 \sin \theta \quad (3.3b)$$

$$\phi_1^1 = \phi_1^2 \cos \theta - \phi_n^2 \sin \theta \quad (3.3c)$$

$$\phi_n^1 = \phi_n^2 \cos \theta + \phi_1^2 \sin \theta \quad (3.3d)$$

The rotation about the normal of a line element originally directed along the ξ_1 -axis is shown in [48] to be

$$\phi_n = \frac{\partial u_2}{\partial \xi_1} \quad (3.4)$$

Using this definition, Eqs. (3.3c) and (3.3d) are written as

$$\phi_1^1 = \phi_1^2 \cos \theta - u_{2,1}^2 \sin \theta \quad (3.5a)$$

$$u_{2,1}^1 = u_{2,1}^2 \cos \theta + \phi_1^2 \sin \theta \quad (3.5b)$$

Using Eqs. (3.3a) and (3.3b) and the definition for γ_{13} , Eq. (2.2d), the previous two equations may be written as

$$\gamma_{13}^1 = \cos \theta \gamma_{13}^2 \quad (3.6a)$$

$$0 = -\sin \theta \gamma_{13}^2 \quad (3.6b)$$

The results shown in Eqs. (3.6a) and (3.6b) indicate that for plates that are not coplanar (i.e., one plate oriented at an arbitrary angle, θ , to the other), the shear strain, γ_{13} , must be set equal to zero for each plate to maintain continuity of rotations. Therefore, if γ_{13} is made a fundamental displacement quantity instead of ϕ_1 , the shear strain can be set equal to zero by simply striking out the appropriate rows and columns in the overall stiffness matrix. Performing this operation reduces the stiffness matrix to the same size as that for CPT. The VICONOPT code utilizes this procedure for plates that are not coplanar. For plates that are coplanar, i.e., $\theta = 0$, the shear strain in plate 1 is equal to that in plate 2. The VICONOPT code handles this situation by creating a substructure using the two plates with all DOF present and eliminating the extra DOF before assembly into the final stiffness matrix.

The use of the shear strain, γ_{13} , as a fundamental displacement quantity requires that the effective transverse-shear force per unit length, \hat{q}_2 , be modified. The modified expression for \hat{q}_2 is obtained from the natural boundary conditions for an edge $\xi_2 = \text{constant}$, that are derived from the virtual work expression, Eq. (2.8), when γ_{13} is used as a fundamental displacement variable. The modified expression is obtained by replacing ϕ_1 with the expression $w_{,1} - \frac{u_1}{R_1} - \gamma_{13}$ in the boundary integral over ξ_2 in Eq. (2.8). Performing this substitution, integrating by parts, and following the procedure outlined in Section 2.6 yields the following modified definition for \hat{q}_2 :

$$\hat{q}_2 = q_2 - N_{12} \left(w_{,1} - \frac{[u_1 - z_c \phi_1]}{R_1} \right) - N_{22} \left(w_{,2} - \frac{[u_2 - z_c \phi_2]}{R_2} \right) + [m_{12} - z_c n_{12}]_{,1} \quad (3.7)$$

The definition for \hat{q}_2 given in Eq. (3.7) replaces that given in Eq. (2.17c). Note that the term $m_{12,1}$ which appears in the Kirchhoff shear term of CPT is also present for the case of SDPT when γ_{13} is used as a fundamental displacement quantity.

3.3 Derivation of the Curved-Plate Stiffness Matrix

Throughout this section, reference is made to force quantities. Although these quantities are forces and moments per unit length, they are designated forces herein for convenience. The first step in implementing the present theory into VICONOPT is to derive a stiffness matrix that relates the force quantities along the two longitudinal edges, $\xi_2 = \pm \frac{b}{2}$, to the displacements along those edges. The desired force and displacement quantities are in the direction of the original (undeformed) coordinates. The displacement variables are

$$\mathbf{d} = \begin{Bmatrix} i & u_1 \\ & u_2 \\ & w \\ & \phi_2 \\ i & \gamma_{13} \end{Bmatrix} \quad (3.8)$$

where the shear strain, γ_{13} , has been introduced as a fundamental displacement quantity instead of the rotation, ϕ_1 . The force variables that correspond to the displacement variables given in Eq. (3.8) are

$$\mathbf{f} = \begin{Bmatrix} i & \hat{n}_{12} \\ & \hat{n}_{22} \\ & \hat{q}_2 \\ & m_{22} \\ i & m_{12} \end{Bmatrix} \quad (3.9)$$

Note that the effective forces at the boundaries, defined by Eqs. (2.17a) and (2.17b) and Eq. (3.7), are being used as the force quantities since, as discussed in Chapter II, they are equal to the forces in the direction of the original (undeformed) coordinates.

The problem may now be reduced to ordinary differential equations in y by assuming that the response of the plate in the longitudinal ξ_1 -direction varies sinusoidally. Therefore, if the displacements and forces in the plate are now considered to be functions of ξ_2 , the variables of Eqs. (3.8) and (3.9) may be written as

$$\mathbf{Z}(\xi_1, \xi_2) = \exp\left(\frac{i \pi \xi_1}{\lambda}\right) \mathbf{z}(\xi_2) \quad (3.10)$$

where

$$\mathbf{z} = \begin{Bmatrix} \mathbf{d} \\ \mathbf{f} \end{Bmatrix}$$

and λ is the half-wavelength of the response in the ξ_1 -direction. Since a sinusoidal variation in the ξ_1 -direction is assumed, the vector \mathbf{z} will involve the amplitudes of the displacement and force quantities. The imaginary number, i , has been used in Eqs. (3.8) and (3.9) to account for the spatial phase shift that occurs between the perturbation forces and displacements which occur at the edges of the plates during buckling for orthotropic plates without shear loading and to result in real plate stiffnesses when using the exponential expression of Eq. (3.10).

The next step in the derivation is to express all unknowns in terms of \mathbf{z} . A partially inverted form of the constitutive relations, Eq. (2.22), is used to express the required quantities as functions of the fundamental variables in \mathbf{d} and \mathbf{f} or terms that may be derived from the fundamental variables. The partially inverted constitutive relations are

$$\begin{Bmatrix} n_{11} \\ \varepsilon_{22} \\ \varepsilon_{12} \\ m_{11} \\ \kappa_{22} \\ \kappa_{12} \end{Bmatrix} = \left[\begin{array}{ccc|ccc} h_{11} & h_{12} & h_{13} & h_{14} & h_{15} & h_{16} \\ -h_{12} & h_{22} & h_{23} & h_{24} & h_{25} & h_{26} \\ -h_{13} & h_{23} & h_{33} & h_{34} & h_{35} & h_{36} \\ \hline h_{14} & -h_{24} & -h_{34} & h_{44} & h_{45} & h_{46} \\ -h_{15} & h_{25} & h_{35} & -h_{45} & h_{55} & h_{56} \\ -h_{16} & h_{26} & h_{36} & -h_{46} & h_{56} & h_{66} \end{array} \right] \begin{Bmatrix} \varepsilon_{11} \\ n_{22} \\ n_{12} \\ \kappa_{11} \\ m_{22} \\ m_{12} \end{Bmatrix} \quad (3.11)$$

$$\begin{Bmatrix} q_1 \\ \gamma_2 \end{Bmatrix} = \begin{bmatrix} h_{77} & h_{78} \\ -h_{78} & h_{88} \end{bmatrix} \begin{Bmatrix} \gamma_1 \\ q_2 \end{Bmatrix}$$

where the linear portion of ε_{11} from Eq. (2.2a) is used

$$\varepsilon_{11} = u_{1,1} + \frac{w}{R_1}$$

The variables κ_{11} and ϕ_1 were defined in Section 2.2 of Chapter II. The constants h_{ij} in the first portion of Eq. (3.11) are calculated from the **A**, **B**, and **D** matrices defined in Eq. (2.25). The constants h_{77} , h_{78} , and h_{88} are shear stiffness terms and are calculated using the theory presented in [44].

Another requirement of the present derivation is to express the relationship between q_2 and \hat{q}_2 without any ξ_2 -derivatives. This expression is

$$q_2 = \frac{\hat{q}_2 + N_{12} \left(w_{,1} - \frac{[u_1 - z_c \phi_1]}{R_1} \right) + N_{22} (\phi_2 - h_{78} \gamma_1) + [m_{12} - z_c n_{12}]_{,1}}{1 - N_{22} h_{88}} \quad (3.12)$$

As with the stability equations, only the linear portion of the strain-displacement relations are considered in the present derivation

$$\gamma_{12} = u_{1,2} + u_{2,1} \quad (3.13a)$$

$$\varepsilon_{22} = u_{2,2} + \frac{w}{R_2} \quad (3.13b)$$

$$\gamma_{23} = w_{,2} - \frac{u_2}{R_2} - \phi_2 \quad (3.13c)$$

$$\kappa_{22} = -\phi_{2,2} \quad (3.13d)$$

$$\kappa_{12} = -(\phi_{1,2} + \phi_{2,1}) \quad (3.13e)$$

The expression for κ_{12} can be re-written after substituting expressions obtained for ϕ_1 and ϕ_2 from Eqs. (2.5a) and (2.5b) and using the linear portion of ε_{12}

$$\kappa_{12} = -\left[\gamma_2 + \left(\frac{1}{R_1} + \frac{1}{R_2} \right) u_2 + 2\phi_2 \right]_{,1} + \frac{\varepsilon_{12}}{R_1} + \gamma_{1,2} \quad (3.13f)$$

Using Eqs. (3.11) and (3.12), the strain displacement equations, Eqs. (3.13a) through (3.13d) and (3.13f) and the equations, Eqs. (2.16a) through (2.16c) and (2.18a) and (2.18b) are written in terms of the elements of \mathbf{z} as

$$\mathbf{T} \mathbf{z}' = \mathbf{P} \mathbf{z} \quad \text{or} \quad \mathbf{z}' = \mathbf{T}^{-1} \mathbf{P} \mathbf{z} \quad (3.14)$$

where a prime denotes differentiation with respect to ξ_2 . The square matrix \mathbf{T} appears in the present study as a result of the inclusion of the effects of N_{22} and N_{12} in the in-plane equilibrium equations. This matrix was shown to be the identity matrix when these terms were neglected in [2]. The presence of off-diagonal terms in this matrix is a fundamental difference between the present theory and that presented in [2].

The elements of \mathbf{z} are now assumed to be given by

$$z_j = c_j \exp\left(\frac{i \beta \xi_2}{b}\right) \quad (3.15)$$

where β is a characteristic root of the differential equation. The number of values of β is equal to the order of the differential equation system. Substitution of Eq. (3.15) into Eq. (3.14) results in the following equation

$$(\mathbf{R} - \beta \mathbf{I}) \mathbf{c} = 0 \quad (3.16a)$$

where

$$\mathbf{R} = b\mathbf{T}^{-1}\mathbf{P} \quad (3.16b)$$

and \mathbf{I} is the identity matrix. The vector \mathbf{c} consists of the c_j of Eq. (3.15). The matrix \mathbf{R} is obtained by premultiplying \mathbf{P} by \mathbf{T}^{-1} . The eigenvalues of the matrix \mathbf{R} are the characteristic roots of the differential equation. This matrix is not symmetric; however, it can be made real by multiplication or division of appropriate rows and columns by the imaginary number, i . The elements of the matrices \mathbf{T} and \mathbf{P} are given in Appendix A for both SDPT and CPT.

For each eigenvalue of \mathbf{R} , there exists an eigenvector, \mathbf{c} . A matrix \mathbf{C} may be defined with columns as the eigenvectors, \mathbf{c} , the upper half of each column, denoted \mathbf{a} , will be associated with displacements, and the lower half, denoted \mathbf{b} , will be associated with forces. The form of \mathbf{C} is therefore

$$\mathbf{C} = \begin{bmatrix} \mathbf{a}_1 & \mathbf{a}_2 & \cdot & \cdot & \cdot & \mathbf{a}_j \\ \mathbf{b}_1 & \mathbf{b}_2 & \cdot & \cdot & \cdot & \mathbf{b}_j \end{bmatrix} \quad (3.17)$$

The next step in the derivation is to write the amplitudes of the displacements and forces at the two edges of the plate. Quantities evaluated at $\xi_2 = -\frac{b}{2}$ are identified with a

superscript 1 and quantities evaluated at $\xi_2 = +\frac{b}{2}$ are identified with a superscript 2 as follows:

$$d_j^1 = \sum_{k=1}^N a_{jk} r_k \exp\left(\frac{-i \beta_k}{2}\right) \quad (3.18a)$$

$$d_j^2 = \sum_{k=1}^N a_{jk} r_k \exp\left(\frac{i \beta_k}{2}\right) \quad (3.18b)$$

$$f_j^1 = \sum_{k=1}^N b_{jk} r_k \exp\left(\frac{-i \beta_k}{2}\right) \quad (3.18c)$$

$$f_j^2 = \sum_{k=1}^N b_{jk} r_k \exp\left(\frac{i \beta_k}{2}\right) \quad (3.18d)$$

where the r_k are constants determined from the edge values and N is the order of the differential equation. Equations (3.18a)-(3.18d) may be written in matrix form as

$$\begin{Bmatrix} \mathbf{d}^1 \\ \mathbf{d}^2 \end{Bmatrix} = \mathbf{E} \mathbf{r} \quad (3.19)$$

$$\begin{Bmatrix} \mathbf{f}^1 \\ \mathbf{f}^2 \end{Bmatrix} = \mathbf{F} \mathbf{r} \quad (3.20)$$

Eliminating \mathbf{r} from Eqs. (3.19) and (3.20) yields

$$\begin{Bmatrix} \mathbf{f}^1 \\ \mathbf{f}^2 \end{Bmatrix} = \mathbf{K} \begin{Bmatrix} \mathbf{d}^1 \\ \mathbf{d}^2 \end{Bmatrix} \quad (3.21)$$

where \mathbf{K} is the stiffness matrix given by

$$\mathbf{K} = \mathbf{F} \mathbf{E}^{-1} \quad (3.22)$$

As for the case of CPT, \mathbf{K} is real and symmetric for orthotropic plates without in-plane shear loading, and it is Hermitian otherwise. Reference [2] presents a discussion of

techniques used to ensure that accurate numerical results for \mathbf{K} are obtained from Eq. (3.22).

3.4 The Wittrick-Williams Eigenvalue Algorithm

A brief discussion of the analysis procedure used in VICONOPT is in order. As previously mentioned, VICONOPT uses a specialized algorithm for determining any natural frequency or buckling load for any given wavelength [29]. The development of this algorithm was necessary because the complex stiffnesses defined in the previous section are transcendental functions of the load factor and half wavelength of the buckling modes of the structure. The eigenvalue problem for determining natural frequencies and buckling load factors is therefore transcendental.

The iterative analysis procedure used in VICONOPT is described in [36]. For this procedure, the plate stiffnesses for a given wavelength are evaluated at a series of trial values of the eigenvalue being determined until convergence is attained. This eigenvalue is either the load factor for buckling or the natural frequency for vibration, and it is different than the eigenvalues of the \mathbf{R} matrix of Eq. (3.16b). Unless otherwise specified by the user, the default initial trial value used in the VICONOPT code is one. For each trial value of the eigenvalue considered, the analysis requires the plate stiffnesses as well as the number of eigenvalues that lie below the trial value for the entire plate assembly assuming the longitudinal edges of each individual to be clamped. A complete description of the eigenvalue algorithm is given in [28]. Determining the number of eigenvalues exceeded by a plate with clamped edges is very difficult except for very specialized cases. Therefore, the procedure developed in [28] is used. This procedure subdivides each plate into sub-elements with a small enough width such that none of the eigenvalues of the sub-elements with clamped edges lie below the trial value. A sub-elements is then used as a substructure and is repeatedly doubled until the original plate element is obtained. Using a simple procedure at each doubling step [29], the number of

eigenvalues that lie below the trial value for the complete plate is returned. This procedure is repeated for each plate in the assembly. Using this information and other information obtained from the stiffness matrix of the entire assembly, the total number of eigenvalues for the entire plate assembly that lie below the trial value is obtained. An iterative procedure is then used to refine the trial value until the desired eigenvalue is calculated to within the accuracy required.

One important piece of information required for the analysis procedure described herein is the number of subdivisions required for each plate. As seen in Appendix A, all of the terms of the \mathbf{R} matrix are proportional to the plate width, b . Therefore, all of the eigenvalues of \mathbf{R} are proportional to b . Furthermore, it is important to note that an eigenvalue equal to π corresponds to buckling or vibration with simply supported longitudinal edges. By successively halving the value for b until all the real eigenvalues of \mathbf{R} are less than π , a value for the width of the sub-elements for which no eigenvalues lie below the eigenvalue for simply supported edges is determined. This width also guarantees that no eigenvalues for the sub-elements lie below the eigenvalue for clamped edges. This width is that used in the iterative analysis procedure described previously.

CHAPTER IV

NUMERICAL RESULTS

In this chapter, numerical results are presented using the newly implemented curved-plate analysis capability in VICONOPT. Results from several example problems are presented to verify the results obtained with this new capability. A convergence study using the segmented-plate approach in VICONOPT is performed for an isotropic cylindrical shell subjected to uniaxial compression to identify a suitable number of segments to be used when comparing results. Results comparing the computational effort required by the new analysis to that of the analysis currently in the VICONOPT program are also presented for this example. Comparisons of results for several curved plates analyzed in Ref. [32] are then made. The effects of including terms related to in-plane transverse loads in the in-plane stability equations are examined using a long cylindrical tube subjected to in-plane transverse loading. Finally, the curved-plate analysis is used to conduct a design-optimization study of a honeycomb-sandwich cylindrical shell subjected to uniaxial compression. Comparisons of analyses using both physical and tensorial strain measures are made for selected examples, and, where appropriate, results using CPT and SDPT are compared.

4.1 Convergence of the Segmented-Plate Approach

The convergence of results using the segmented-plate approach in VICONOPT is examined for the case of an aluminum cylindrical shell subjected to uniaxial compression, see Figure 4.1. The values of the material properties used for this example are $E = 10.0 \times 10^6$ psi and $\nu_{12} = 0.33$. The wall thickness, t , is 0.1 in., and the radius, R_2 is 60 in. As shown in Reference [49], the critical value for the stress resultant, N_{11cr} , for the axisymmetric buckling of a long isotropic cylindrical shell is

$$N_{11cr} = \frac{Et^2}{R_2 \sqrt{3(1-\nu_{12}^2)}} = 1019.354 \text{ lb/in.} \quad (4.1)$$

For $\nu_{12} = 0.33$, the critical half wavelength, λ_{cr} , for axisymmetric buckling is shown in [49] to be

$$\lambda_{cr} = \pi \sqrt[4]{\frac{R_2^2 t^2}{12(1-\nu_{12}^2)}} = 1.74 \sqrt{R_2 t} = 4.255 \text{ in.} \quad (4.2)$$

Results illustrating the convergence of the VICONOPT segmented-plate results for N_{11cr} as a function of the number of segments used to approximate the cylinder are shown in Figure 4.2. In this figure, the results of the segmented-plate analysis are shown as the solid curve. The theoretical value obtained from Reference [49] is shown as the dashed horizontal line. The value obtained using the present curved-plate analysis with two curved-plate elements is shown as the open symbol. All results in this figure are calculated for the value of λ_{cr} given in Eq. (4.2). The VICONOPT results presented in this figure are obtained using CPT with tensorial strain measures. As shown in Figure 4.2, the segmented-plate results converge to the theoretical value when 120 segments are used. Therefore, to ensure that converged results are obtained when the segmented-plate approach is used to analyze the remaining example problems, sixty segments will be used when analyzing curved plates with an included angle of 180 degrees or less, and 120 segments will be used when analyzing full cylinders.

This example problem is also used to study the computational requirements of the new curved-plate analysis in relation to the segmented-plate approach. A plot of normalized CPU time as a function of the number of plate segments used in the approximation is shown in Figure 4.3 for the segmented-plate analysis using either CPT or SDPT. The normalized CPU time shown in this figure is the CPU time required for

the segmented-plate analyses normalized with respect to the CPU time required for the curved-plate analysis using two curved-plate elements. The horizontal dashed line is at a normalized CPU time of 1.0, and it represents the curved-plate analysis results. As shown in the figure, to achieve convergence with 120 flat-plate segments requires approximately 3.5 times and 16.7 times as much CPU time as the curved-plate analysis for CPT and SDPT, respectively. (For the analysis using SDPT, $G_{12} = G_{13} = G_{23}$). One consideration to note at this time is that the segmented-plate analysis in VICONOPT is implemented to handle the general case of variable geometry, stiffness and loading in the ξ_2 -direction. This approach is therefore not as computationally efficient as it could be for the case of constant curvature, stiffness, and loading in that direction (as is the case for the curved-plate analysis). One approach to determining the additional computational efficiency that may be obtained with the segmented-plate analysis involves defining a single, small flat plate that is repeatedly doubled using the substructuring capability in VICONOPT until the curved-plate segment is obtained. This technique is referred to herein as ‘doubling’. Results relating the computational effort of this approach to the curved-plate analysis indicate that further reduction in the computational effort required for the segmented-plate analysis can be obtained using this technique. This result occurs because the in-plane and out-plane equations are uncoupled in the segmented-plate analysis, and analytical expressions for the plate stiffnesses can be used. However, this approach is currently not automated in the VICONOPT code, and a separate ‘doubling’ effort would have to be made for every curved-plate segment in any given analytical model.

4.2 Buckling of Curved Plates With Widely Varying Curvatures

The example problems presented in the next two sections are taken from Ref. [32], and they are used to verify the results obtained using the new curved-plate analysis in VICONOPT. The positive sense of the applied in-plane loadings to be considered in all

of the following examples is given in Figure 4.4. The first example problem considered studies the buckling of a symmetrically laminated curved plate with clamped longitudinal edges as a function of the curvature of the plate. The geometry of the plate is shown in Figure 4.5. As shown in the figure, the plate is constructed from symmetrically laminated boron/epoxy plies with a $[0/90/\pm 45]_s$ layup. To allow for direct comparison of results with those presented in [32], the SI units are used for this example and the example in the following section. The material properties for a boron/epoxy ply are given in Table 1.

The following loadings are considered for this example problem: N_{11} only, N_{22} only, N_{12} only, and combined $N_{11} = N_{22} = N_{12}$. The buckling of this plate subject to these four different loadings was investigated while varying the value of the curvature parameter, $\frac{b^2}{R_2 t}$, from 1 to 1000. The values of b , R_2 , and β used for these analyses are summarized

in Table 2. Both physical and tensorial strains are used with the new curved-plate analysis, while physical strains only are used for the segmented-plate analysis. The analysis of [32] uses physical strains. All analysis results presented in this section are for CPT. The terms involving N_{22} and N_{12} are included in the in-plane stability equations for all analyses. The results of this study are presented in Table 3 for N_{11} loading, in Table 4 for N_{22} loading, in Table 5 for N_{12} loading, and in Table 6 for combined $N_{11} = N_{22} = N_{12}$ loading. The critical values of the stress resultants presented in these tables were calculated using for the values of $\frac{\lambda}{b}$ given in the tables. These values of $\frac{\lambda}{b}$ were presented in Reference [32]. The critical values of these stress resultants are also plotted as a function of the curvature parameter in Figure 4.6 through Figure 4.9, respectively. As shown in these tables, the present analysis compares very well with that presented in [32] and with the segmented-plate analysis for widely varying values of the curvature

parameter. As shown in Tables 3-6, there is no appreciable difference in the results obtained using physical and tensorial strains.

4.3 Buckling of an Unsymmetrically Laminated Curved Plate

This example problem includes the effect of bending-stretching coupling and shear-extension coupling on the buckling of an unsymmetrically laminated curved plate with simply supported longitudinal edges. The geometry of the curved plate is shown in Figure 4.10. As shown in the figure, the laminate being studied consists of a 0.0508-cm.-thick layer of 2024 aluminum that is reinforced on the inner surface with pairs of $\pm 45^\circ$ boron/epoxy plies. The material properties for 2024 aluminum are given in Table 1. For this example, the number of pairs of $\pm 45^\circ$ boron/epoxy plies is increased from one to seven. The analyses used for this example are identical to those used for the previous example. The critical values for buckling of the stress resultants N_{11} and N_{12} are presented in Tables 7 and 8, respectively. These values are also plotted as a function of the number of boron/epoxy plies used in the laminate in Figure 4.11 and Figure 4.12, respectively. The agreement between all the analyses is very good. As with the previous example, there is no appreciable difference in the results obtained using physical and tensorial strains. Results were also computed using SDPT. However, for the case of seven pairs of pairs of $\pm 45^\circ$ boron/epoxy plies, the R/t ratio is still approximately 300, and the effects of transverse-shear deformation are minimal. Therefore, as expected, the critical values for buckling of the stress resultants N_{11} and N_{12} were slightly less than those for CPT, but the differences were less than 0.2 percent. With regards to the CPU time requirements for this example, the segmented-plate analysis using SDPT required approximately 35 times as much CPU time as the curved-plate analysis for the case of 14 boron/epoxy plies. Furthermore, the results obtained using the 'doubling' approach described in Section 4.1 indicate that the computational efficiencies offered by that approach were not realized for this example problem. This result occurs because the

coupling that occurs due to the unsymmetric laminate prevents the in-plane and out-of-plane equations from being uncoupled, and the same numerical approach for calculating the plate stiffnesses as that used for the curved-plate analysis must be used.

4.4 Effect of N_{22} Terms in the In-Plane Stability Equations

As stated previously, the original segmented-plate analysis in the VICONOPT code neglects the effects of the terms involving N_{22} and N_{12} in the in-plane stability equations. This example problem illustrates the effect these terms may have on the buckling of an isotropic (aluminum) long cylindrical tube subjected to uniform external pressure. The material properties in English units for aluminum are given in Table 9. The geometry of this example problem is shown in Figure 4.13. As shown in the figure, only half of the tube is modeled since the buckling mode being studied is symmetric (i.e., two full waves in the circumferential direction). The pressure load is modeled as an applied N_{22} hoop loading. The value of the external pressure that would generate this hoop load is obtained from the following expression [49]

$$p = \frac{N_{22}}{R_2} \quad (4.3)$$

Simitses [50] presents a detailed discussion of the buckling of a thin circular ring uniformly compressed by external pressure. When considering the behavior of the pressure load as the ring buckles, Simitses describes three possible cases. In Case 1, the pressure load is assumed to remain normal to the deflected surface. This loading is referred to as a live pressure load. In Case 2, the pressure load is assumed to remain parallel to its original direction. This loading is referred to as a dead pressure load. In Case 3, the pressure load is assumed to always be directed toward the center of curvature of the ring. This loading is referred to as a centrally directed pressure load. Only Cases 1 and 2 will be discussed in the present thesis.

In Reference [50], Simitses presents in-plane and out-of-plane stability equations for the thin circular ring which may be rewritten in the notation used in the present thesis as

$$n_{22,2} + \frac{q_2}{R_2} - p_{cr} \left(w_{,2} - \frac{u_2}{R_2} \right) - p_2 = 0 \quad (4.4)$$

$$q_{2,2} - \frac{n_{22}}{R_2} - p_{cr} (R_2 w_{,22} - u_{2,2}) - p_3 = 0 \quad (4.5)$$

where p_2 and p_3 are the perturbation values of the applied pressure load in the buckled state in the ξ_2 - and ξ_3 -directions, respectively. For the case of a live pressure load in which the applied pressure is assumed to remain normal to the deflected surface, p_2 and p_3 are (for small deformations)

$$p_2 = -p_{cr} \left(w_{,2} - \frac{u_2}{R_2} \right) \quad \text{and} \quad p_3 = 0 \quad (4.6)$$

For the case of a dead pressure load in which the applied pressure is assumed to remain parallel to its original direction, p_2 and p_3 are

$$p_2 = 0 \quad \text{and} \quad p_3 = 0 \quad (4.7)$$

Substituting Eqs. (4.3) and (4.6) into Eqs. (4.4) and (4.5), yields the following stability equations for the case of live pressure loading:

$$n_{22,2} + \frac{q_2}{R_2} = 0 \quad (4.8)$$

$$q_{2,2} - \frac{n_{22}}{R_2} - N_{22cr} \left(w_{,22} - \frac{u_{2,2}}{R_2} \right) = 0 \quad (4.9)$$

Substituting Eqs. (4.3) and (4.7) into Eqs. (4.4) and (4.5), yields the following stability equations for the case of dead pressure loading:

$$n_{22,2} + \frac{q_2}{R_2} - \frac{N_{22cr}}{R_2} \left(w_{,2} - \frac{u_2}{R_2} \right) = 0 \quad (4.10)$$

$$q_{2,2} - \frac{n_{22}}{R_2} - N_{22cr} \left(w_{,22} - \frac{u_{2,2}}{R_2} \right) = 0 \quad (4.11)$$

For live pressure, the critical value of pressure is shown in [50] to be

$$p_{cr} = \frac{3EI}{R_2^3} \quad (4.12)$$

Therefore,

$$N_{22cr} = \frac{3EI}{R_2^2} \quad (4.13)$$

For dead pressure, the critical value of pressure is shown in [50] to be

$$p_{cr} = \frac{4EI}{R_2^3} \quad (4.14)$$

Therefore,

$$N_{22cr} = \frac{4EI}{R_2^2} \quad (4.15)$$

As discussed in Reference [49], results for the case of a long cylindrical tube uniformly compressed by external pressure, may be obtained by considering an elemental ring of unit width and using Eqs. (4.12) through (4.15) with E replaced by $E/(1-\nu^2)$ and I replaced by $t^3/12$.

External pressure loads are not included in the present analysis. However, an equivalent N_{22} loading may be calculated using Eq. (4.3). The present analysis treats the applied loads as dead loads since no effort is made to modify the applied loads as the plate deforms. The stability equations in the ξ_2 and ξ_3 directions, Eqs. (2.11b) and (2.11c) for the present analysis are written for a thin circular ring subjected to N_{22} loading by ignoring any terms that involve N_{12} , ξ_1 , or derivatives with respect to ξ_1 . These equations are

$$n_{22,2} + \frac{q_2}{R_2} - \frac{N_{22}}{R_2} \left(w_{,2} - \frac{u_{2,2}}{R_2} \right) - \underline{E} N_{22} \left(\frac{w_{,2}}{R_2} + u_{2,2} \right) = 0 \quad (4.16)$$

$$q_{2,2} - \frac{n_{22}}{R_2} - N_{22} \left(w_{,22} - \frac{u_{2,2}}{R_2} \right) + \frac{\underline{E} N_{22}}{R_2} \left(\frac{w}{R_2} + u_{2,2} \right) = 0 \quad (4.17)$$

Comparing Eqs. (4.9), (4.11), and (4.17), reveals that if physical strains are used in the present analysis (i.e., $\underline{E} = 0$), the out-of-plane stability equation is identical to that given by Simitses for both live and dead pressure loads. Furthermore, the in-plane stability equation for the live pressure load case is recovered by the present analysis if the N_{22} term is neglected in Eq. (4.16). The dead pressure load case is seen to be recovered when the N_{22} term is included in Eq. (4.16). Comparing Eqs. (4.6), (4.7), and (4.16), shows that

for the case of physical strains, the remaining term involving N_{22} is actually equivalent to the component of a live pressure load in the ξ_2 direction (see Eq. (4.6)).

Buckling results for this example are presented in Table 10. The VICONOPT results presented in this table are for physical strains. As previously discussed, the VICONOPT result when the N_{22} term is neglected in the in-plane stability equation corresponds to the case of live pressure load, and the VICONOPT result when the N_{22} term is included in the in-plane stability equation corresponds to the case of dead pressure load. The results for physical strains for the segmented-plate analysis always equal those for the case of dead pressure load since the N_{22} term in the in-plane stability equation also involves $1/R_2$ and it therefore drops out of that equation altogether. These results illustrate the dramatic effect that the N_{22} and N_{12} terms in the in-plane stability equations can have on the buckling results for curved plates.

4.5 Design Optimization of a Cylindrical Shell Subject to Uniaxial Compression

The final example utilizes the new curved-plate analysis with the design optimization capability of VICONOPT to perform a structural optimization of two different cylindrical shell concepts subject to uniform axial compression (N_{11} loading). The two concepts are solid-wall construction and honeycomb-sandwich construction. The geometry of this example problem is shown in Figure 4.14. As shown in the figure, the facesheets of the honeycomb-sandwich concept are aluminum, and the core is Korex™ aramid paper honeycomb core [51]. The solid-wall concept is aluminum. The material properties used for the facesheets and core are presented in Table 9.

Before results for this example are presented, a discussion of the modeling technique used to model this cylinder is presented. An analysis of a complete cylinder was performed using only one plate element with the new curved-plate analysis capability in

VICONOPT. The cylinder is modeled by defining a repetitive cross-section in which there is only one node that is connected to itself. However, numerical problems were encountered when analyzing closed cylinders with very small wavelengths. The following procedure was used to avoid this problem. First, a 45° arc segment is defined. Second, a 90° arc segment is defined as a substructure by connecting the original 45° arc segment to itself. Similarly, a 180° arc segment is constructed from two 90° arcs. Finally, a 360° arc is constructed from two 180° arcs. This substructure is then used to define the repetitive cross-section of the cylinder as previously discussed. This modeling technique is used for all closed cylinders analyzed in the present thesis, and no numerical problems were encountered when using this technique.

The design variables for the structural optimization are the thicknesses of the facesheets and the core for the sandwich concept and the wall thickness for the solid-wall construction. There is no minimum-gage restriction for any design variables. The nominal values for these variables are 0.1 in., 0.5 in., and 0.1 in., respectively. The design constraints are that the strain in the facesheets or the solid wall cannot exceed 0.005 in/in and that the stress in the core cannot exceed 115 psi in the ξ_1 -direction and 55 psi in the ξ_2 -direction. The results of this study, including the mass of the optimized cylinder and the final values of the design variables are given in Table 11 for the honeycomb-sandwich concept and in Table 12 for the solid-wall concept. Results from both CPT and SDPT are given in these tables. The optimized mass values are also plotted as a function of the applied loading in Figure 4.15. As seen in the tables and the figure, the values for optimized mass obtained using CPT are slightly less than those for SDPT for the honeycomb-sandwich cylinder as the applied loading is increased. However, the values for core thickness obtained using CPT are significantly less than those for SDPT for the honeycomb-sandwich cylinder as the applied loading is increased. These results are expected because CPT results in an overly stiff approximation since the

effects of transverse-shear deformation are neglected. This overly stiff approximation results in higher buckling loads for a given core thickness. Therefore, the core thickness and the optimum mass obtained is less than that obtained using SDPT. The optimized mass values for the solid-wall construction are much greater than those for the honeycomb-sandwich construction. The results for CPT and SDPT are nearly identical for the solid-wall construction, as expected.

CHAPTER V

CONCLUDING REMARKS

The VICONOPT computer code is an exact analysis and optimum design program that includes the buckling and vibration analyses of prismatic assemblies of flat, in-plane-loaded anisotropic plates. In the present thesis, the capability to analyze curved-plate segments exactly has been added to the VICONOPT code. Non-linear curved-plate equilibrium equations have been formulated using the principle of virtual work, and linearized stability equations that describe the response of the plate just after buckling occurs were derived following the application of several simplifying assumptions. Finally, modifications to these equations were made to allow the reference surface of the plate to be located at a distance z_c from the centroidal surface.

The analysis methodology described in the present thesis improves upon the existing methodology in the VICONOPT code (referred to herein as the segmented-plate analysis) which requires that curved-plate segments be subdivided into several flat-plate elements that must be subsequently joined at their longitudinal edges to approximate the curved-plate geometry. The new analysis formulation allows either classical plate theory (CPT) or first-order shear deformation plate theory (SDPT) to be used. Furthermore, anisotropic laminates having fully populated **A**, **B**, and **D** stiffness matrices may be analyzed. The analysis described in the present thesis is an example of an exact finite-strip method (FSM) since it uses a stiffness matrix that is derived by direct solution to the stability equations.

One additional capability that has been incorporated into the VICONOPT code as part of the present thesis is the option to use plate elements (flat or curved) that are based upon nonlinear strain-displacement relations that contain terms from either physical or tensorial strain measures. A second capability that has been added is the ability to

include the effect of terms associated with in-plane transverse and in-plane shear loading in the in-plane stability equations. The original VICONOPT code neglects these terms.

Results from the present curved-plate analysis capability compare very well with a closed-form solution and the existing segmented-plate analysis for the buckling of a long isotropic cylinder. The present analysis also compares well with results from the literature for symmetrically laminated curved plates with widely varying curvatures and with unsymmetrically laminated plates that include the effect of extensional-bending and shear-extension coupling. No appreciable effects of using tensorial versus physical strains are noted in these examples. The present curved-plate analysis was also shown to require significantly less computational effort than the segmented-plate analysis. An alternate approach for the segmented-plate analysis that offers additional computational savings for certain classes of problems has been investigated. However, this approach requires greater user effort, and it is currently not implemented in the VICONOPT code.

A significant effect of either including or neglecting the terms associated with an applied in-plane transverse loading (i.e., N_{22} loading) in the in-plane stability equations was noted when analyzing a long cylindrical tube subjected to uniform external pressure. The symmetry of the buckling mode for this problem allowed it to be modeled as a half cylinder, and the pressure load was simulated with an equivalent hoop (N_{22}) loading. The buckling results for this problem were shown to change by a factor of 3/4 when the terms associated with the N_{22} loading were neglected in the in-plane stability equations. This result illustrates the effect that the treatment of the in-plane stability equations can have on the buckling results for curved plates.

Finally, the present curved-plate analysis was used to conduct a design-optimization study of two different cylindrical shells subject to uniform axial compression (N_{11} loading). One shell was constructed from a honeycomb-sandwich wall construction, and the other was a solid-wall construction. The values of mass for the optimized solid-wall design were consistently higher than those for the honeycomb-sandwich construction.

However, there was no difference between results using CPT and SDPT for the solid-wall cylinder. The values of mass for the optimized honeycomb-sandwich cylinder using CPT were slightly less than those for SDPT as the applied loading was increased. However, the values of core thickness for the optimized honeycomb-sandwich cylinder using CPT were significantly less than those for SDPT as the applied loading was increased. This trend occurred because CPT results in an overly stiff approximation since the effects of transverse-shear flexibility are neglected. This overly stiff approximation results in higher buckling loads and, thus, a lower optimum mass.

One area for future work includes retaining the curvature terms in the longitudinal direction and implementing the capability to analyze shells of revolution. The analysis can also be modified to allow vibration analyses to be performed. Another enhancement that can be made to the present analysis is to remove the restriction that when the terms associated with in-plane transverse and in-plane shear loading are retained in the in-plane stability equations, the centroidal surface and reference surface must coincide.

REFERENCES

1. Williams, F. W.; Kennedy, D.; Anderson, M. S.; and Edwards, D. A.: "User Manual for VICONOPT," Release 1.3, April 1996.
2. Anderson, M. S.; and Kennedy, D.: "Inclusion of Transverse Shear Deformation in the Exact Buckling and Vibration Analysis of Composite Plate Assemblies," Presented at the AIAA/ASME/ASCE/AHS/ASC 32nd Structures, Structural Dynamics and Materials Conference, Dallas, Texas, April 13-15, 1992. AIAA Paper No. 92-2287.
3. Cheung, Y. K.: *The Finite Strip Method in Structural Analysis*, Pergamon Press, Oxford, England, 1976.
4. Zienkiewicz, O. C.: *The Finite Element Method in Engineering Science*, McGraw Hill, London, England, 1971.
5. Cheung, Y. K.: "The Finite Strip Method in the Analysis of Elastic Plates with Two Opposite Simply Supported Ends," Proceedings of the Institute of Civil Engineers, Vol. 40, No. 1, 1968.
6. Cheung, M. S.; and Cheung, Y. K.: "Natural Vibrations of Thin Flat-Walled Structures With Different Boundary Conditions," Journal of Sound and Vibration, Vol. 18, 1971, pp. 325-337.
7. Przemieniecki, J. S.: "Finite Element Structural Analysis of Local Instability," AIAA Journal, Vol. 11, 1973, pp. 33-39.
8. Plank, R. J.; and Wittrick, W. H.: "Buckling Under Combined Loading of Thin Flat-Walled Structures By a Complex Finite-Strip Method," International Journal for Numerical Methods in Engineering, Vol. 8, 1974, pp. 323-339.
9. Dawe, D. J.: "Static Analysis of Diaphragm-Supported Cylindrical Shells Using a Curved Finite Strip," International Journal for Numerical Methods in Engineering, Vol. 11, 1977, pp. 1347-1364.
10. Dawe, D. J.: "Finite Strip Buckling Analysis of Curved Plate Assemblies Under Biaxial Loading," International Journal for Numerical Methods in Engineering, Vol. 13, 1977, pp. 1141-1155.
11. Morris, I. R.; and Dawe, D. J.: "Free Vibration of Curved-Plate Assemblies With Diaphragm Ends," Journal of Sound and Vibration, Vol. 73, 1980, pp. 1-17.
12. Dawe, D. J.: "Finite Strip Models for Vibration of Mindlin Plates," Journal of Sound and Vibration, Vol. 59, 1978, pp. 441-452.
13. Mindlin, R. D.: "Influence of Rotatory Inertia and Shear on Flexural Motions of Isotropic Elastic Plates," Journal of Applied Mechanics, Vol. 18, 1951, pp. 31-38.

14. Roufaeil, O. L.; and Dawe, D. J.: "Vibration Analysis of Rectangular Mindlin Plates by the Finite Strip Method," Computers & Structures, Vol. 12, 1980, pp. 833-842.
15. Dawe, D. J.; and Roufaeil, O. L.: "Buckling of Rectangular Mindlin Plates," Computers & Structures, Vol. 15, 1982, pp. 461-471.
16. Craig, T. J.; and Dawe, D. J.: "Flexural Vibration of Symmetrically Laminated Composite Rectangular Plates Including Transverse Shear Effects," International Journal of Solids and Structures, Vol. 22, No. 2, 1986, pp. 155-169.
17. Dawe, D. J.; and Craig, T. J.: "The Vibration and Stability of Symmetrically Laminated Composite Rectangular Plates Subjected to In-Plane Stresses," Composite Structures, Vol. 5, 1986, pp. 281-307.
18. Craig, T. J.; and Dawe, D. J.: "Vibration of Shear-Deformable Laminated Plate Structures by the Finite Strip Method," Computers & Structures, Vol. 27, No. 1, 1987, pp. 61-72.
19. Dawe, D. J.; and Craig, T. J.: "Buckling and Vibration of Shear Deformable Prismatic Plate Structures by a Complex Finite Strip Method," International Journal of Mechanical Sciences, Vol. 30, No. 2, 1988, pp. 77-99.
20. Dawe, D. J.; and Peshkam, V.: "Buckling and Vibration of Finite-Length Composite Prismatic Plate Structures With Diaphragm Ends, Part I: Finite Strip Formulation," Computer Methods in Applied Mechanics and Engineering, Vol. 77, 1989, pp. 1-30.
21. Peshkam, V.; and Dawe, D. J.: "Buckling and Vibration of Finite-Length Composite Prismatic Plate Structures With Diaphragm Ends, Part II: Computer Programs and Buckling Applications," Computer Methods in Applied Mechanics and Engineering, Vol. 77, 1989, pp. 227-252.
22. Dawe, D. J.; and Peshkam, V.: "Buckling and Vibration of Long Plate Structures by Complex Finite Strip Methods," International Journal of Mechanical Sciences, Vol. 32, No. 9, 1990, pp. 743-766.
23. Wittrick, W. H.: "A Unified Approach to the Initial Buckling of Stiffened Panels in Compression," The Aeronautical Quarterly, Vol. 19, 1968, pp. 265-283.
24. Wittrick, W. H.; and Curzon, P. L. V.: "Stability Functions for the Local Buckling of Thin Flat-Walled Structures with the Walls in Combined Shear and Compression," Aeronautical Quarterly, November 1968, vol. 19, pp. 327-351.
25. Wittrick, W. H.: "General Sinusoidal Stiffness Matrices for Buckling and Vibration Analysis of Thin Flat-Walled Structures," International Journal of Mechanical Sciences, Vol. 10, 1968, pp. 949-966.
26. Smith, C. S.: "Bending, Buckling and Vibration of Orthotropic Plate-Beam Structures," Journal of Ship Research, Vol. 12, 1968, pp. 249-268.

27. Williams, F. W.: "Computation of Natural Frequencies and Initial Buckling Stresses of Prismatic Plate Assemblies," Journal of Sound and Vibration, Vol. 21, 1972, pp. 87-106.
28. Wittrick, W. H.; and Williams, F. W.: "Buckling and Vibration of Anisotropic or Isotropic Plate Assemblies Under Combined Loadings," International Journal of Mechanical Sciences, Vol. 16, 1974, pp. 209-239.
29. Wittrick, W. H.; and Williams, F. W.: "An Algorithm for Computing Critical Buckling Loads of Elastic Structures," Journal of Structural Mechanics, Vol. 1, 1973, pp. 497-518.
30. Viswanathan, A. V.; and Tamekuni, M.: "Elastic Buckling Analysis For Composite Stiffened Panels and other Structures Subjected to Biaxial Inplane Loads," NASA CR-2216, 1973.
31. Viswanathan, A. V.; Tamekuni, M.; and Tripp, L. L.: "Elastic Stability of Biaxially Loaded Longitudinally Stiffened Composite Structures," Proceedings of the AIAA/ASME/SAE 14th Structures, Structural Dynamics, and Materials Conference, Williamsburg, VA, March 20-22, 1973. AIAA Paper No. 73-367.
32. Viswanathan, A. V.; Tamekuni, M.; and Baker, L. L.: "Elastic Stability of Laminated, Flat and Curved, Long Rectangular Plates Subjected to Combined Loads," NASA CR-2330, 1974.
33. Williams, F. W.; and Anderson, M. S.: "Incorporation of Lagrangian Multipliers into an Algorithm for Finding Exact Natural Frequencies or Critical Buckling Loads," International Journal of Mechanical Sciences, Vol. 25, 1983, No. 8, pp. 579-584.
34. Anderson, M. S.; Williams, F. W.; and Wright, C. J.: "Buckling and Vibration of any Prismatic Assembly of Shear and Compression Loaded Anisotropic Plates with an Arbitrary Supporting Structure," International Journal of Mechanical Sciences, Vol. 25, No. 8, 1983, pp. 585-596.
35. Kennedy, D.; and Williams, F. W.: "Vibration and Buckling of Anisotropic Plate Assemblies with Winkler Foundations," Journal of Sound and Vibration, Vol. 138, No. 3, 1990, pp. 501-510.
36. Williams, F. W.; Kennedy, D.; and Anderson, M. S.: "Analysis Features of VICONOPT, an Exact Buckling and Vibration Program for Prismatic Assemblies of Anisotropic Plates," Proceedings of the 31st AIAA/ASME/ASCE/AHS/ASC Structures, Structural Dynamics and Materials Conference, Long Beach, California, pp. 920-929, April 1990. AIAA Paper 90-0970.
37. Butler, R.; and Williams, F. W.: "Optimum Design Features of VICONOPT, an Exact Buckling and Vibration Program for Prismatic Assemblies of Anisotropic Plates," Proceedings of the 31st AIAA/ASME/ASCE/AHS/ASC Structures, Structural Dynamics and Materials Conference, Long Beach, California, pp. 1289-1299, April 1990. AIAA Paper 90-1068.

38. Sanders, J. L., Jr.: "An Improved First-Approximation Theory For Thin Shells," NASA TR R-24, 1959.
39. Sanders, J. L., Jr.: "Nonlinear Theories for Thin Shells," Quarterly of Applied Mathematics, Vol. 21, 1963, pp. 21-36.
40. Wolfram, S.: *MATHEMATICA: A System for Doing Mathematics by Computer*, Addison-Wesley Publishing Company, Inc., Redwood City, CA, 1988.
41. Novozhilov, V. V.: *Foundations of the Nonlinear Theory of Elasticity*, Graylock Press, Rochester, New York, 1963.
42. Stein, M.: "Nonlinear Theory for Plates and Shells Including the Effects of Transverse Shearing," AIAA Journal, Vol. 24, No. 9, September 1986, pp. 1537-1544.
43. Shames, I. H. and Dym, C. L.: *Energy and Finite Element Methods in Engineering Mechanics*, Hemisphere Publishing Corporation, New York, New York, 1985.
44. Cohen, G. A.: "Transverse Shear Stiffness of Laminated Anisotropic Shells," Computer Methods in Applied Mechanics and Engineering, Vol. 13, 1978, pp. 205-220.
45. Jones, R. M.: *Mechanics of Composite Materials*, Hemisphere Publishing Corp., New York, New York, 1975.
46. Langhaar, H. L.: *Energy Methods in Applied Mechanics*, Kreiger Publishing Company, Malabar, Florida, 1989.
47. Cohen, G. A.: "FASOR - A Second Generation Shell of Revolution Code," Computers & Structures, Vol. 10, 1979, pp. 301-309.
48. Shames, I. H.: *Mechanics of Deformable Solids*, Kreiger Publishing Company, Malabar, Florida, 1985.
49. Timoshenko, S. P.; and Gere, J. M.: *Theory of Elastic Stability*, McGraw-Hill Book Company, New York, New York, 1961.
50. Simitses, G. J.: *An Introduction to the Elastic Stability of Structures*, Kreiger Publishing Company, Malabar, Florida, 1986.
51. Anonymous: DuPont KOREX™ Honeycomb Core for High Performance Applications, DuPont Technical Data Specification Sheet.

APPENDIX A

MATRICES FOR DETERMINING CHARACTERISTIC ROOTS

The eigenvalues of matrix \mathbf{R} in Eq. (3.16a) are the characteristic roots of the differential equations describing the behavior of the plate. The 10-by-10 matrix \mathbf{R} is calculated from the matrices \mathbf{T} and \mathbf{P} as shown in Eq. (3.16b). The non-zero elements of the \mathbf{T} matrix are

$$t_{3,3}^* = t_{4,4}^* = t_{5,5}^* = t_{6,6}^* = t_{7,7}^* = t_{8,8}^* = t_{9,9}^* = t_{10,10}^* = 1$$

$$t_{1,1}^* = 1 - \frac{(\underline{E} \ h_{33}N_{22} - \underline{G} \ h_{23}N_{12})}{b} \quad t_{1,2}^* = \frac{-\underline{F} \ h_{23}N_{22} + \underline{G} \ h_{33}N_{12}}{b}$$

$$t_{2,1}^* = -\frac{(\underline{E} \ h_{23}N_{22} - \underline{G} \ h_{22}N_{12})}{b} \quad t_{2,2}^* = 1 - \frac{(\underline{F} \ h_{22}N_{22} - \underline{G} \ h_{23}N_{12})}{b}$$

$$t_{4,1}^* = \frac{\underline{E} \ h_{35}N_{22} - \underline{G} \ h_{25}N_{12}}{b} \quad t_{4,2}^* = \frac{\underline{F} \ h_{25}N_{22} - \underline{G} \ h_{35}N_{12}}{b}$$

$$t_{5,1}^* = -\frac{(\underline{E} \ h_{36}N_{22} - \underline{G} \ h_{26}N_{12})}{b} \quad t_{5,2}^* = \frac{-\underline{F} \ h_{26}N_{22} + \underline{G} \ h_{36}N_{12}}{b}$$

$$t_{6,1}^* = \frac{\alpha}{b} \left(\frac{\underline{E} \ \underline{H} \ h_{33}N_{22}N_{12} - \underline{G} \ \underline{H} \ h_{23}N_{12}^2 - \underline{E} \ h_{13}N_{22} + \underline{G} \ h_{12}N_{12}}{b} \right)$$

$$t_{6,2}^* = \frac{\alpha}{b} \left(\frac{\underline{F} \ \underline{H} \ h_{23}N_{22}N_{12} - \underline{G} \ \underline{H} \ h_{33}N_{12}^2 - \underline{F} \ h_{12}N_{22} + \underline{G} \ h_{13}N_{12}}{b} \right)$$

$$t_{7,1}^* = \frac{\alpha}{b} \left(\frac{\underline{E} \ \underline{H} \ h_{23}N_{22}N_{12} - \underline{G} \ \underline{H} \ h_{22}N_{12}^2 - \underline{E} \ N_{22}}{b} \right)$$

$$t_{7,2}^* = \frac{\alpha}{b} \left(\frac{\underline{F} \ \underline{H} \ h_{22}N_{22}N_{12} - \underline{G} \ \underline{H} \ h_{23}N_{12}^2 + \underline{G} \ N_{12}}{b} \right)$$

$$t_{8,1}^* = \frac{\alpha}{b} t_{10,1} = \frac{\alpha^2}{b^2} (\underline{E} \ h_{34}N_{22} - \underline{G} \ h_{24}N_{12})$$

$$t_{8,2}^* = \frac{\alpha}{b} t_{10,2} = \frac{\alpha^2}{b^2} (\underline{F} \ h_{24}N_{22} - \underline{G} \ h_{34}N_{12})$$

The underlined terms given above and subsequently are those terms that drop out of the equation when the effects of N_{22} and N_{12} in the in-plane stability equations are neglected.

The non-zero elements of the \mathbf{P} matrix are

$$p_{1,1}^* = -\alpha(h_{13} - \underline{H} h_{33}N_{12})$$

$$p_{1,2} = -\alpha(1 - \underline{H} h_{23}N_{12})$$

$$p_{1,3}^* = -\frac{\alpha^2}{b}h_{34} - \frac{b}{R_2}(\underline{F} h_{23}N_{22} - \underline{G} h_{33}N_{12})$$

$$p_{1,5} = p_{10,6} = \alpha h_{34}$$

$$p_{1,6}^* = -bh_{33}$$

$$p_{1,7}^* = p_{2,6}^* = -bh_{23}$$

$$p_{1,9}^* = -p_{4,6}^* = -bh_{35}$$

$$p_{1,10} = p_{5,6} = -bh_{36}$$

$$p_{2,1}^* = -\alpha(h_{12} - \underline{H} h_{23}N_{12})$$

$$p_{2,2} = \underline{\alpha H} h_{22}N_{12}$$

$$p_{2,3}^* = \frac{b}{R_2} - \frac{\alpha^2 h_{24}}{b} - \frac{b}{R_2}(\underline{F} h_{22}N_{22} - \underline{G} h_{23}N_{12})$$

$$p_{2,5} = p_{10,7} = \alpha h_{24}$$

$$p_{2,7}^* = -bh_{22}$$

$$p_{2,9}^* = -p_{4,7}^* = -bh_{25}$$

$$p_{2,10} = p_{5,7} = -bh_{26}$$

$$p_{3,2}^* = \frac{b}{R_2}$$

$$p_{3,3} = p_{8,8} = \frac{\alpha N_{12} h_{88}}{S}$$

$$p_{3,4} = \frac{b}{S}$$

$$p_{3,5} = p_{10,8} = -\frac{bh_{78}}{S}$$

$$p_{3,10} = -p_{5,8} = -\frac{\alpha}{b}p_{3,8} = -\frac{\alpha h_{88}}{S}$$

$$p_{4,1}^* = \alpha(h_{15} - \underline{H} h_{35}N_{12})$$

$$p_{2,2} = \underline{-\alpha H} h_{25}N_{12}$$

$$p_{4,3}^* = -\frac{\alpha^2 h_{45}}{b} - \frac{b}{R_2} (\underline{F} h_{25} N_{22} - \underline{G} h_{35} N_{12})$$

$$p_{4,5} = -\frac{\alpha}{b} p_{10,9} = \alpha h_{45}$$

$$p_{4,9}^* = b h_{55}$$

$$p_{4,10} = -p_{5,9} = b h_{56}$$

$$p_{5,1} = -\alpha (h_{16} - \underline{H} h_{36} N_{12})$$

$$p_{5,2} = \frac{\alpha}{R_2} + \underline{H} \alpha h_{26} N_{12}$$

$$p_{5,3} = \frac{\alpha^2}{b} \left(h_{46} + \frac{N_{12} h_{88}}{S} \right) - \frac{b}{R_2} (\underline{F} h_{26} N_{22} - \underline{G} h_{36} N_{12})$$

$$p_{5,4} = \alpha + \frac{\alpha}{S}$$

$$p_{5,5} = p_{10,10} = -\alpha \left(h_{46} + \frac{h_{78}}{S} \right)$$

$$p_{5,10} = -b h_{66} - \frac{\alpha^2 h_{88}}{b S}$$

$$p_{6,1}^* = \frac{-\underline{C} \pi^2 b N_{11}}{\lambda^2} + \frac{\alpha^2}{b} \left(h_{11} + \underline{2H} h_{13} N_{12} - \underline{H}^2 h_{33} N_{12}^2 \right)$$

$$p_{6,2} = \frac{\alpha^2 N_{12}}{b} (\underline{G} + \underline{H} [1 + h_{12} - \underline{H} h_{23} N_{12}])$$

$$p_{6,3}^* = \frac{\alpha^3}{b^2} (-h_{14} + \underline{H} h_{34} N_{12}) + \frac{\alpha}{R_2} (N_{12} [\underline{G} h_{13} - \underline{G} \underline{H} h_{33} N_{12} + \underline{F} \underline{H} h_{23} N_{22}]$$

$$- \underline{F} h_{12} N_{22}) + \frac{\underline{C} \alpha \pi^2 N_{11} z_c}{\lambda^2}$$

$$p_{6,5} = \frac{\alpha^2}{b} \left(h_{14} - \underline{H} h_{34} N_{12} \right) - \frac{\underline{C} \pi^2 b N_{11} z_c}{\lambda^2}$$

$$p_{6,6}^* = \alpha(-h_{13} + \underline{\underline{Hh}}_{33}N_{12})$$

$$p_{6,7}^* = \alpha(-h_{12} + \underline{\underline{Hh}}_{23}N_{12})$$

$$p_{6,9}^* = \alpha(-h_{15} + \underline{\underline{Hh}}_{35}N_{12})$$

$$p_{6,10} = \alpha(-h_{16} + \underline{\underline{Hh}}_{36}N_{12})$$

$$p_{7,1} = \frac{\alpha^2}{b} \left(N_{12} \left[\underline{G} + \underline{H} \{ 1 + h_{12} - \underline{\underline{Hh}}_{23}N_{12} \} \right] \right)$$

$$p_{7,2} = -\underline{B} \frac{\pi^2 b N_{11}}{\lambda^2} - \frac{b N_{22}}{R_2^2} - \frac{\alpha^2 \underline{H}^2 h_{22} N_{12}^2}{b}$$

$$p_{7,3} = -\frac{\alpha N_{12}}{R_2} \left(\frac{1}{S} - \frac{1 - \underline{G} + \underline{G} \underline{\underline{Hh}}_{23}N_{12} - \underline{F} \underline{\underline{Hh}}_{22}N_{22}}{\underline{S}} \right) + \frac{\alpha^3 \underline{\underline{Hh}}_{24}N_{12}}{b^2}$$

$$p_{7,4} = -\frac{b N_{22}}{R_2 S} (1 - \underline{1}) + \frac{\underline{B} \pi^2 b N_{11} z_c}{\lambda^2}$$

$$p_{7,5} = \frac{b h_{78} N_{12}}{R_2 S} (1 - \underline{1}) - \frac{\alpha^2 \underline{\underline{Hh}}_{24}N_{12}}{b}$$

$$p_{7,6} = -\alpha(1 - \underline{\underline{Hh}}_{23}N_{12})$$

$$p_{7,7} = \alpha \underline{\underline{Hh}}_{22}N_{12}$$

$$p_{7,8} = -\frac{b}{S R_2} \left(1 - \underline{\alpha h_{88} N_{22}} \right)$$

$$p_{7,9} = \alpha \underline{\underline{Hh}}_{25}N_{12}$$

$$p_{7,10} = \alpha \left(\frac{1}{S R_2} - \frac{h_{88} N_{22}}{S R_2} + \underline{\underline{Hh}}_{26}N_{12} \right)$$

$$p_{8,1}^* = \frac{\alpha^3}{b^2} (h_{14} - \underline{\underline{Hh}}_{34}N_{12}) - \frac{\underline{C} \alpha \pi^2 N_{11} z_c}{\lambda^2}$$

$$p_{8,2} = -\frac{\alpha^3 \underline{\underline{Hh}}_{24}N_{12}}{b^2}$$

$$p_{8,3} = \frac{\pi^2 b N_{11}}{\lambda^2} + \frac{\alpha^2}{b} \left(\frac{\underline{F} h_{24} N_{22}}{R_2} - \frac{\underline{G} h_{34} N_{12}}{R_2} + \frac{N_{12}^2 h_{88}}{S} \right) - \frac{\alpha^4 h_{44}}{b^3} + \frac{\underline{C} \alpha^2 \pi^2 N_{11} z_c^2}{b \lambda^2}$$

$$p_{8,4} = \alpha N_{12} \left(\frac{1}{S} + \frac{z_c}{R_2} \right)$$

$$p_{8,5} = -\frac{\alpha N_{12} h_{78}}{S} + \frac{\alpha^3 h_{44}}{b^2} - \frac{\underline{C} \alpha \pi^2 N_{11} z_c^2}{\lambda^2}$$

$$p_{8,6} = \frac{\alpha^2 h_{34}}{b}$$

$$p_{8,7} = \frac{\alpha^2 h_{24}}{b} - \frac{b}{R_2}$$

$$p_{8,8} = \frac{\alpha h_{88} N_{12}}{S}$$

$$p_{8,9} = -\frac{\alpha^2 h_{45}}{b}$$

$$p_{8,10} = -\frac{\alpha^2}{b} \left(h_{46} + \frac{h_{88} N_{12}}{S} \right)$$

$$p_{9,2} = -\frac{\underline{B} \pi^2 b N_{11} z_c}{\lambda^2}$$

$$p_{9,3} = \frac{\alpha N_{12}}{S} \left(1 - \frac{z_c}{R_2} \right)$$

$$p_{9,4} = \frac{b N_{22}}{S} \left(1 - \frac{z_c}{R_2} \right) + \frac{\underline{B} \pi^2 b N_{11} z_c^2}{\lambda^2}$$

$$p_{9,5} = -\frac{b h_{78} N_{22}}{S} \left(1 - \frac{z_c}{R_2} \right)$$

$$p_{9,8} = \frac{b}{S} \left(1 - \frac{z_c}{R_2} \right)$$

$$p_{9,10} = -\alpha \left(1 + \frac{1}{S} - \frac{z_c}{R_2 S} \right)$$

$$p_{10,1} = \frac{\alpha^2}{b} \left(h_{14} - \frac{\underline{H} h_{34} N_{12}}{S} \right) - \frac{\underline{C} \pi^2 b N_{11} z_c}{\lambda^2}$$

$$p_{10,2} = -\frac{\alpha^2 \underline{H} h_{24} N_{12}}{b}$$

$$p_{10,3} = \frac{\alpha h_{78} N_{12}}{S} + \frac{\alpha}{R_2} (\underline{F} h_{24} N_{22} - \underline{G} h_{34} N_{12}) - \frac{\alpha^3 h_{44}}{b^2} + \frac{\underline{C} \alpha \pi^2 N_{11} z_c^2}{\lambda^2}$$

$$p_{10,4} = \frac{b h_{78} N_{22}}{S}$$

$$p_{10,5} = b h_{77} - \frac{b h_{78}^2 N_{22}}{S} + \frac{\alpha^2 h_{44}}{b} - \frac{\underline{C} \pi^2 b N_{11} z_c^2}{\lambda^2}$$

where

$$\alpha = \frac{\pi b}{\lambda}$$

$$S = 1 - h_{88}N_{22}$$

The expressions for the elements of the **T** and **P** matrices for the case of classical plate theory are obtained by setting the transverse-shear strains, γ_{13} and γ_{23} , equal to zero and using the resulting expression $\phi_1 = w_{,1}$ (recall that $\frac{1}{R_1}$ equals to zero). The partially inverted stress-strain relations given in Eq. (3.11), are modified such that m_{12} and κ_{12} are interchanged. For the classical case, only four stability equations, Eqs. (2.16a), (2.16b), (2.16c), and (2.18a) are used since Eq. (2.18b) is satisfied by incorporation into the final form of Eq. (2.16c). The same steps used for the transverse-shear case are followed to generate **T** and **P** matrices of order eight. The elements of the **T** and **P** matrices with a superscript * given previously for the transverse-shear case also apply for the classical case if 1 is subtracted from any index greater than 4. The non-zero elements of the **T** matrix that are not given in the results for transverse shear are

$$t_{6,1} = \frac{\alpha}{b} \left(\underline{E} \underline{H} h_{23} N_{22} N_{12} - \underline{G} \underline{H} h_{22} N_{12}^2 - \underline{E} N_{22} - \frac{1}{R_2} [\underline{E} h_{36} N_{22} - \underline{G} h_{26} N_{12}] \right)$$

$$t_{6,2} = \frac{\alpha}{b} \left(\underline{F} \underline{H} h_{22} N_{22} N_{12} - \underline{G} \underline{H} h_{23} N_{12}^2 + \underline{G} N_{12} - \frac{1}{R_2} [\underline{F} h_{26} N_{22} - \underline{G} h_{36} N_{12}] \right)$$

$$t_{8,1} = \frac{2\alpha}{b} (\underline{E} h_{36} N_{22} - \underline{G} h_{26} N_{12})$$

$$t_{8,2} = \frac{2\alpha}{b} (\underline{E} h_{26} N_{22} - \underline{G} h_{36} N_{12})$$

The non-zero elements of the **P** matrix that are not given in the results for transverse shear are

$$p_{1,2} = -\alpha \left(1 + \frac{h_{36}}{R_2} - \frac{\underline{\underline{H}}h_{23}N_{12}}{R_2} \right)$$

$$p_{1,4} = -2\alpha h_{36}$$

$$p_{2,2} = -\alpha \left(\frac{h_{26}}{R_2} - \frac{\underline{\underline{H}}h_{22}N_{12}}{R_2} \right)$$

$$p_{2,4} = -2\alpha h_{26}$$

$$p_{3,4} = b$$

$$p_{4,2} = \alpha \left(\frac{h_{56}}{R_2} - \frac{\underline{\underline{H}}h_{25}N_{12}}{R_2} \right)$$

$$p_{4,4} = 2\alpha h_{56}$$

$$p_{5,2} = \frac{\alpha^2 N_{12}}{b} \left(\underline{\underline{G}} + \underline{\underline{H}} \left[1 + h_{12} + \frac{h_{36}}{R_2} - \underline{\underline{H}} h_{23}N_{12} \right] \right) - \frac{\alpha^2 h_{16}}{bR_2}$$

$$p_{5,4} = \frac{-2\alpha^2}{b} (h_{16} - \underline{\underline{H}}h_{36}N_{12})$$

$$p_{6,1} = \frac{\alpha^2 N_{12}}{b} \left(\underline{\underline{G}} + \underline{\underline{H}} \left[1 + h_{12} + \frac{h_{36}}{R_2} - \underline{\underline{H}} h_{23}N_{12} \right] \right) - \frac{\alpha^2 h_{16}}{bR_2}$$

$$p_{6,2} = \frac{\alpha^2}{b} \left(\frac{h_{66}}{R_2^2} + \underline{\underline{H}}N_{12} [2h_{26} - \underline{\underline{H}}h_{22}N_{12}] \right) - \frac{\underline{\underline{B}}\pi^2 b N_{11}}{\lambda^2}$$

$$p_{6,3} = \frac{\alpha^3}{b^2} \left(\frac{h_{46}}{R_2} + \underline{\underline{H}}h_{24}N_{12} \right) + \frac{\alpha N_{12}}{R_2} \left(1 + \underline{\underline{G}} - \underline{\underline{G}} \underline{\underline{H}}h_{23}N_{12} + \underline{\underline{F}} \underline{\underline{H}}h_{22}N_{22} + \frac{\underline{\underline{G}}h_{36}}{R_2} \right) - \frac{\alpha \underline{\underline{F}}h_{26}N_{22}}{R_2^2} - \frac{\alpha N_{12}}{R_2}$$

$$p_{6,4} = \frac{2\alpha^2}{b} \left(\frac{h_{66}}{R_2} + \underline{\underline{H}}h_{26}N_{12} \right) - \frac{bN_{22}}{R_2} (1 - 1) + \frac{\underline{\underline{B}}\pi^2 b N_{11} z_c}{\lambda^2}$$

$$p_{6,5} = -\alpha \left(1 + \frac{h_{36}}{R_2} - \frac{\underline{\underline{H}}h_{23}N_{12}}{R_2} \right)$$

$$p_{6,6} = -\alpha \left(\frac{h_{26}}{R_2} - \frac{\underline{\underline{H}}h_{22}N_{12}}{R_2} \right)$$

$$p_{6,7} = -\frac{b}{R_2}$$

$$p_{6,8} = -\alpha \left(\frac{h_{56}}{R_2} - \frac{\underline{H}h_{25}N_{12}}{\underline{H}h_{25}N_{12}} \right)$$

$$p_{7,1} = \frac{\alpha^3}{b^2} \left(h_{14} - \frac{\underline{H}h_{34}N_{12}}{\underline{H}h_{34}N_{12}} \right) - \frac{\underline{C}\alpha\pi^2 N_{11}z_c}{\lambda^2}$$

$$p_{7,2} = -\frac{\alpha^3}{b^2} \left(\frac{h_{46}}{R_2} + \frac{\underline{H}h_{24}N_{12}}{\underline{H}h_{24}N_{12}} \right)$$

$$p_{7,3} = \frac{\pi^2 b N_{11}}{\lambda^2} + \frac{\alpha^2}{b R_2} (\underline{F}h_{24}N_{22} - \underline{G}N_{12}h_{34}) - \frac{\alpha^4 h_{44}}{b^3} + \frac{\underline{C}\alpha^2 \pi^2 N_{11}z_c^2}{b\lambda^2}$$

$$p_{7,4} = \alpha N_{12} - \frac{2\alpha^3 h_{46}}{b^2} + \frac{\alpha N_{12}z_c}{R_2}$$

$$p_{7,5} = \frac{\alpha^2 h_{34}}{b}$$

$$p_{7,6} = \frac{\alpha^2 h_{24}}{b} - \frac{b}{R_2}$$

$$p_{7,8} = -\frac{\alpha^2 h_{45}}{b}$$

$$p_{8,1} = \frac{\alpha^2}{b} \left(h_{16} \left[2 - \frac{z_c}{R_2} \right] - \frac{2\underline{H}h_{36}N_{12}}{\underline{H}h_{36}N_{12}} \right)$$

$$p_{8,2} = -\frac{\alpha^2}{b R_2} \left(h_{66} \left[2 - \frac{z_c}{R_2} \right] - \frac{2\underline{H}h_{26}N_{12}}{\underline{H}h_{26}N_{12}} \right) - \frac{\underline{B}\pi^2 b N_{11}z_c}{\lambda^2}$$

$$p_{8,3} = -\frac{\alpha^3 h_{46}}{b^2} \left(2 - \frac{z_c}{R_2} \right) + \alpha N_{12} \left(1 - \frac{z_c}{R_2} \right) + \frac{2\alpha}{R_2} (\underline{F}h_{26}N_{22} - \underline{G}h_{36}N_{12})$$

$$p_{8,4} = -\frac{2\alpha^2 h_{66}}{b} \left(2 - \frac{z_c}{R_2} \right) + b N_{22} \left(1 - \frac{z_c}{R_2} \right) + \frac{\underline{B}\pi^2 b N_{11}z_c^2}{\lambda^2}$$

$$p_{8,5} = \alpha h_{36} \left(2 - \frac{z_c}{R_2} \right)$$

$$p_{8,6} = \alpha h_{26} \left(2 - \frac{z_c}{R_2} \right)$$

$$p_{8,7} = b \left(1 - \frac{z_c}{R_2} \right)$$

$$p_{8,8} = \alpha h_{56} \left(2 - \frac{z_c}{R_2} \right)$$

Table 1. Material properties for boron/epoxy plies and 2024 aluminum (SI units).

Material	$E_{11} \times 10^{-10}$, N/m ²	$E_{22} \times 10^{-10}$, N/m ²	$G_{12} \times 10^{-10}$, N/m ²	ν_{12}	ρ , kg/m ³
Boron/epoxy	20.69	1.86	0.48	0.21	2006.8
Aluminum 2024	7.38	7.38	2.76	0.33	2768.0

Table 2. Geometric parameters used to vary the curvature parameter, $\frac{b^2}{R_2 t}$.

$\frac{b^2}{R_2 t}$	b, cm.	R_2 , cm.	β , degrees
1	24.4002	5760.3570	0.25264
5	24.4005	1152.1180	1.2632
10	25.4020	576.12905	2.5262
30	25.4185	192.2917	7.5738
50	25.4513	115.67310	12.6067
100	25.6036	58.53098	25.0633
300	27.1026	21.86161	71.0315
500	29.6186	15.66554	108.3281
700	32.6900	13.63059	137.4115
1000	37.7873	12.75046	169.8018

Table 3. Critical value of stress resultant N_{11} for buckling of a symmetrically laminated long curved plate with clamped longitudinal edges.

$\frac{b^2}{R_2 t}$	$\frac{\lambda}{b}$	$N_{11cr}, \text{ N/m}$ Reference 32	$N_{11cr}, \text{ N/m}$ VICONOPT			
			Physical strains		Tensorial strains	
			Curved-plate theory	Segmented-plate theory	Curved-plate theory	Curved-plate theory
1	0.75	9 788	9 857	9 857	9 857	9 857
5	0.69	11 434	11 511	11 511	11 511	11 511
10	0.58	15 426	15 522	15 552	15 552	15 552
30	0.38	36 578	36 818	36 818	36 817	36 817
50	0.32	56 750	57 120	57 119	57 119	57 119
100	0.26	101 540	102 220	102 214	102 218	102 218
300	0.19	241 585	243 024	242 973	242 984	242 984
500	0.16	324 986	326 894	326 794	326 795	326 795
700	0.13	366 870	368 915	368 788	368 773	368 773
1000	0.13	386 498	388 410	388 274	388 207	388 207

Table 4. Critical value of stress resultant N_{22} for buckling of a symmetrically laminated long curved plate with clamped longitudinal edges.

$\frac{b^2}{R_2 t}$	$\frac{\lambda}{b}$	$N_{22cr}, \text{ N/m}$ Reference 32	VICONOPT ^a , $N_{22cr}, \text{ N/m}$		
			Physical strains Curved-plate theory	Segmented-plate theory	Tensorial strains Curved-plate theory
1	250	5 813	5 856	5 856	5 856
5	250	8 020	8 077	8 077	8 077
10	250	11 607	11 780	11 780	11 780
30	250	11 607	11 767	11 767	11 767
50	250	11 662	11 743	11 743	11 743
100	250	11 557	11 632	11 632	11 632
300	250	10 541	10 607	10 607	10 607
500	250	9 088	9 143	9 144	9 143
700	250	7 652	7 696	7 697	7 696
1000	250	5 866	5 887	5 888	5 887

^a N_{22} terms included in the in-plane stability equations.

Table 5. Critical value of stress resultant N_{12} for buckling of a symmetrically laminated long curved plate with clamped longitudinal edges.

$\frac{b^2}{R_2t}$	$\lambda \over b$	N_{12cr} , N/m Reference 32	N_{12cr} , N/m			
			Physical strains		Tensorial strains Curved-plate theory	
			Curved-plate theory	Segmented-plate theory		
1	0.85	12 415	12 491	12 491	12 491	
5	0.80	13 413	13 501	13 501	13 501	
10	0.72	15 580	15 683	15 683	15 683	
30	0.58	24 200	24 342	24 341	24 344	
50	0.59	31 170	31 345	31 344	31 350	
100	0.62	44 840	45 058	45 053	45 068	
300	0.86	74 120	73 773	73 748	73 794	
500	1.03	82 860	81 458	81 418	81 479	
700	1.02	82 630	80 528	80 479	80 547	
1000	1.32	75 630	72 204	72 160	72 217	

^a N_{22} and N_{12} terms included in the in-plane stability equations.

Table 6. Critical value of stress resultant $N_{11} = N_{22} = N_{12}$ for buckling of a symmetrically laminated long curved plate with clamped longitudinal edges.

$\frac{b^2}{R_2 t}$	$\frac{\lambda}{b}$	$N_{cr}, N/m$	$VICONOPT^a, N_{cr}, N/m$			
			Curved-plate theory	Physical strains Segmented-plate theory	Tensorial strains Curved-plate theory	
1	1.10	4 290	4 318	4 318	4 318	4 318
5	0.90	5 110	5 149	5 149	5 149	5 149
10	0.79	6 600	6 651	6 651	6 651	6 651
30	0.92	10 560	10 633	10 633	10 633	10 633
50	250	11 660	11 743	11 743	11 743	11 743
100	250	11 560	11 631	11 631	11 631	11 631
300	250	10 540	10 607	10 607	10 607	10 607
500	250	9 090	9 143	9 144	9 143	9 143
700	250	7 650	7 696	7 697	7 696	7 696
1000	250	5 880	5 887	5 888	5 887	5 887

^a N_{22} and N_{12} terms included in the in-plane stability equations.

Table 7. Critical value of stress resultant N_{11} for buckling of an unsymmetrically laminated long curved plate with simply supported longitudinal edges.

Number of B/E plies	N_{11cr} , N/m	N_{11cr} , N/m			
		Physical strains		Tensorial strains	
		Curved-plate theory	Segmented-plate theory	Curved-plate theory	Curved-plate theory
2	24 545	24 981	24 969		24 973
4	40 000	41 367	41 336		41 347
6	63 636	64 331	64 265		64 289
8	92 727	94 318	94 198		94 241
10	129 545	131 905	131 708		131 775
12	177 273	177 722	177 416		177 517
14	232 727	232 424	231 976		232 118

Table 8. Critical value of stress resultant N_{12} for buckling of an unsymmetrically laminated long curved plate with simply supported longitudinal edges.

Number of B/E plies	N_{12cr} , N/m	N_{12cr} , N/m			
		Physical strains		Tensorial strains	
		Curved-plate theory	Segmented-plate theory	Curved-plate theory	Curved-plate theory
2	7 273	8 070	8 066		8 070
4	14 318	16 346	16 336		16 345
6	26 818	28 830	28 811		28 829
8	43 182	46 229	46 194		46 229
10	66 818	69 265	69 205		69 264
12	95 454	98 668	98 573		98 666
14	130 454	135 180	135 037		135 177

Table 9. Material properties for aluminum and Korex™ honeycomb core (English Engineering units).

Material	$E_{11} \times 10^{-6}$, lb/in ²	$E_{22} \times 10^{-6}$, lb/in ²	$G_{12} \times 10^{-6}$, lb/in ²	$G_{13} \times 10^{-6}$, lb/in ²	$G_{23} \times 10^{-6}$, lb/in ²	ν_{12}	ρ , lb/in ³
Aluminum	10.0	10.0	3.846	3.846	3.846	0.3	0.1
Korex™ H/C core	0.0001	0.0001	0.0001	0.012	0.004	0.3	0.00116

Table 10. Critical value of hoop stress resultant N_{22} for buckling of a long, isotropic cylinder subject to uniform external compression (results are in lbs/in.).

Reference [49]		VICONOPT (physical strains)		
		Curved-plate analysis		Segmented-plate analysis
Live load	Dead load	N_{22} terms neglected	N_{22} terms included	N_{22} terms neglected
28.1180	37.4906	28.1180	37.4906	37.4950
				37.4950

Table 11. Design-optimization results for a honeycomb-sandwich cylinder subjected to N_{11} loading.

N_{11} , lb/in.	Classical plate theory (physical strains)			Transverse shear plate theory (physical strains)		
	t_{fs} , in.	t_{core} , in.	mass, lb _m	t_{fs} , in.	t_{core} , in.	mass, lb _m
1 000	0.010	0.310	213.53	0.010	0.313	213.85
2 000	0.020	0.334	397.00	0.020	0.339	397.43
3 000	0.030	0.324	576.88	0.030	0.331	577.64
4 000	0.040	0.280	753.17	0.040	0.349	760.47
5 000	0.050	0.270	933.02	0.050	0.367	943.44
10 000	0.100	0.250	1835.8	0.100	0.606	1873.2
15 000	0.150	0.194	2734.7	0.150	0.909	2809.7
20 000	0.200	0.135	3633.3	0.200	1.212	3746.3

Table 12. Design-optimization results for a solid-wall cylinder subjected to N_{11} loading.

N_{11} , lb/in.	Classical plate theory (physical strains)		Transverse shear plate theory (physical strains)	
	t_{wall} , in.	mass, lb _m	t_{wall} , in.	mass, lb _m
1 000	0.102	924.68	0.102	924.69
2 000	0.143	1296.8	0.143	1296.8
3 000	0.179	1622.0	0.179	1622.0
4 000	0.207	1873.8	0.207	1873.9
5 000	0.230	2082.1	0.230	2082.2
10 000	0.324	2931.8	0.324	2931.9
15 000	0.409	3697.5	0.409	3697.7
20 000	0.474	4291.3	0.474	4291.6

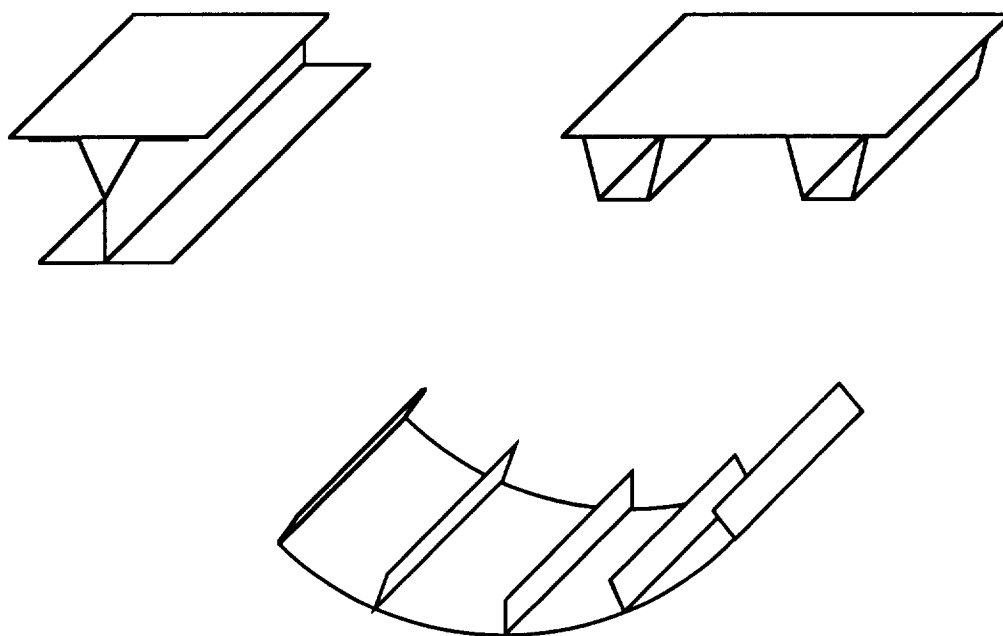


Figure 1.1 Typical longitudinally stiffened plate structures.

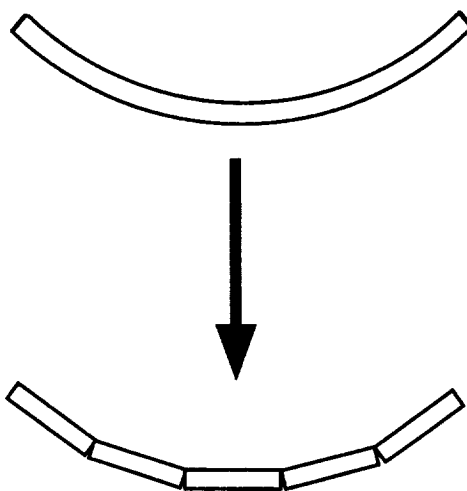


Figure 1.2 Segmented representation of curved plate geometry currently used by VICONOPT.

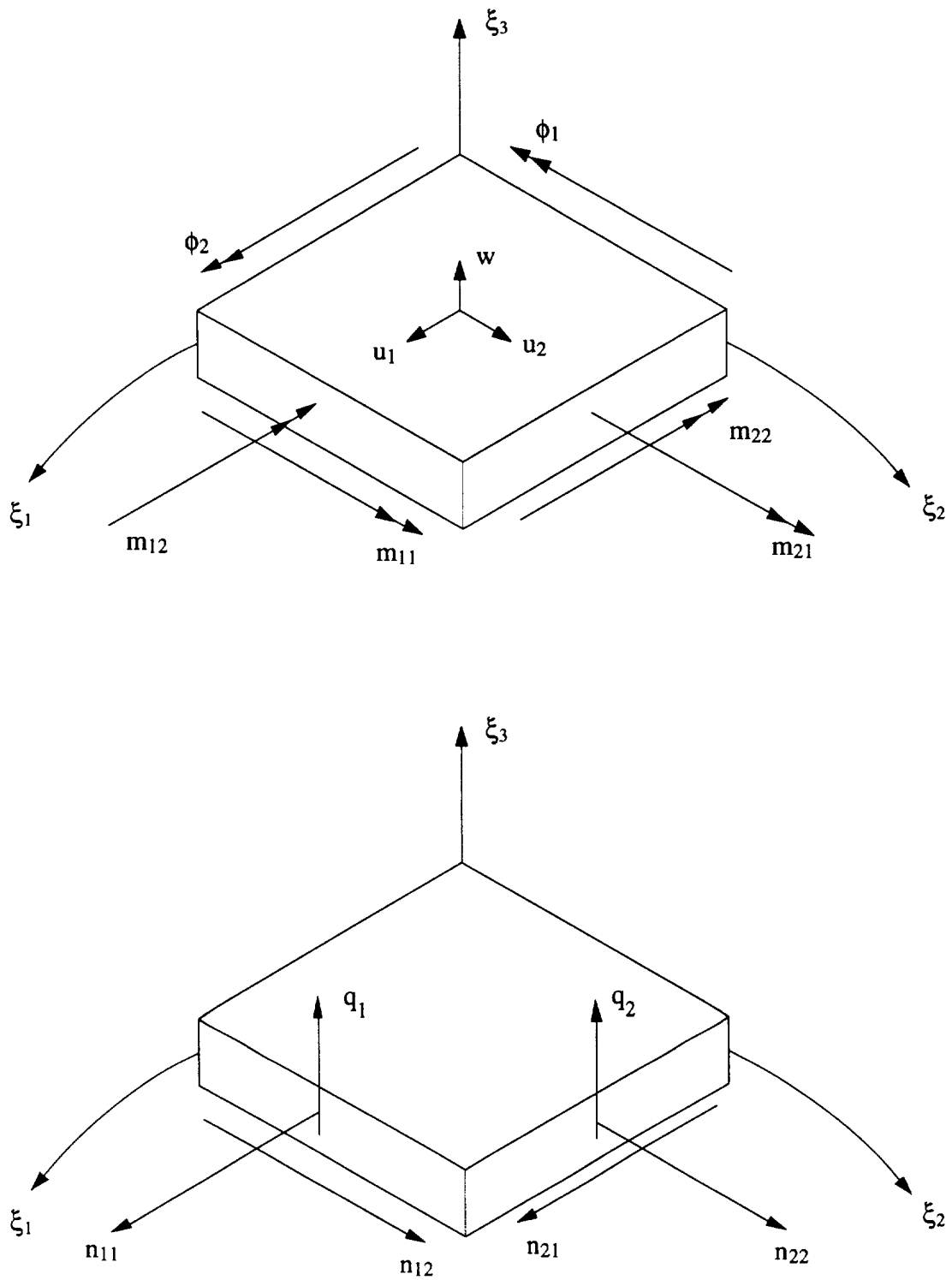


Figure 2.1. Curved-plate geometry and sign convention for buckling displacements, rotations, moments, and forces.

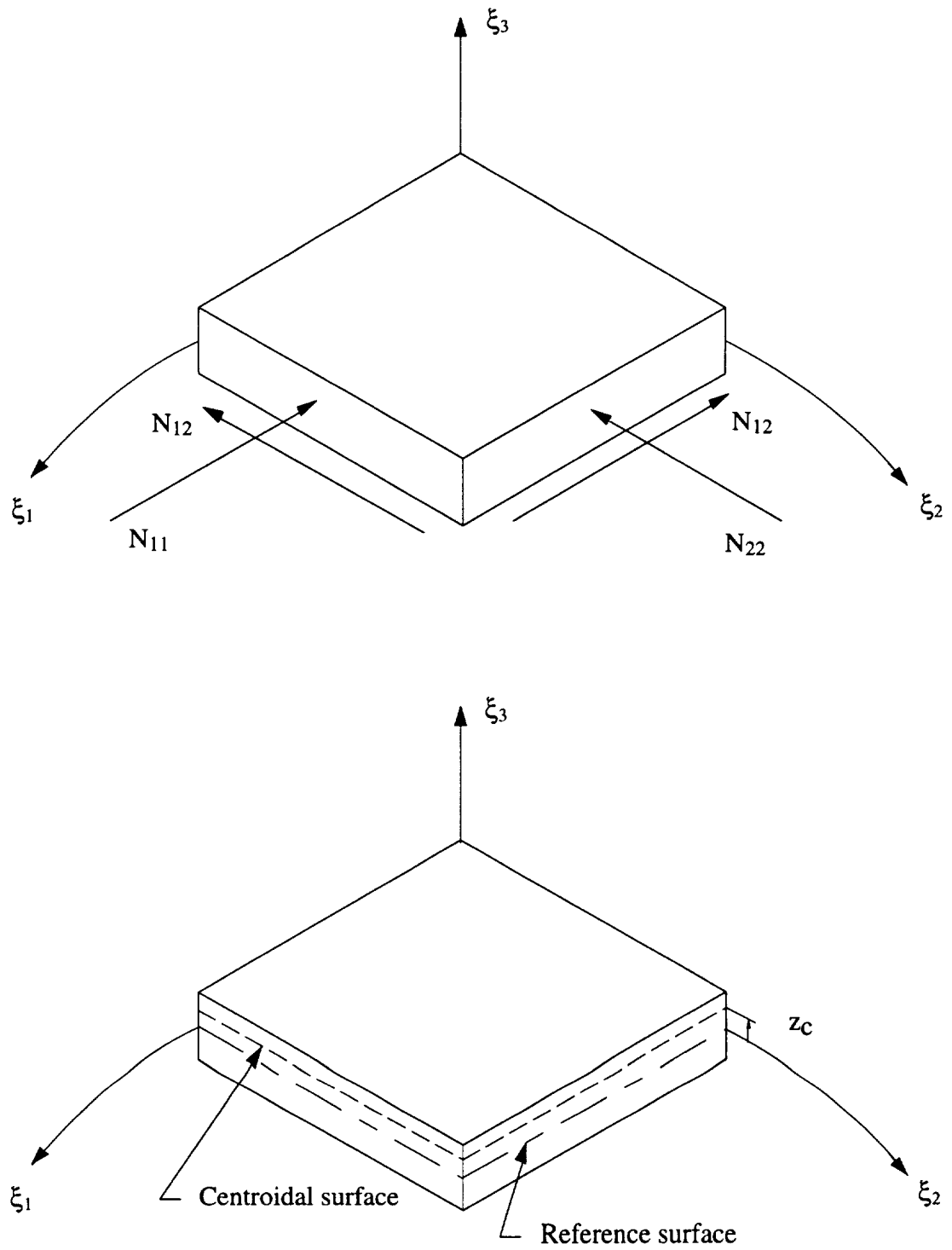


Figure 2.2 Sign convention for applied in-plane loads and relation of reference surface to centroidal surface.

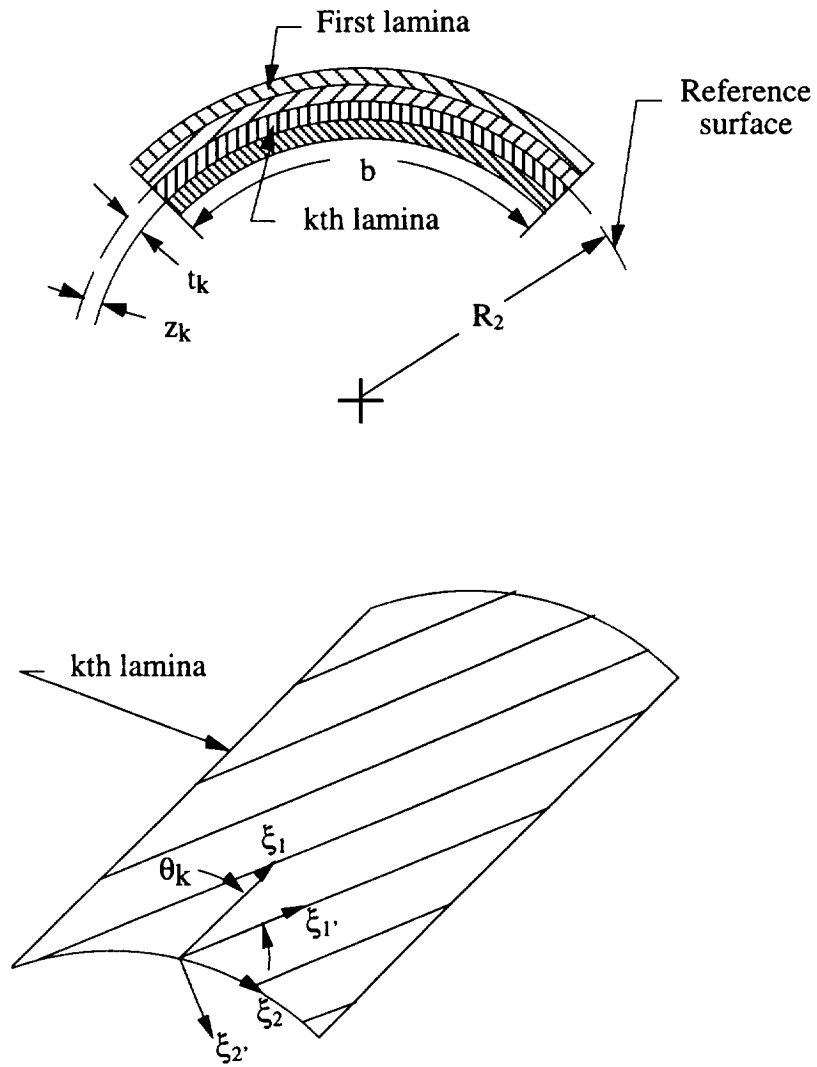
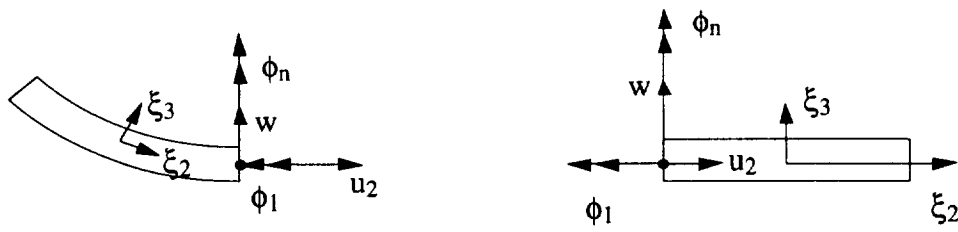


Figure 2.3 Curved-laminate geometry.

Plate 1Plate 2

(a) plates 1 and 2 coplanar

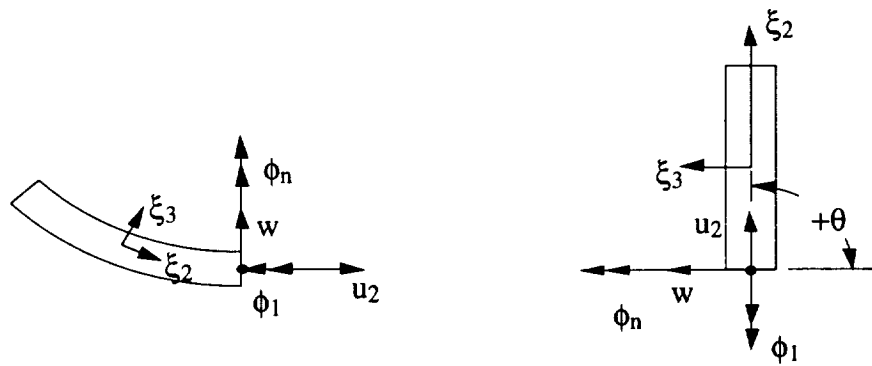
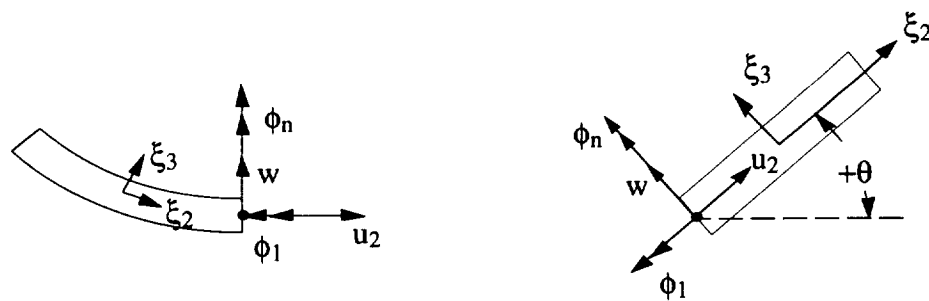
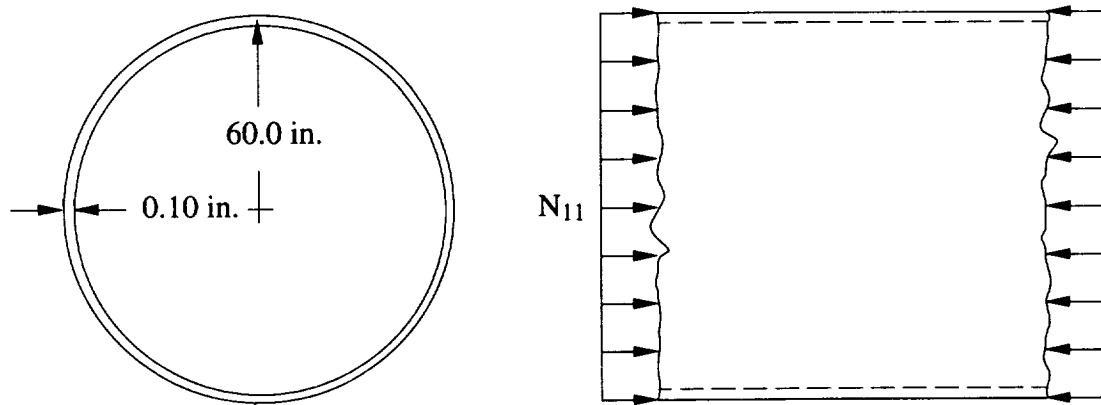
(b) plate 2 rotated to $\theta = +90^\circ$ (c) plate 2 rotated to arbitrary angle, θ

Figure 3.1 Displacements and rotations at a typical plate junction.



$$E = 10.0 \times 10^6 \text{ psi}$$

$$\nu_{12} = 0.33$$

$$\rho = 0.1 \text{ lb/in.}^3$$

Figure 4.1 Long isotropic (aluminum) cylinder subjected to uniaxial compression.

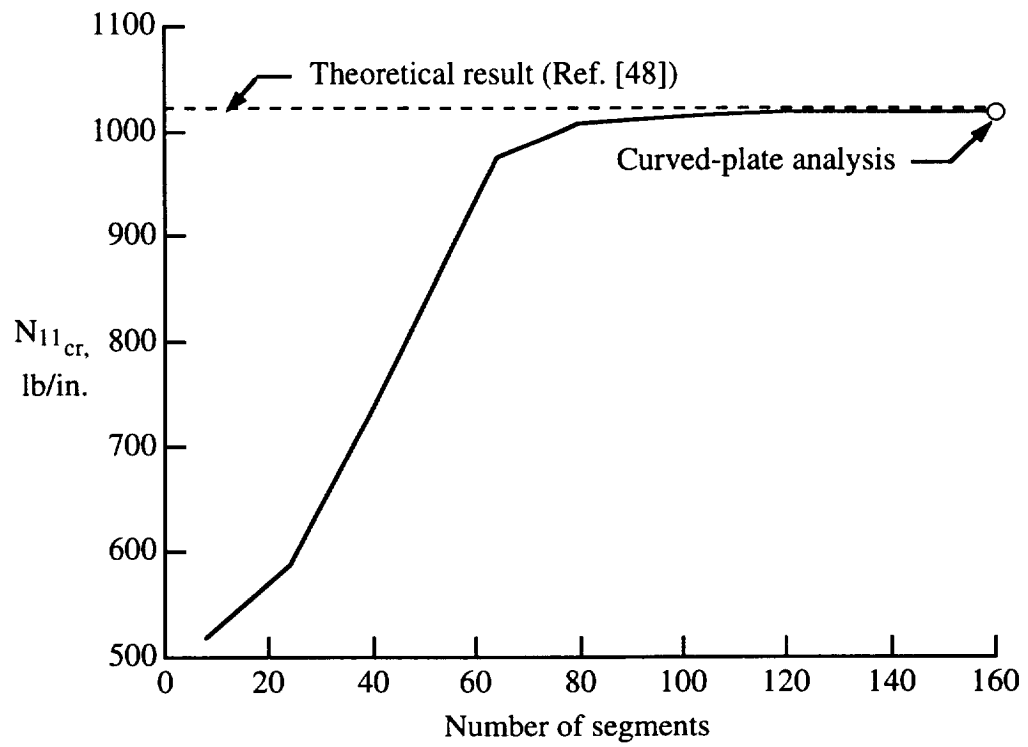


Figure 4.2 Convergence of VICONOPT segmented-plate results as a function of the number of segments used in the approximation.

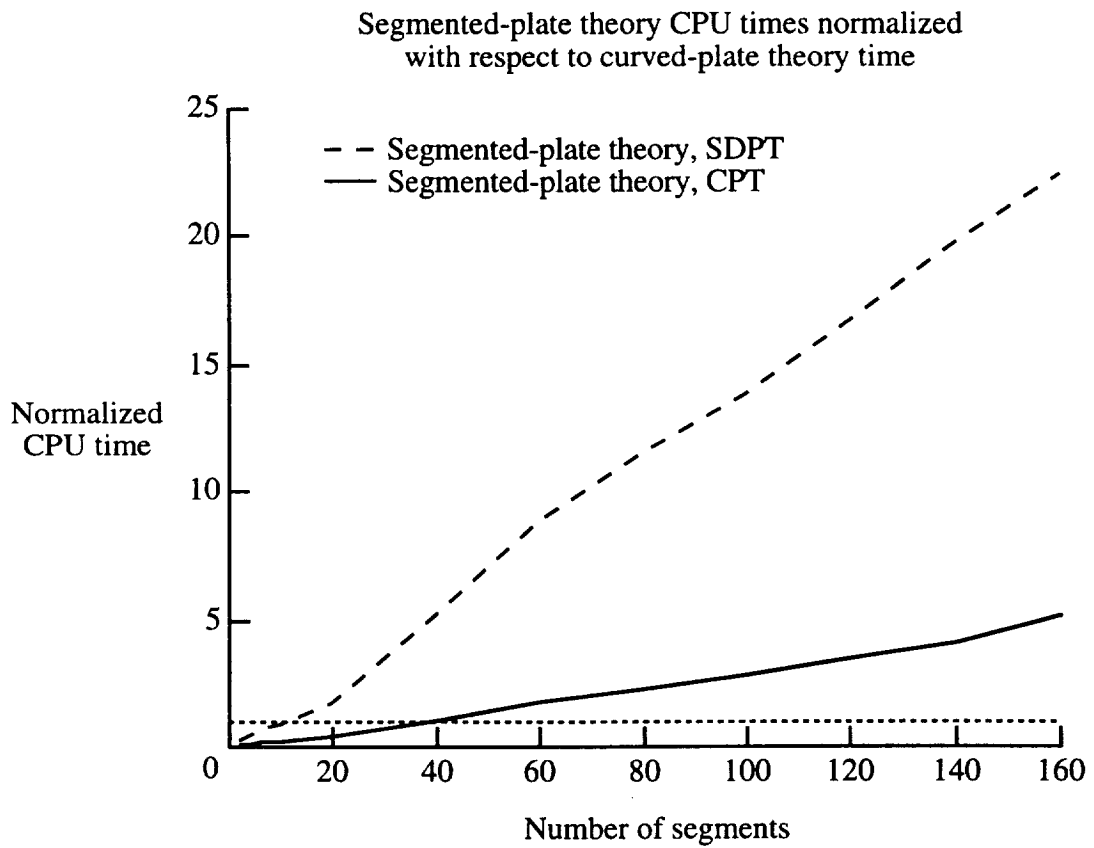


Figure 4.3 Normalized CPU time requirements for the segmented-plate approach as a function of the number of segments used in the approximation.

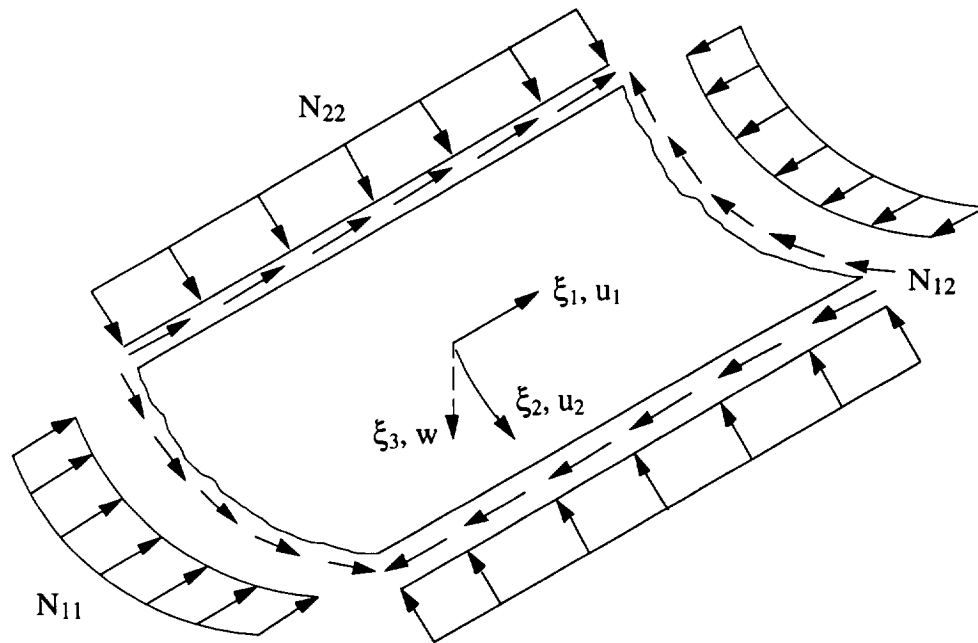


Figure 4.4 Positive applied in-plane loads on a long curved plate.

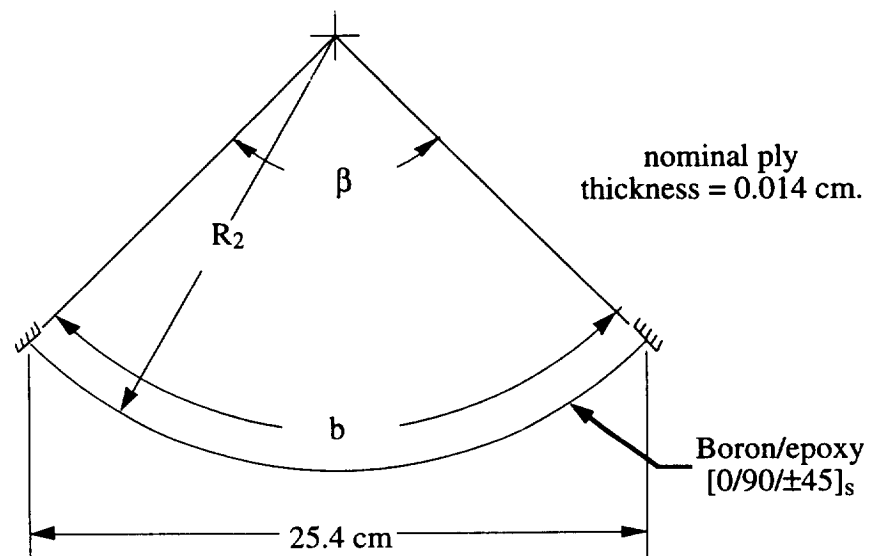


Figure 4.5 Symmetrically laminated long curved plate with clamped longitudinal edges subjected to applied in-plane loads.

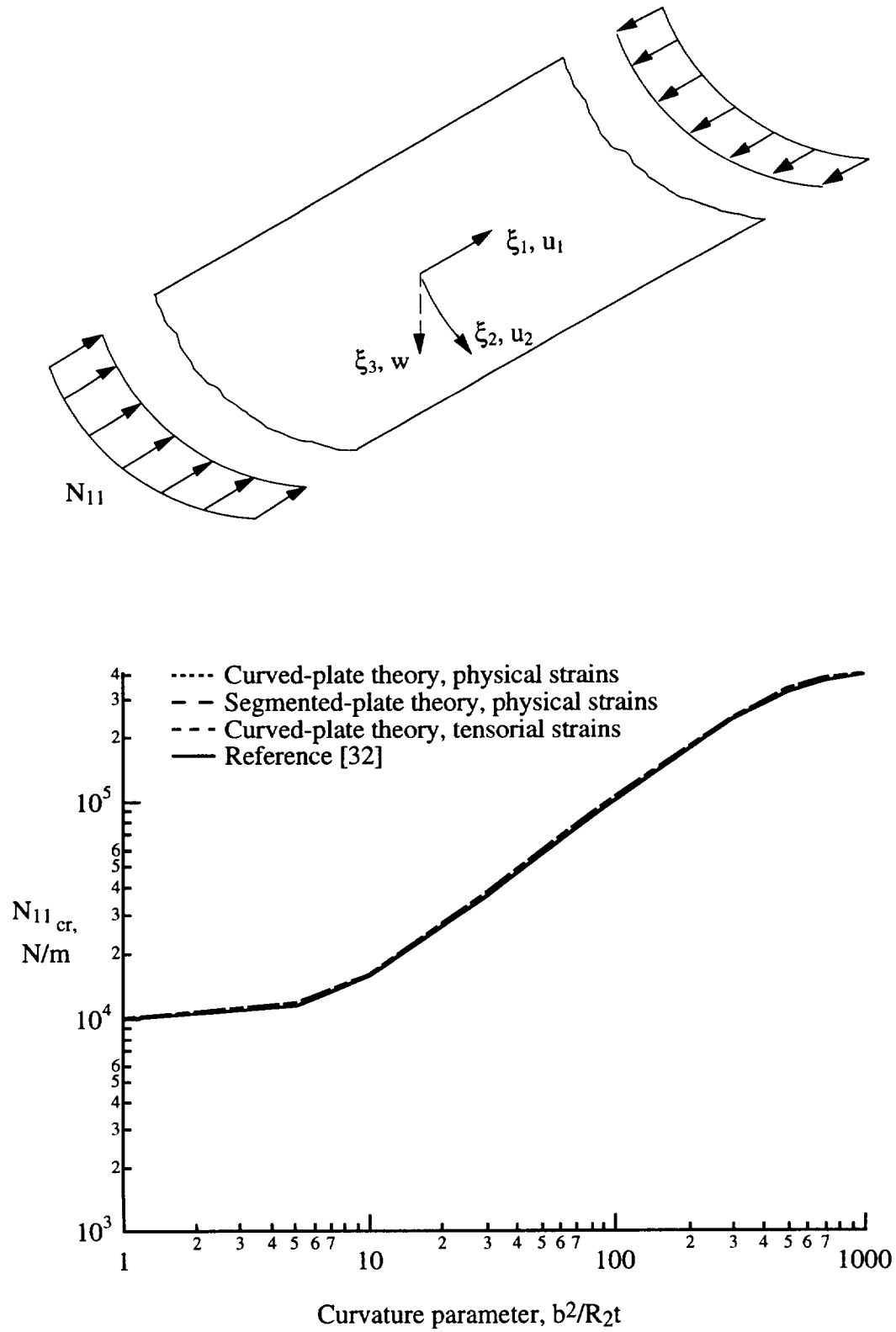


Figure 4.6 Critical value of stress resultant N_{11} for buckling of a symmetrically laminated curved plate with clamped longitudinal edges.

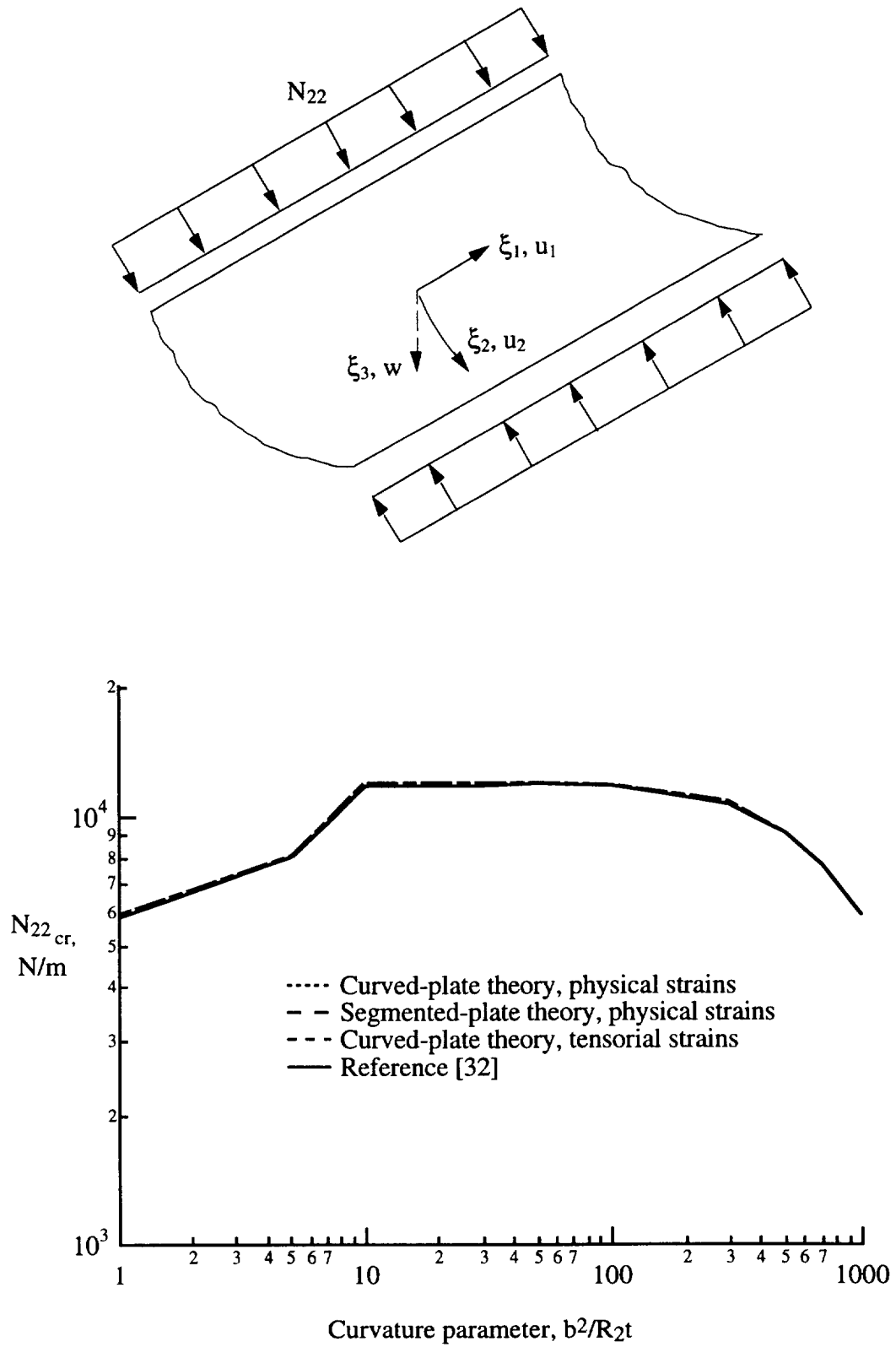


Figure 4.7 Critical value of stress resultant N_{22} for buckling of a symmetrically laminated curved plate with clamped longitudinal edges.

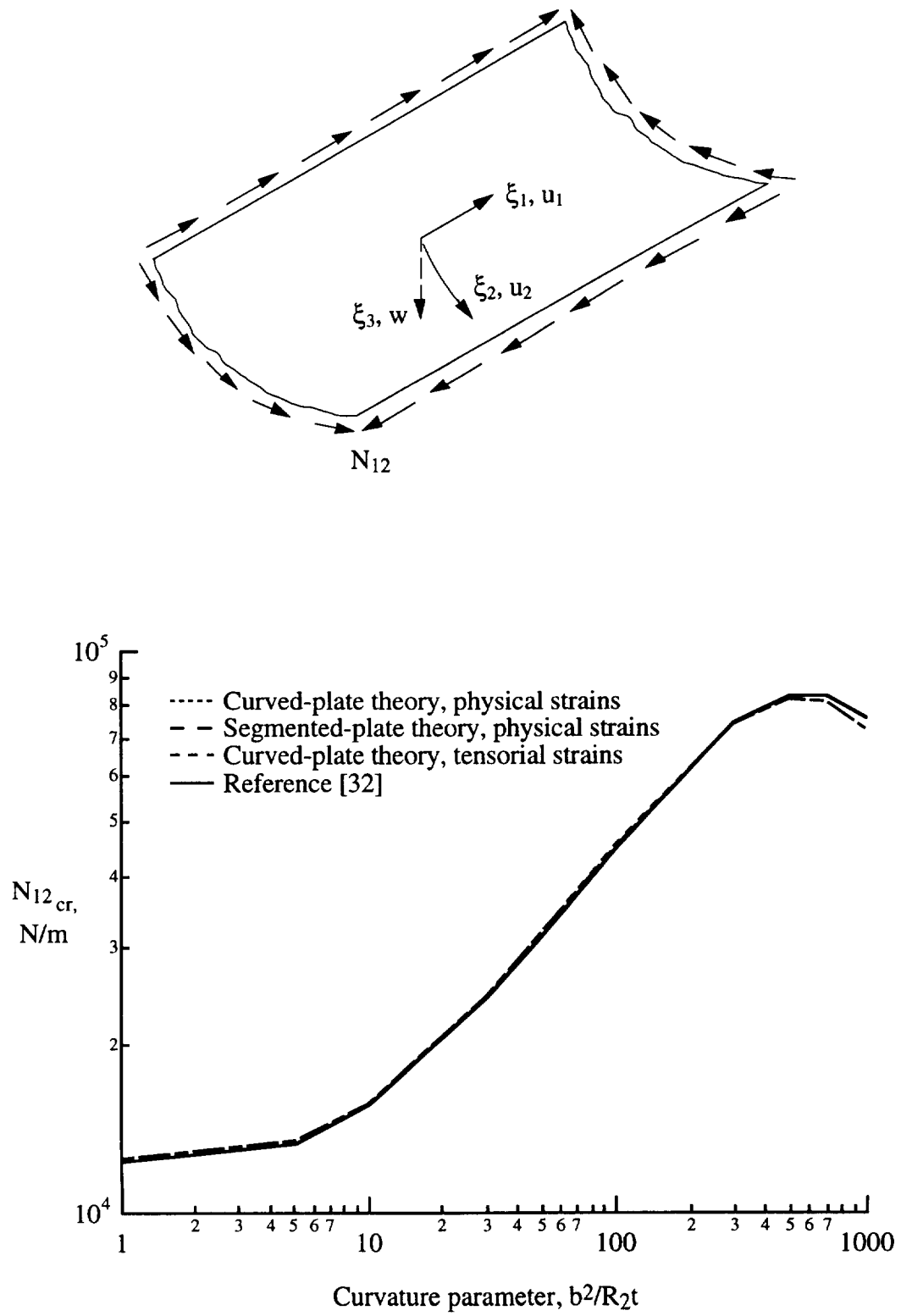


Figure 4.8 Critical value of stress resultant N_{12} for buckling of a symmetrically laminated curved plate with clamped longitudinal edges.

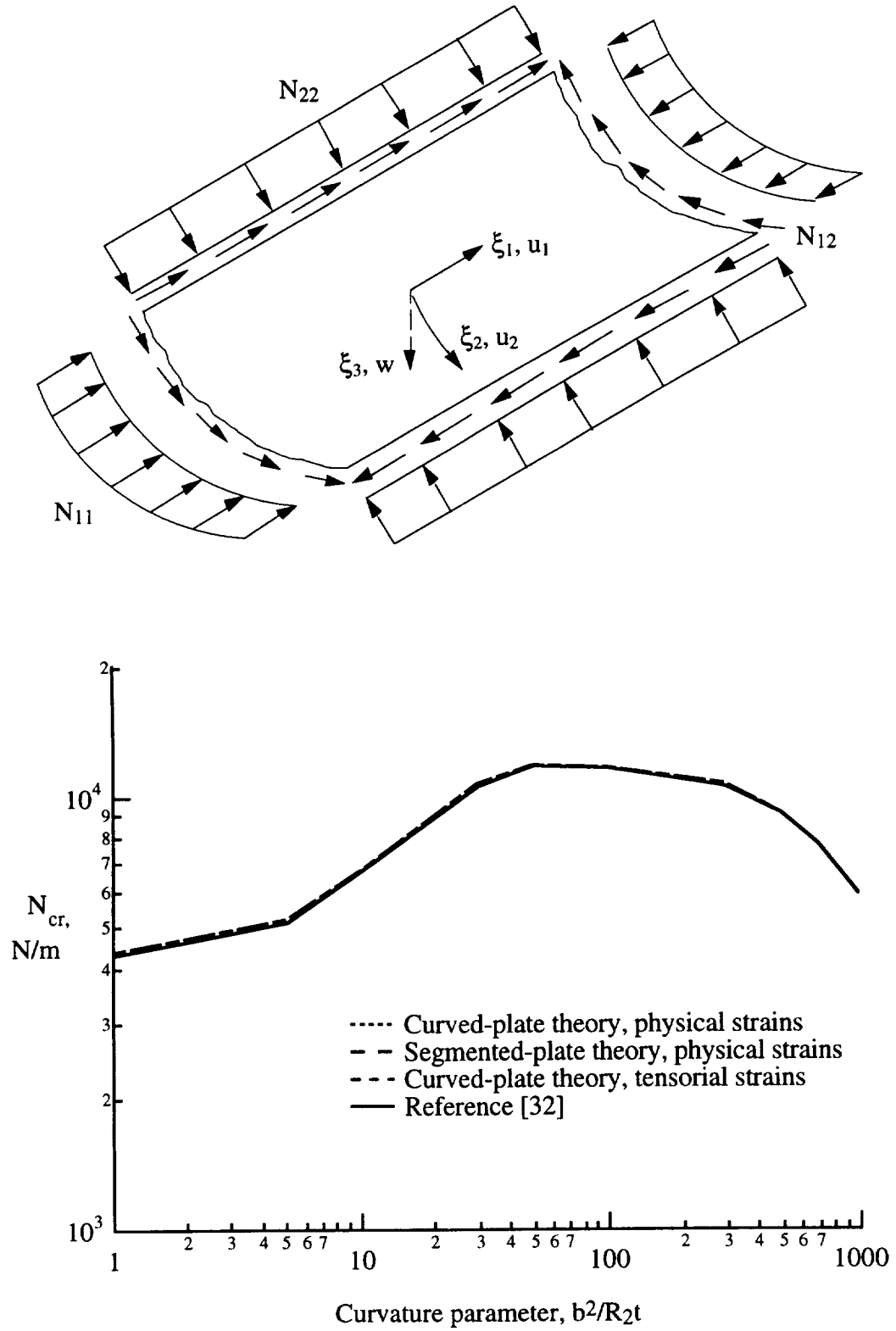


Figure 4.9 Critical value of stress resultants $N_{11} = N_{22} = N_{12}$ for buckling of a symmetrically laminated curved plate with clamped longitudinal edges.

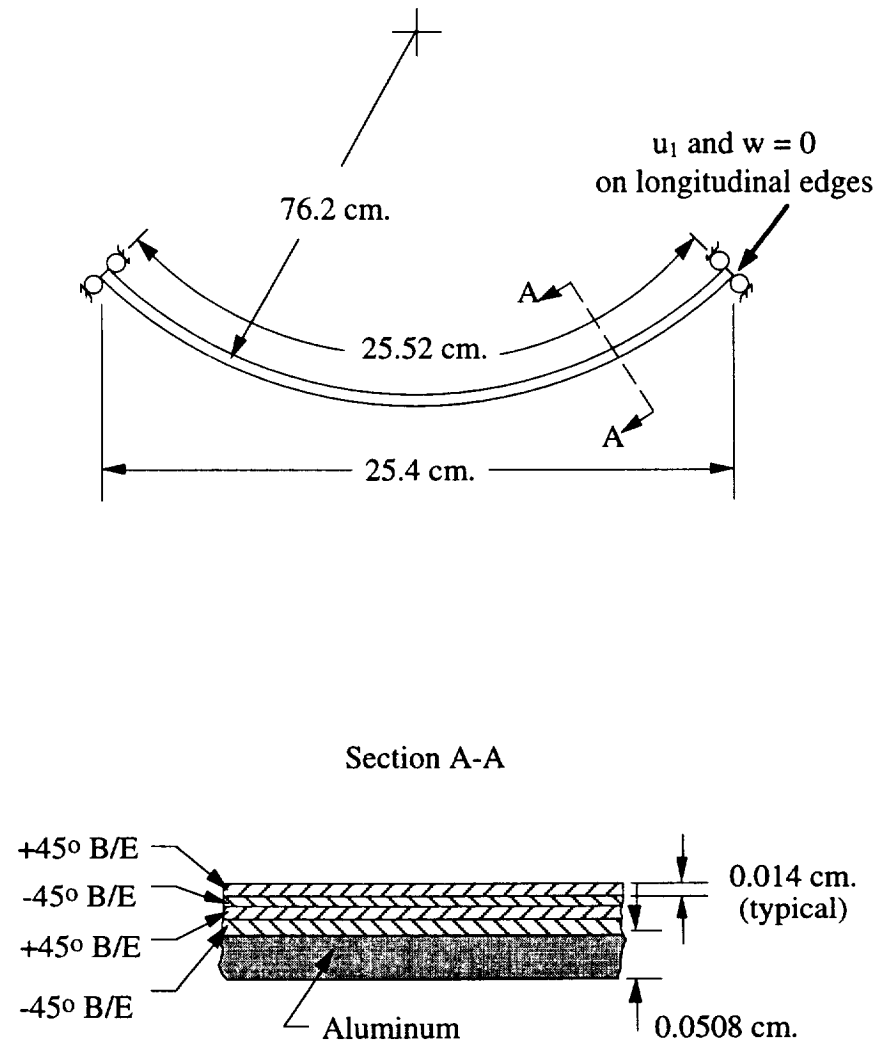


Figure 4.10 Unsymmetrically laminated aluminum and boron/epoxy (B/E) curved plate with simply supported edges subjected to applied in-plane loads.

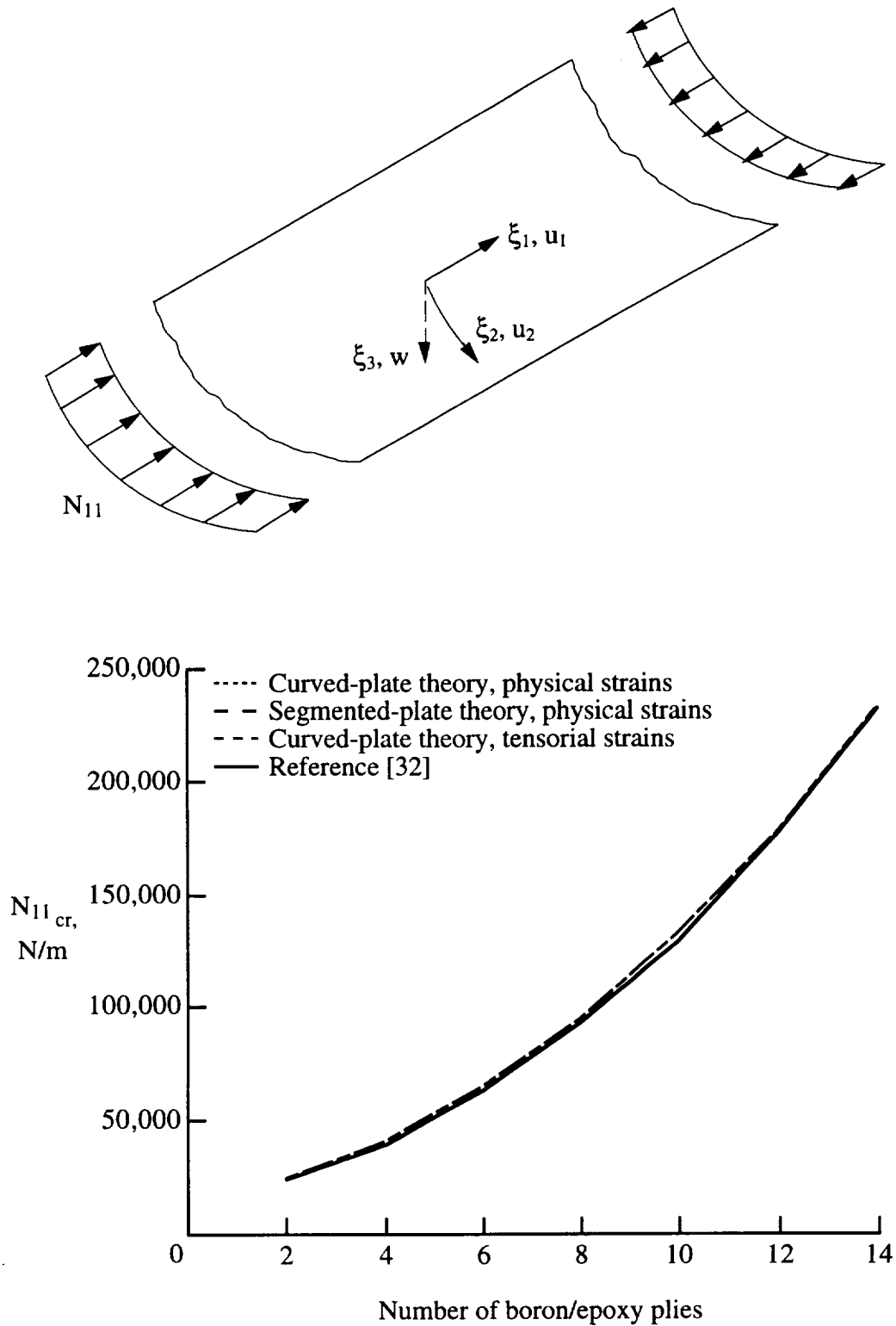


Figure 4.11 Critical value of stress resultant N_{11} for buckling of an unsymmetrically laminated aluminum and boron/epoxy (B/E) curved plate with simply supported longitudinal edges.

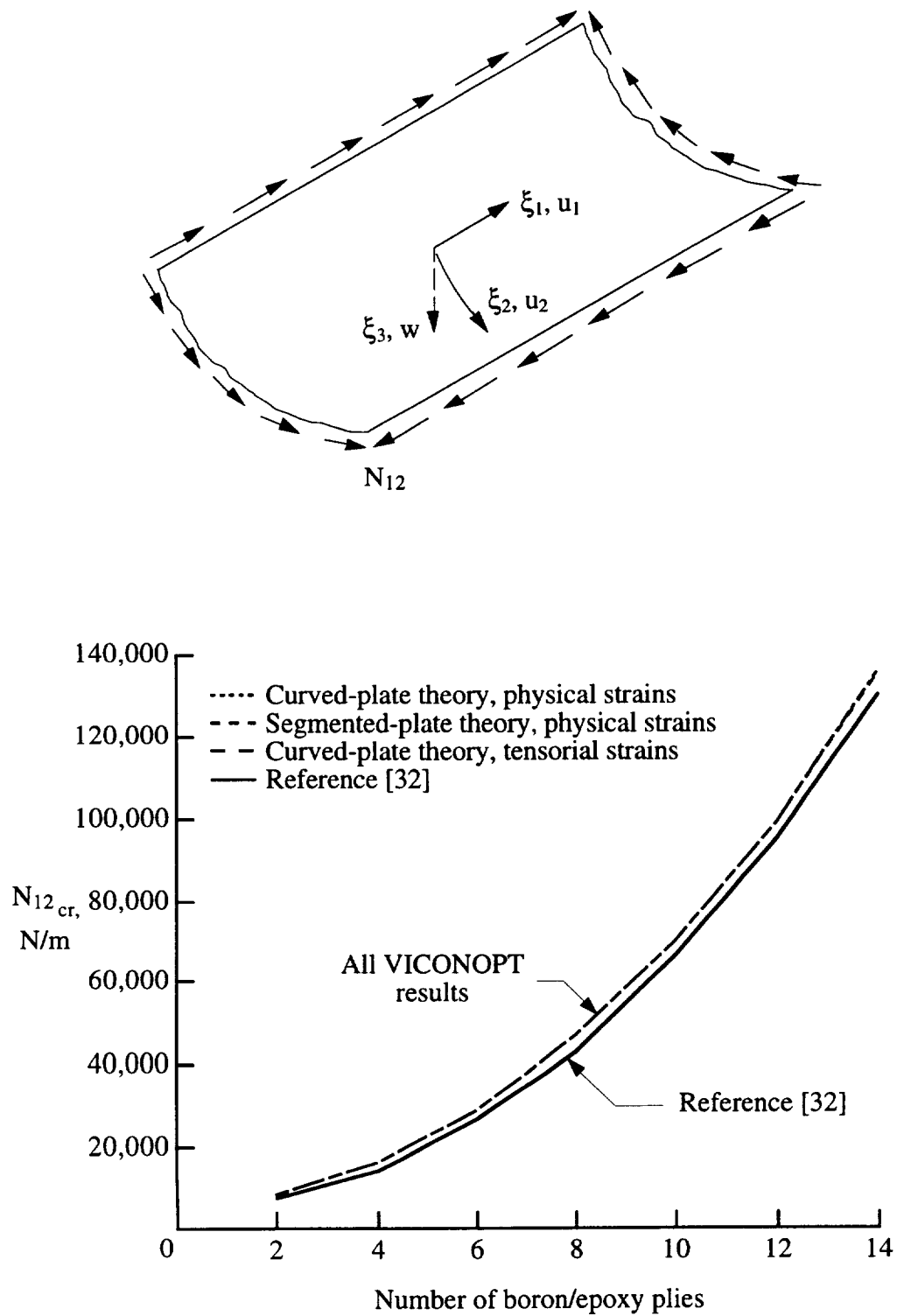


Figure 4.12 Critical value of stress resultant N_{12} for buckling of an unsymmetrically laminated aluminum and boron/epoxy (B/E) curved plate with simply supported longitudinal edges.

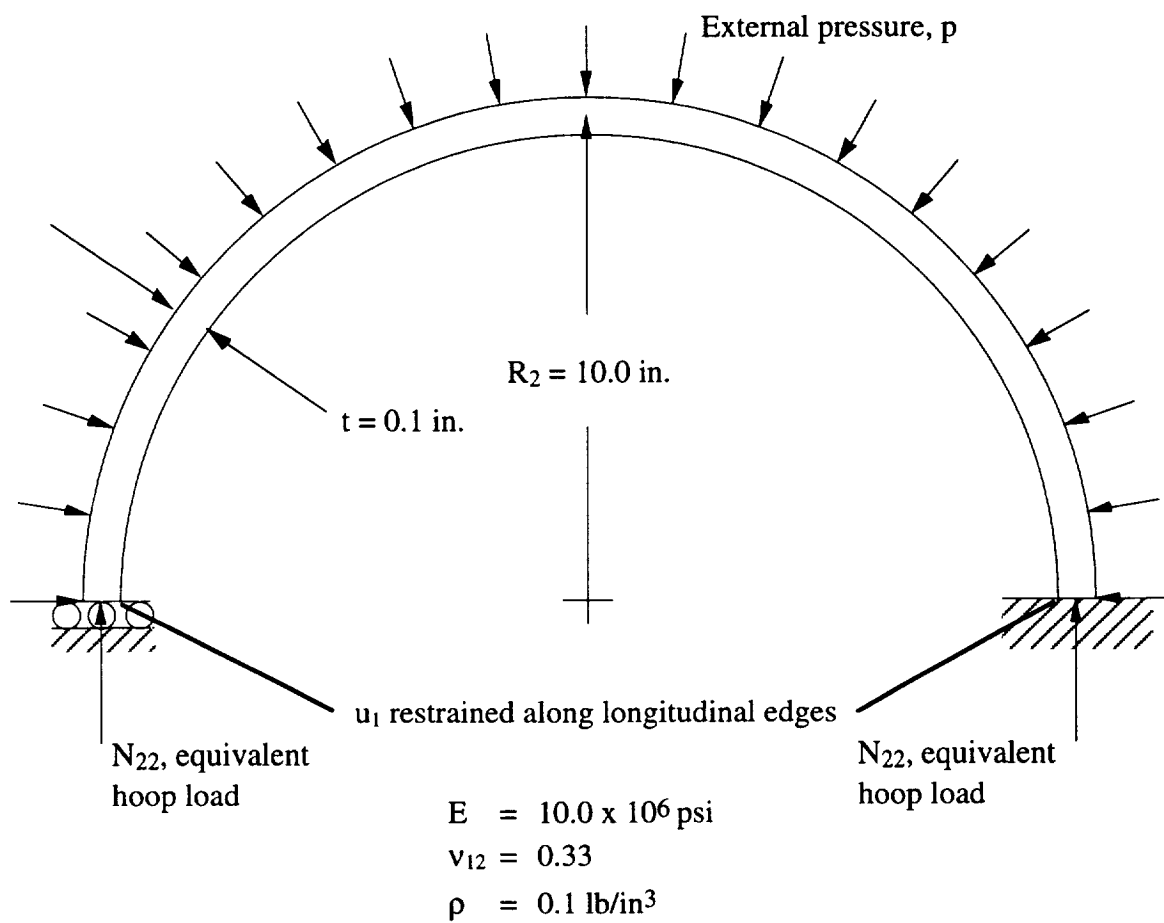


Figure 4.13 Isotropic (aluminum) long cylindrical tube subjected to uniform external pressure loading.

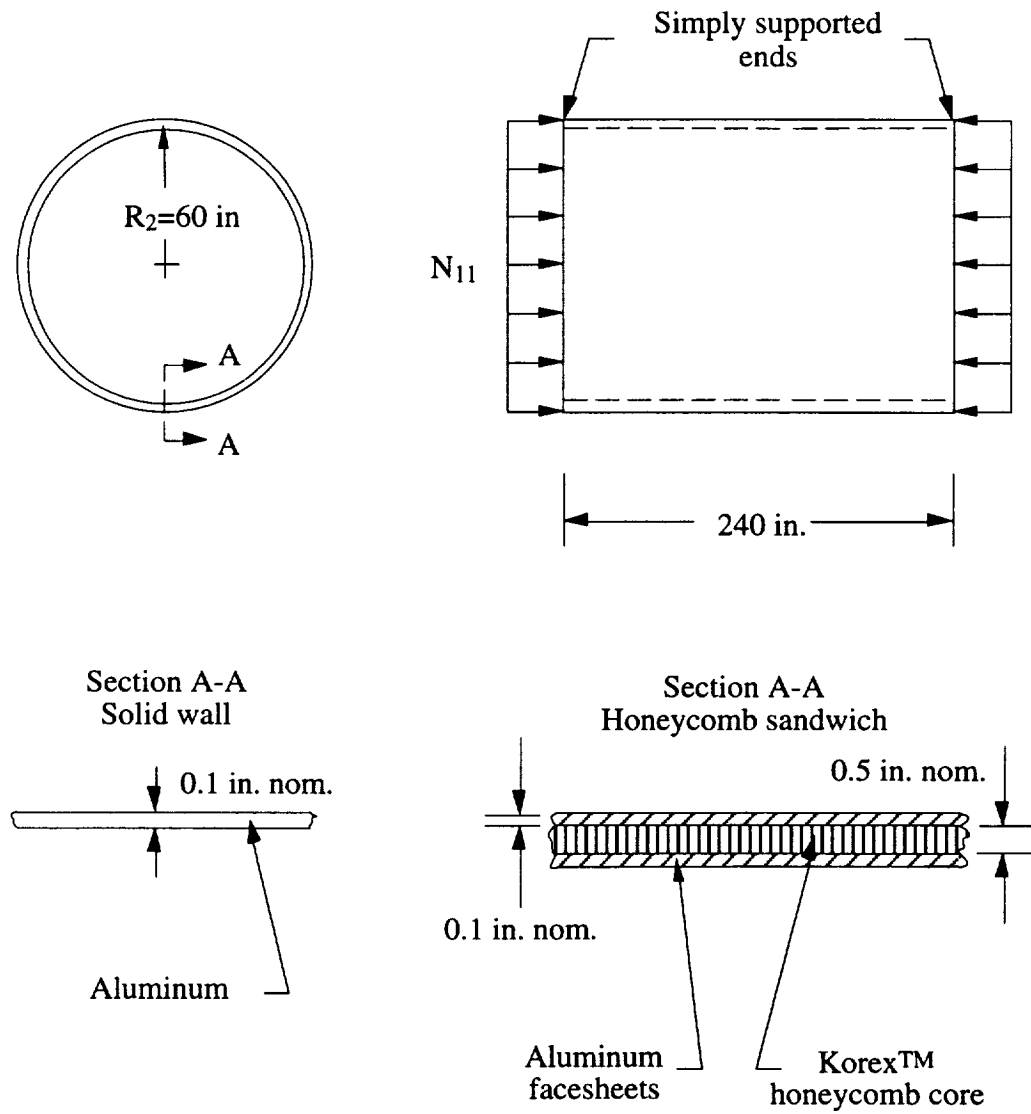


Figure 4.14 Cylindrical shell subjected to uniform axial compression (N_{11} loading).

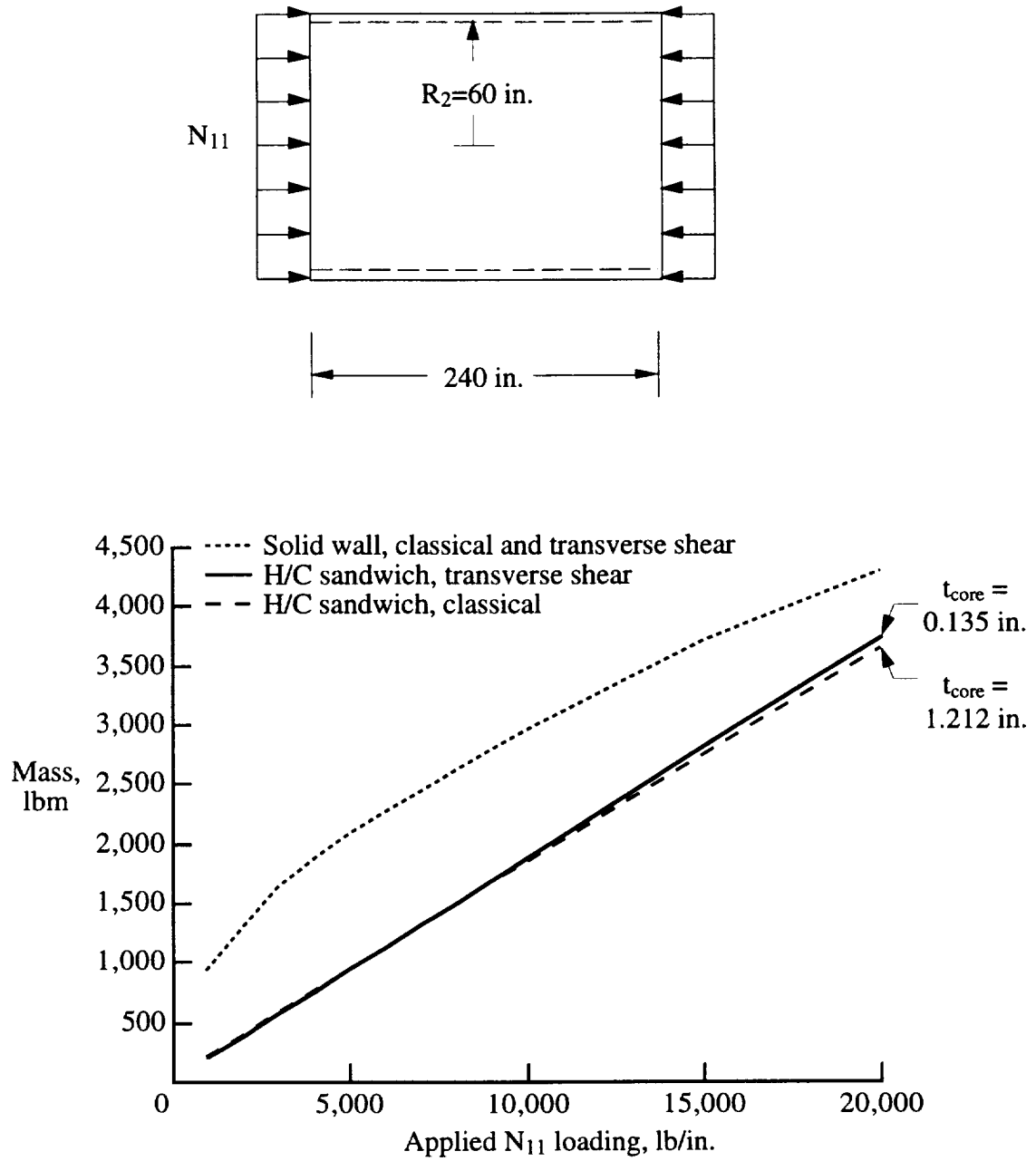


Figure 4.15 Optimized cylinder mass as a function of the applied loading for a cylindrical shell.